



^b
UNIVERSITÄT
BERN

OESCHGER CENTRE
CLIMATE CHANGE RESEARCH

Sugar Beet Yield Analysis with the WOFOST Simulation Model and Remote Sensing in Switzerland

Master thesis
Faculty of Science, University of Bern

handed in by
Manuel Kunz
2025

Supervision:
PD Dr. Annelie Holzkämper
Oeschger Center for Climate Change Research & Agroscope

Co-supervision:
Prof. Dr. Stefan Wunderle
Institute of Geography, University of Bern
and
Thomas Steinger
Agroscope

Abstract

Climate change is projected to impact agricultural production. Sugar beet production is an important part of Swiss agriculture, which is why assessing potential climatic impacts is relevant. Since cropping simulation models are useful in such assessments, this thesis evaluated the performance of the World Food Studies (WOFOST) cropping simulation model for simulating the growth of sugar beets under Swiss conditions. The model's performance was evaluated using yield observations from 20 locations for the period from 1990 to 2022, as well as yield observations from 950 sugar beet fields located across the Swiss Plateau in the year 2020. It was found that WOFOST performed better regarding the temporal variability of the yield observations (1990-2022) compared to the spatial variability (2020). In 2020, Swiss sugar beet production was impacted by the Beet Yellow Virus (BYV), resulting in decreased sugar beet yields. For the 950 sugar beet fields examined, information regarding the level of BYV contamination, alongside the location and harvested yield, was gathered through a survey of sugar beet farmers. A remote sensing analysis was conducted in which 101 different vegetation indices were calculated for the examined sugar beet field to identify the vegetation index that correlates best with the harvested yield and the BYV contamination category. The Chlorophyll Index Green (CIG), the Simple Ratio (SR), and the Green Ratio Vegetation Index (GRVI) showed the strongest correlation with observed yield, while the Anthocyanin Reflectance Index (ARI) demonstrated the best correlation with the BYV categories. Lastly, the combination of WOFOST and remote sensing parts showed that WOFOST predicted more frequent water stress for fields heavily affected by BYV, suggesting that water stress increased the vulnerability to BYV infections.

Acknowledgement

Firstly, I would like to thank Annelie Holzkämper for giving me the opportunity to write my thesis in her group at Agroscope, as well as for her support and guidance throughout the process. Secondly, I would also like to thank Stefan Wunderle for his support with the remote sensing part. Further, I am grateful to Thomas Steinger, who supported the data analysis process and provided access to his survey data. I would also like to thank Maria Eliza Turek, Malve Heinz and Tamara Baumgartner for their support in the data analysis. Lastly, I am grateful to my family and friends for their support throughout the process of my master's thesis.

Table of content

1	Introduction	5
2	Data and methods	10
2.1	WOFOST – Model description	10
2.2	WOFOST simulations 1990-2022.....	12
2.2.1	Meteorological data.....	12
2.2.2	Soil parameter set and WOFOST model	14
2.2.3	Yield comparison.....	14
2.3	WOFOST simulations and remote sensing analysis in 2020	15
2.3.1	Meteorological data.....	16
2.3.2	Soil parameters	17
2.3.3	Yield comparison.....	18
2.4	Model evaluation with reference data from Reckenholz.....	18
2.5	Remote sensing data.....	20
3	Results	23
3.1	WOFOST evaluation at Reckenholz	23
3.1.1	Evapotranspiration	25
3.1.2	Soil moisture content.....	25
3.2	WOFOST simulations 1990-2022.....	27
3.3	WOFOST simulations 2020	30
3.4	Remote sensing results	35
4	Discussion	38
4.1	WOFOST simulations	38
4.2	Remote sensing	40
5	Conclusion.....	42
6	References	44
7	Annex	51

List of Figures

Figure 1: Map showing the locations with available sugar beet yield data in Switzerland	12
Figure 2: Map showing the locations with available sugar beet yield data and daily meteorological records	13
Figure 3: Map showing the locations used for WOFOST simulation and the location of the two sugar factories.	15
Figure 4: Map showing the locations of sugar beet fields for which data were collected in the survey of 2020 ..	16
Figure 5: Map showing the location and the BYV contamination category from the survey in 2020.	20
Figure 6: Soil moisture content and hydraulic conductivity plotted against the pressure heads.	24
Figure 7: Simulated and observed evapotranspiration at Reckenholz.....	25
Figure 8: Simulated and observed (red) soil moisture contents at Reckenholz.....	26
Figure 9: Map showing Willmott's Index of Agreement values (d) for all examined locations.....	28
Figure 10: Boxplot showing the calculated values for Willmott's Index of Agreement per crop parameter set. ..	29
Figure 11: Boxplot difference between observed and simulated yield (2020).	30
Figure 12: Map showing the mean absolute error (mae) for all examined fields (2020)	31
Figure 13: Boxplot showing the difference between observed and simulated yield (2020).....	32
Figure 14: Scatterplot with the observed yield simulated yield per BYV category	33
Figure 15: Violin plots showing the statistical distribution of selected meteorological variables	34
Figure 16: Pearson's correlation coefficient (R) for observed sugar beet yield and various vegetation indices ...	35
Figure 17: Feature importance derived from the initial random forest model.....	36
Figure 18: Confusion matrices for the three random forest models	37

List of Tables

Table 1: Meteorological variables required in WOFOST.....	10
Table 2: Meteorological parameters obtained from IDAWEB and used for crop simulations	13
Table 3: Meteorological parameters obtained from MeteoSwiss spatial climate analyses dataset.....	16
Table 4: Soil properties of the soil in the lysimeter systems	19
Table 5: Van Genuchten-Mualem parameters for the Grafenried soil at Reckenholz	23
Table 6: Willmott's Index of Agreement values (d) for all examined locations (1990-2022)	27

1 Introduction

In Chapter 5 of the Sixth Assessment Report from the Intergovernmental Panel on Climate Change (IPCC), Working Group II summarises the scientific literature regarding the "past, current, and future climate change effects on managed ecosystems that provide provisioning and cultural services" (Bezner Kerr et al., 2022: 720). Regarding the observation of climate change effects, the authors state with high confidence that climate change has led to mostly adverse impacts on crop yields (Bezner Kerr et al., 2022: 724). For example, studies (Challinor et al., 2014; D. Shindell et al., 2019; D. T. Shindell, 2016) have identified and calculated the size of yield losses due to increased temperatures caused by anthropogenic emissions of greenhouse gases (GHG) in the past. Similarly, Mulla et al. (2020) state that current climate models "predict an increase of global warming leading to exposure of major crops to temperature stress and a decrease of yields of an uncertain magnitude for every region" (Mulla et al., 2020: 424). While it is evident that these climatic changes will impact agricultural ecosystems, Henne et al. (2018) stress that an agricultural ecosystem's yield production depends on various other factors (e.g., management) besides climatic conditions. Therefore, it is difficult to identify and attribute climate change impacts on agricultural ecosystems in general.

In 2018, the National Centre for Climate Services (NCCS) of Switzerland published its "CH2018 – Technical Report" which contains detailed information and data about observed and projected climatic changes in Switzerland. This report clearly states that the temperatures in Switzerland in the 21st century will increase in all areas and every season. The magnitude of the temperature increase depends on the emission scenario (CH2018, 2018: 8). Additionally, climate change will influence current precipitation patterns, especially seasonal patterns and snowfall. Various studies investigated how these described climatic changes impact agriculture in Switzerland: Using the CH2018 climate scenario datasets (published by the NCCS), Tschurr et al. (2020) found that projected increases in temperature will prolong the growing season. This is especially the case in the Alpine region (Rammig et al., 2010). While a prolonged growing season could benefit crop production, the frequency and intensity of droughts will also increase, which is why "... Switzerland's climate will become rougher and more challenging" (Tschurr et al., 2022: 19) for agriculture. Furthermore, a study analysing the impact of climate change on grain maize production in Switzerland found that increased temperatures could benefit grain maize production but that an increased drought risk could offset these effects (Holzkämper et al., 2013). Additionally, a study found "an increasing likelihood of climatic

extremes” (Fuhrer et al., 2006), which will increase the risk for agricultural production (Brönnimann et al., 2014).

In 2012, a study aimed at assessing the impact of climate change on the yield of four different crop types cultivated in Europe by using a cropping simulation model (WOFOST), historic crop and weather data, and data from a global climate model (GCM). Switzerland was not part of the study area. Nevertheless, the results from the crop simulations for the regions close to Switzerland (e.g. South Germany and Eastern France) show that depending on the time and the emission scenario, the potential impact of climate change on sugar beet yields can either be positive or negative (Supit et al., 2012). Similarly, a study conducted in Germany found that due to increasing temperatures, sugar beets can be planted earlier in the year, which could potentially lead to an increase in produced yield (Kremer, 2017).

Sugar beets are predominantly cultivated in the region of the Swiss plateau. Two factories in Switzerland process the harvested sugar beet plants. One factory is located in Aarberg in the Seeland region; the other is situated in Frauenfeld in the northeastern part of Switzerland. In their publication about sugar beet production in Switzerland, the Federal Statistical Office (FSO) shows that the share of land used to produce sugar beets is highest in areas close to either one of the two sugar factories (Bundesamt für Statistik, 2020: 2). In total, approximately 1.8% of usable arable land in Switzerland is used to produce sugar beets (Bundesamt für Statistik, 2020: 1). In 2017, 72% of consumed sugar was produced in Switzerland (Bundesamt für Statistik, 2020: 1). In Switzerland, sugar is classified as a “basic supply good” which is why its production is subsidised by the Federal Government (Bundesamt für Statistik, 2020: 2). As described at the beginning of the chapter, climate change will affect agricultural systems in Switzerland (increasing temperatures and changes in precipitation patterns). Given its importance in agricultural production and food supply, assessing potential climate change impacts on sugar beet production in Switzerland is consequently relevant.

The impact of climatic changes like increasing temperatures and changes in precipitation on agricultural production depends on the crop and the location (Imtiaz Safa and Shahid, 2024: 287). Therefore, Mulla et al. (2020) state that cropping simulation models are useful for analysing the potential impacts of climate change on agricultural production, as they can include local climatic conditions, soil parameters and agricultural practices. Cropping simulation models have evolved in recent years and find a wide range of applicability, like climate change and adaptation, food security, policy assessment or farmer advice (Holzworth et al., 2015: 277).

For example, the CropSyst crop model was used in a study to identify climate change adaptation measures for agricultural practices in western Switzerland (Klein et al., 2014). Another study used the WOFOST cropping simulation model from Wageningen University to assess climate change's impact on winter wheat production in Switzerland as well as to investigate if the WOFOST cropping simulation model is suitable for simulating winter wheat production in Switzerland (Conway et al., 2023).

WOFOST is a cropping simulation model developed in the 1980s that is used in the MARS Crop Yield Forecasting System (M-CYFS) to create crop yield forecasts for member states of the European Union since 1993 (Lecerf et al., 2019: 192). WOFOST has been used in various studies for crop yield forecasts (A. De Wit et al., 2010; Lecerf et al., 2019), to assess climate change effects on crop yields (Bassu et al., 2014; Supit et al., 2012) or in combination with remote sensing data (Curnel et al., 2011; Huang et al., 2019). WOFOST can be used to simulate various crops. One or multiple calibrated crop files containing crop parameters are available for each crop. Most of the calibrated crop parameter sets were developed in a study by Boons-Prins et al. (1993). For sugar beet, four crop parameter sets exist that are ready to use and cover the area of Western, Central, and South Europe. As the crop parameter sets were created on behalf of the Joint Research Centre of the Commission of the European Community, Switzerland was not included since it is not part of the European Union. Therefore, the first goal of this study is to evaluate whether the existing crop parameter sets in WOFOST are suitable to simulate the growth of sugar beets in Switzerland. To achieve this goal, the four sugar beet crop parameter sets will be used to simulate the growth of sugar beet for 20 different Swiss locations in a historic period ranging from 1990 to 2022. The simulated yield output from WOFOST will be compared to data about the actual sugar beet yield harvested by farmers to determine the accuracy of each crop parameter set.

As outlined above, even though crop simulation models can be useful for assessing crop growth in various climate conditions and locations, it is also important to consider their limitations. Here, it is helpful to consider the concept of three agricultural production levels proposed by van Ittersum & Rabbinge (1997): Agricultural production is ultimately the result of growth-defining, growth-limiting and growth-reducing factors (Rabbinge, 1993, as cited in van Ittersum & Rabbinge, 1997). Growth-defining factors are, for example, the climatic conditions, crop characteristics, location or sowing time. These factors determine the *potential production*. Under growth-limiting factors, the supply of water and nutrients is understood. Lastly, growth-reducing factors consist of various influences that reduce the growth of a plant, like pollutants

or diseases. Ultimately, the *actual production* depends on the water and nutrient supply and the presence of growth-reducing factors (van Ittersum & Rabbinge, 1997). In WOFOST, it is possible to simulate the potential production of a crop as well as the water-limited production. However, it is not possible to include nutrient supply or growth-reducing factors in the simulations (de Wit and Boogaard, 2024: 5).

In 2020, sugar beet production in Switzerland was affected by the Beet Yellow Virus (BYV): A study found that in some areas, up to 50% of sugar yield was lost due to the virus (Groux et al., 2021). In 2019, three neonicotinoid pesticides were banned in Switzerland. While pesticides could have been used in previous years to control the vectors that transmit the virus, this was no longer possible in 2020. The high number of diseased areas could also have been caused by high spring temperatures, resulting in an earlier and more numerous occurrence of vectors (Groux et al., 2021). Due to this significant occurrence of the BYV, a research group from Agroscope¹ surveyed over 1'000 sugar beet farmers in Switzerland. This survey collected the size and the location of sugar beet fields, the level of contamination by the virus yellows, the sowing date, and the resulting sugar beet yield. On the basis of this dataset, two different analysis were carried out in this thesis which will be described in the following.

The leaves of a sugar beet plant infected with the BYV begin to turn yellow approximately three weeks after the contamination by the vector and reach the maximum degree of yellow colour in the later stages of the phenological development (Hossain et al., 2021: 588). In general, remote sensing can identify such damages caused by diseases and pests. In fact, Zhang et al. (2019) define the following four categories of damages to plants that are detectable through remote sensing: Reduction of biomass/decrease of leaf area index, lesions or pustules due to infection, destruction of pigments systems and wilting (Zhang et al., 2019: 2). Using remote sensing data from Sentinel-2, Zheng et al. (2018) created a new multispectral index to identify yellow rust (a fungal disease) in winter wheat in China. Overall, the study found that the newly created red-edge disease stress index (REDSI) showed yellow rust classification accuracy of about 85%, which was higher compared to other common vegetation indices (Zheng et al., 2018). As the authors propose, it would be interesting to see whether the REDSI index is also suitable for identifying diseases of other cultivars. Therefore, this study will also use Sentinel-2 data to calculate the REDSI index for the sugar beet fields from the 2020 survey and compare the results with the farmers' assessment of the disease intensity. Additionally, the most common

¹ Swiss centre of excellence for agricultural research

vegetation indices will be calculated to find the index that best identifies the fields with high disease contamination.

As mentioned above, the exact amount of harvested sugar beet yield was collected for approximately 950 sugar beet fields in the 2020 survey among sugar beet farmers. The sugar beet fields cover the area of the Swiss plateau. Such detailed and regionally distributed yield data is very suitable for comparing the actual harvested yield with the simulated yield output from WOFOST. Therefore, for each of the fields with sugar beet yield data available from the survey, WOFOST will be used to simulate the growth of the sugar beet plants, and the resulting yield amount will be compared to the observed harvested yield.

This study can be divided into two parts: The first part consists of the WOFOST simulations. Here, simulations are carried out for a historical period (1990-2020) for 20 locations in Switzerland and for the year 2020 for approximately 950 different sugar beet fields in Switzerland. For the simulations, all four available crop parameter sets are used, and the results will be compared to identify the best suitable crop parameter set for Switzerland. The second part of this study contains the remote sensing analysis: In the first step, various vegetation indices (including REDSI proposed by Zheng et al. (2018)) will be calculated for every sugar beet field of the 2020 survey and for various time steps. Furthermore, the resulting index values will be compared to the harvested yield amount as well as to the farmers' assessment of virus intensity. Lastly, the two parts (WOFOST and remote sensing) will be combined: For fields with high virus contamination, WOFOST is expected to overestimate the yield, as it only simulates water-limited production and not the actual production that is reduced by the disease.

Chapter 2 describes the data and materials used. It contains descriptions about the use and functionality of the cropping simulation model WOFOST and the data used for the simulations. Additionally, the observed yield data that will be used to compare the simulation results is described. Lastly, the chapter includes descriptions about the data used for the remote sensing part. Chapter 3 contains the results for the different analyses and in Chapter 4 the results are discussed. Lastly, the most important findings of this study are summarised in Chapter 5.

2 Data and methods

The used data and methods are listed and described in this Chapter. There is a subchapter for every analysis, that contains detailed descriptions of the used data and the applied methods. Additionally, since the simulations with WOFOST are the main methodological part of this thesis, Chapter 2.1 contains a WOFOST model description.

2.1 WOFOST – Model description

This thesis uses the WOFOST cropping simulation model developed by Wageningen University. Generally, “WOFOST computes daily biomass accumulation and its distribution over crop organs during the growth period using a photosynthesis approach” (Boogaard et al., 2013, p. 131). More precisely, the crop processes simulated by WOFOST include phenological development, CO₂ assimilation, respiration, partitioning, leaf growth and senescence, stems and storage organs, roots, transpiration and soil moisture (A. de Wit et al., 2019). In WOFOST, a crop's dry matter formation relies on irradiation, temperature, and the crop characteristics defined in the crop parameter set. The daily dry matter formation is determined by the daily rate of CO₂ assimilation, calculated from “...the absorbed radiation and the photosynthesis-light response curve of individual leaves”(A. de Wit et al., 2019). Ultimately, the resultant dry matter is allocated to the various plant organs based on the crop's characteristics and current phenological development stage (A. de Wit et al., 2019).

As outlined in Chapter 1, WOFOST can be utilised to simulate the potential or water-limited production of one or multiple crops for specified locations. Meteorological data from these locations are needed to simulate the growth of certain crops at a given site. Table 1 presents the necessary meteorological variables in WOFOST, including the required units. In addition to meteorological conditions, specific soil parameters or agricultural management practices can also be included in the simulations.

Table 1: Meteorological variables required in WOFOST (table content from (A. de Wit, 2024))

Parameter	Description	Unit
TMAX	Daily maximum temperature	°C
TMIN	Daily minimum temperature	°C
VAP	Mean daily vapour pressure	hPa
WIND	Mean daily wind speed at 2 m above ground level	msec ⁻¹
RAIN	Precipitation (rainfall or water equivalent in case of snow or hail)	cmday ⁻¹
IRRAD	Daily global radiation	Jm ⁻² day ⁻¹
SNOWDEPTH	Depth of snow cover (optional)	cm

WOFOST was developed in the 1980s (de Wit et al., 2020: 1) and has since been utilised in various studies. Timsina et al. (2018) used WOFOST to simulate the potential yield for wheat in Bangladesh, Boogaard et al. (2013) estimated the yield of autumn-sown wheat in Europe with WOFOST, and Kulig et al. (2020) compared the potential and water-limited yields simulated with WOFOST for two potato cultivars in Poland. WOFOST is an open-source model (de Wit et al., 2019: 164). Since its first publication in the 1980s, WOFOST has undergone updates and improvements, which will be necessary in the future given the increasing demand to consider climate variability driven by climate change in crop simulations (A. de Wit et al., 2019). Specifically, concerning the impacts of climate change, Gilardelli et al. (2018) noted that cropping simulation models frequently fail to accurately account for extreme climate impacts on crop production. Their study compared WOFOST with a modified version of WOFOST created to account for extreme weather conditions and identified differences between the two versions through sensitivity analyses. Ultimately, they concluded that adjusting WOFOST to accommodate extreme climate conditions is important for forecasting crop yields (Gilardelli et al., 2018: 7). Such adaptations of WOFOST are only feasible due to the aforementioned open-source design of the model. Another benefit of using WOFOST is that it features a Python implementation called Python Crop Simulation Environment PCSE² (A. de Wit et al., 2019). With PCSE, large numbers of WOFOST simulations can be carried out.

As previously mentioned, WOFOST is continually being developed, which is why there is not one single model but a multitude of models. Each model is available in PCSE and can be selected to perform cropping simulations. The “Wofost72” model is the first basic crop model used to simulate the phenology of a crop, as well as its potential or water-limited production. This model does not consider the impact of CO₂, biomass reallocation, or nitrogen dynamics, and the water-limited model features a simple, so-called “classic” water balance, viewing the soil as a single layer. In “Wofost73”, it is possible to factor in CO₂ impact and biomass reallocation in the simulations. Additionally, a more complex water balance module that accommodates multi-layered soils can be utilised. Finally, “Wofost81” represents the latest WOFOST model, which allows for the inclusion of nitrogen dynamics in the simulation runs (A. de Wit, 2024a). In WOFOST, different calibrated crop parameter sets are available for various crops (A. de Wit, 2024b). Four different crop parameter sets exist for sugar beet. The parameters were calibrated for different geographical regions.

² Detailed information about PCSE is available at <https://pcse.readthedocs.io/en/stable/>

2.2 WOFOST simulations 1990-2022

The primary objective of this thesis is to assess which of the four sugar beet crop parameter sets available in WOFOST is most suitable for simulating the growth of sugar beet plants in Switzerland. As outlined in Chapter 1, the simulation results will be compared with actual harvested sugar beet yield data. Consequently, the spatial scope is confined to locations where sugar beet yield data is available for the period 1990-2022. Figure 1 shows the locations where sugar beet yield data is available for 1990-2022. It is essential to note that these locations do not represent sugar beet fields but rather the site of a MeteoSwiss measurement station. The sugar beet yield data is aggregated: for each MeteoSwiss measurement station, all sugar beet yields harvested within a 15 km radius of the measurement station were averaged. This resulted in 88 locations, predominantly situated in the Swiss Plateau (Figure 1).

Locations with sugar beet yield data

Number: 88

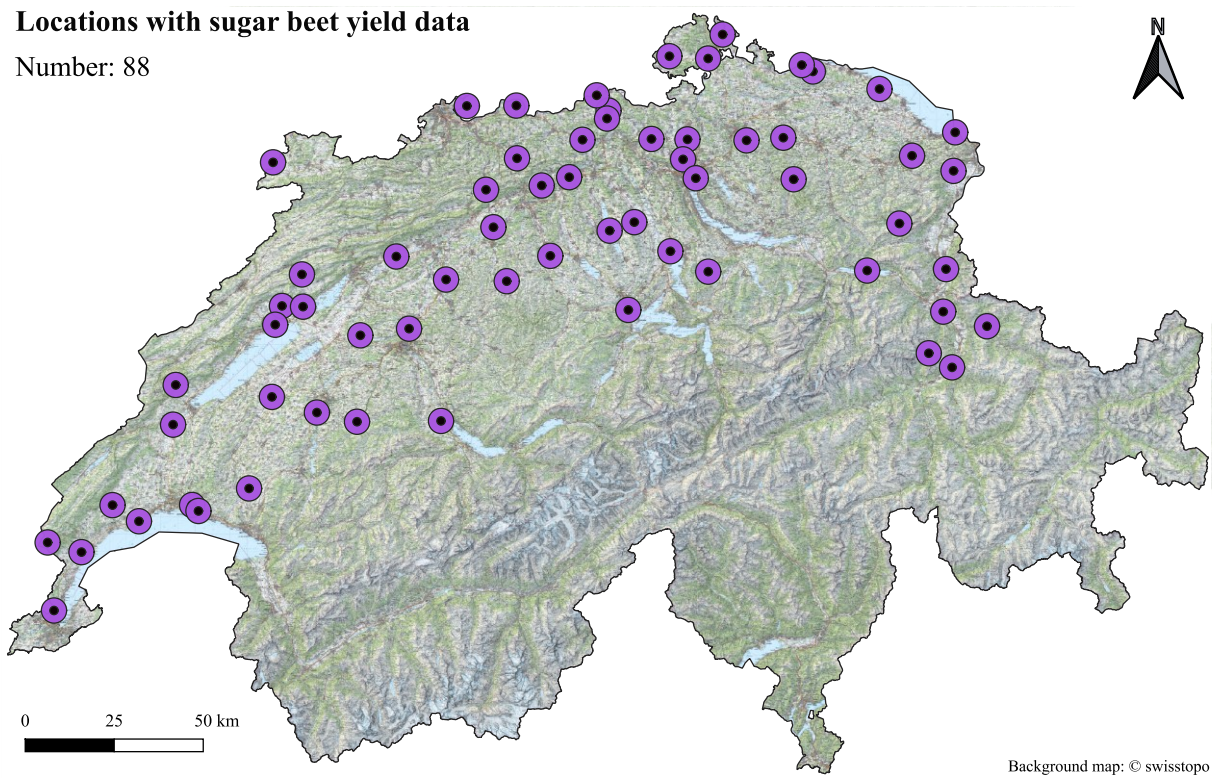


Figure 1: Map showing the locations with available sugar beet yield data in Switzerland

2.2.1 Meteorological data

As mentioned in Chapter 2.1, site-specific meteorological parameters are needed for the WOFOST simulations. Daily meteorological parameters can be accessed via the data portal “IDAweb” provided by MeteoSwiss. Table 2 displays each meteorological parameter required in WOFOST, along with the name, unit, and description of the corresponding parameter from IDAweb. A comparison of the units for the parameters needed in WOFOST and those provided

by IDAweb shows that the precipitation data obtained from IDAweb must be converted from mm to cm. Additionally, the radiation data was converted from Watts per square metre to Joules per square metre.

Table 2: Meteorological parameters obtained from IDAWEB and used for crop simulations

WOFOST parameter	IDAweb parameter	Unit	Description
TMAX	Maximum temperature	°C	Air temperature 2 m above ground; daily maximum
TMIN	Minimum temperature	°C	Air temperature 2 m above ground; daily minimum
VAP	Pressure	hPa	Vapour pressure 2 m above ground; daily mean
WIND	Wind	m/s	Wind speed scalar; daily mean
RAIN	Precipitation	mm	Precipitation; daily total 0 UTC – 0 UTC
IRRAD	Radiation	W/m ²	Global radiation; daily mean

Daily meteorological data records from 1990 to 2022 were available on IDAweb for 64 stations. Since meteorological data and sugar beet yield data are both necessary for the WOFOST simulation, only the stations for which both observations are available were selected. The selected locations are shown in Figure 2.

Locations with sugar beet yield and meteorological data from 1990-2022

Number: 38

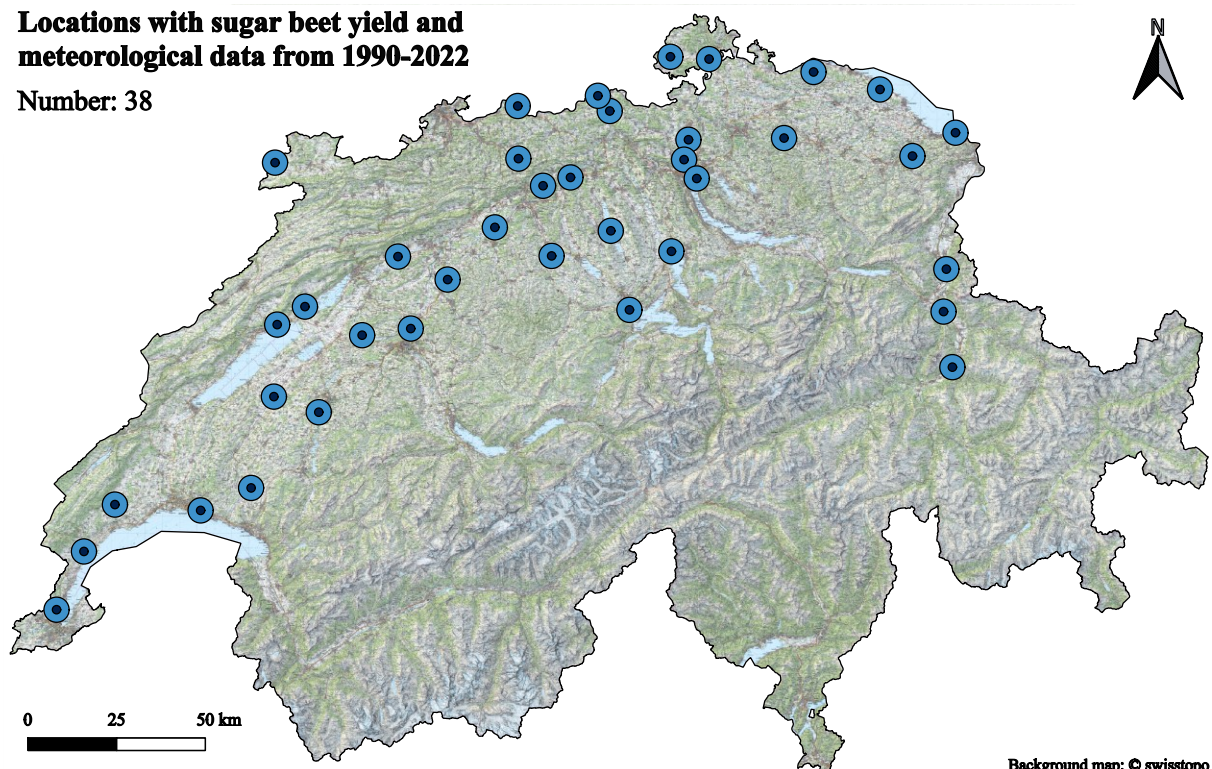


Figure 2: Map showing the locations with available sugar beet yield data and daily meteorological records for 1990-2022 in Switzerland

2.2.2 Soil parameter set and WOFOST model

WOFOST was run for all four different sugar beet crop parameter sets available in WOFOST, using the “EC3-medium fine” soil parameter set for each location. The EC3 soil parameter set is a standard parameter set from WOFOST, in the middle of a scale that ranges from EC1, which is suited for very coarse soils, to EC6, that is used for very fine and permeable soils. Since the yield data for each of the 38 stations are averages derived from multiple sugar beet fields with varying soil characteristics, the EC3 soil parameter set was selected as it represents average soil conditions. Given that site-specific soil conditions were unavailable and not included in the simulation, the WOFOST model “Wofost81_WLP_CWB” was used. This model simulates water-limited production through a classical water balance. As the sowing and harvest dates are unknown, typical sowing and harvest dates were set: the 30th of March was used for the sowing date, while the 30th of November was chosen for the harvest date. Finally, WOFOST was run without any additional agricultural management practices, such as irrigation or fertiliser application.

2.2.3 Yield comparison

WOFOST simulates the formation of a crop's dry matter. Consequently, the yield resulting from a simulation run represents only the crop's dry matter weight in tonnes per hectare. In contrast, the fresh weight of harvested and washed sugar beet plants measured in decitonnes per hectare were observed. Therefore, the observation data was converted from decitonnes per hectare to tonnes per hectare, as this is the standard unit for crop yields. Likewise, the simulated dry matter had to be converted to fresh weight to compare of the simulated output with the observations. A study conducted in New Zealand measured both the fresh weight of sugar beet plants and the dry matter percentages in an experimental setting. The findings indicated that, across different sugar beet varieties, the dry matter proportion was approximately 25% (Martin, 1980). Furthermore, researchers at Agroscope measured the dry matter content of sugar beet cultivated at Reckenholz in 2020, discovering a dry matter content of approximately 24.4%. For this reason, the simulated dry matter from WOFOST was divided by 0.244 to calculate the simulated fresh weight. Once the results for all stations and all years (1990-2022) were simulated and calculated, they were compared to the observations. For this comparison, Willmott's index of agreement d was used. The formula for calculating d is presented below, with P representing the observed data, O as the simulated data, and \bar{O} as the mean of the simulated data.

$$d = 1 - \frac{\sum_{i=1}^n (P_i - O_i)^2}{\sum_{i=1}^n (|P_i - \bar{O}| + |O_i - \bar{O}|)^2}$$

To calculate Willmott's Index of Agreement for a location, observations of sugar beet yield and meteorological data are required. For some locations, only a limited number of observations were available. To ensure data reliability, a filter was applied to include only those locations with more than five years of observations. Twenty locations met this criterion and were included in the analysis. As shown in Figure 3, these locations are distributed across the Swiss Plateau, mostly situated near one of the two sugar factories in Aarberg and Frauenfeld.

Locations WOFOST simulations 1990-2022

Number: 20

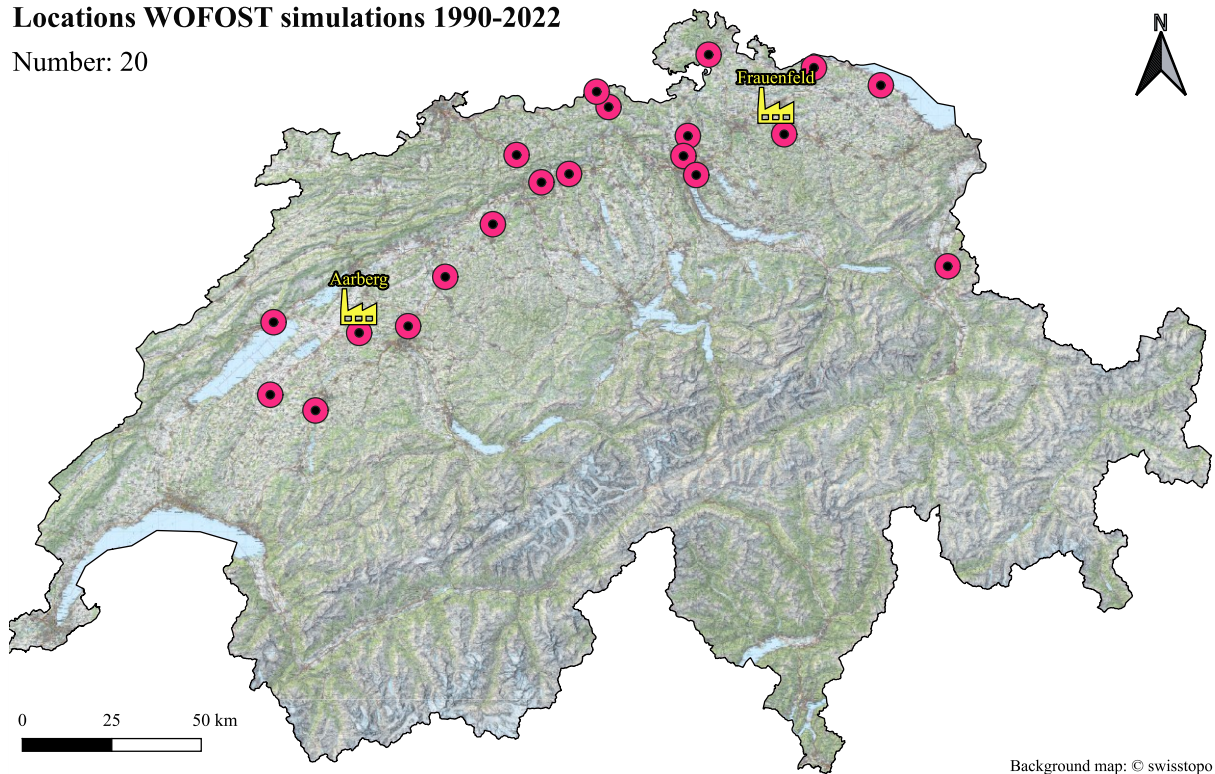


Figure 3: Map showing the locations used for WOFOST simulation and the location of the two sugar factories.

2.3 WOFOST simulations and remote sensing analysis in 2020

As described in Chapter 1, following an increase in sugar beet fields infected with the BYV in 2020, a research group from Agroscope conducted a survey among sugar beet farmers. In addition to information regarding the harvested sugar beet yield, the variety of sugar beet used, the sowing date, and the location of the field, farmers were also asked to estimate the level of BYV contamination per field on a scale from 1 (no contamination) to 4 (more than 50% of the field contaminated). Figure 4 shows the spatial distribution of the sugar beet fields for which data were collected in the 2020 survey. As can be seen, most sugar beet fields are situated in the area of the Swiss Plateau, with two clusters centred around the two sugar factories in Aarberg and Frauenfeld. This dataset will be used for WOFOST simulations on one hand and for calculating and analysing vegetation indices through remote sensing on the other hand.

Locations sugar beet fields from survey 2020

Number: 948

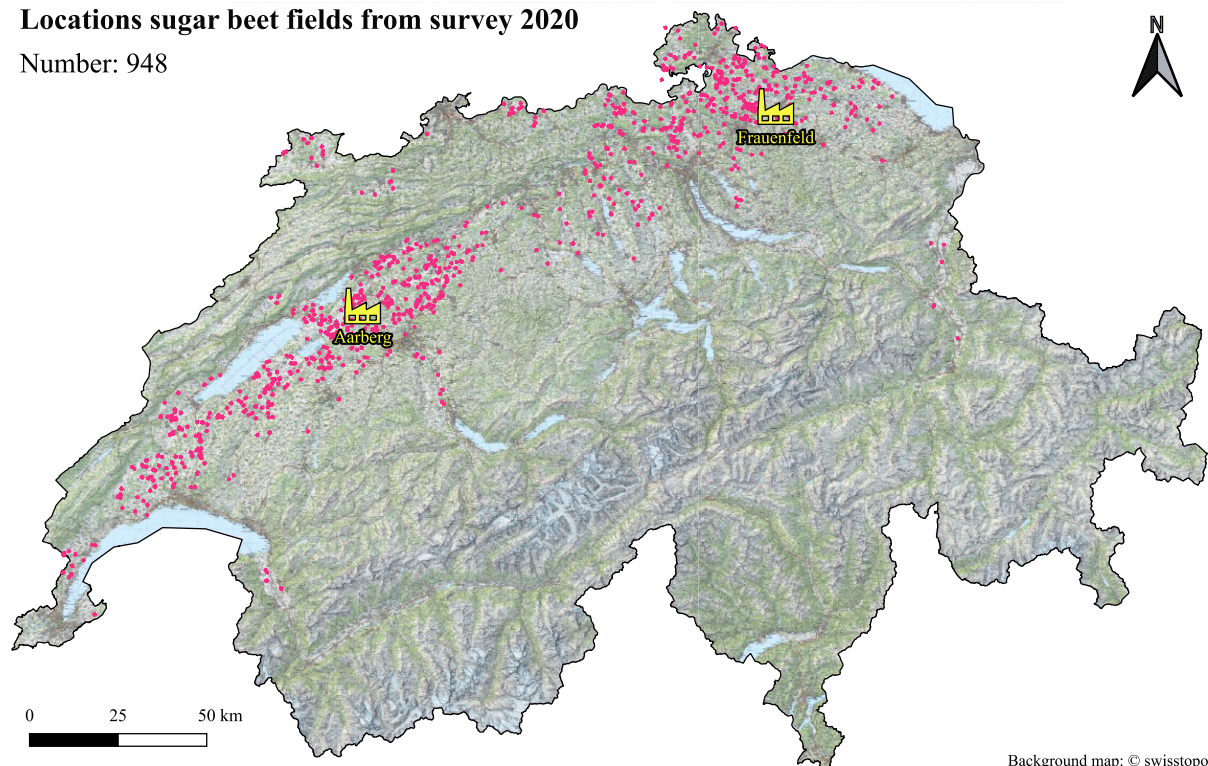


Figure 4: Map showing the locations of sugar beet fields for which data were collected in the survey of 2020

2.3.1 Meteorological data

To run WOFOST, meteorological input data is needed. As the dataset contains numerous sugar beet fields from various locations across Switzerland, meteorological records with a higher spatial resolution were used to include site-specific meteorological conditions. MeteoSwiss offers a range of datasets for climate analyses in Switzerland, featuring a grid size of 1 km. Table 3 summarises the datasets used in this thesis. Meteorological parameters from the nearest grid cell were extracted for each sugar beet field.

Table 3: Meteorological parameters obtained from MeteoSwiss spatial climate analyses dataset

WOFOST parameter	Dataset	Period	Grid	Unit	Description
TMAX	TmaxD	01.01.2020-31.12.2020	ch01.r.swiss.lv95	°C	Daily maximum temperature
TMIN	TminD	01.01.2020-31.12.2020	ch01.r.swiss.lv95	°C	Daily minimum temperature
RAIN	RhiresD	01.01.2020-31.12.2020	ch01.r.swiss.lv95	mm	Daily precipitation
IRRAD	SISD	01.01.2020-31.12.2020	ch01.r.swiss.lv95	W/m ²	Daily satellite-based global radiation

Such gridded datasets are not available for pressure and wind. Since pressure and wind records are needed for WOFOST simulations, these records were acquired from meteorological measurement stations via IDAWEB (following a similar procedure as described in Chapter 2.2). The pressure and wind records from the nearest meteorological measurement station were extracted for each sugar beet field.

2.3.2 Soil parameters

In addition to site-specific meteorological observations, WOFOST can also include site-specific soil conditions into the crop growth simulation. The Swiss Competence Center for Soil (KOBO) (2023) created models of soil property maps for Switzerland based on soil property measurements from the Swiss Soil Dataset (Service Center NABODAT, 2022). These maps are available for the entire area of Switzerland. Data regarding soil texture and organic carbon at three different depths can be exported from these soil property maps for each sugar beet field based on their coordinates. The soil texture data includes proportions of sand, clay, and silt. The exported data on soil texture and organic matter was used to develop a site-specific soil file that could ultimately be included in the WOFOST simulations. In the first step, the Van Genuchten-Mualem soil hydraulic parameters (Van Genuchten, 1980) were computed for each sugar beet field from the soil texture and organic matter data using two different pedotransfer functions (“PTF-01” and “PTF-02”) from the R package “euptf2” (Weber et al., 2020). Subsequently, the derived Van Genuchten-Mualem parameters were used to calculate soil moisture and hydraulic conductivity as a function of the hydraulic head. The “vangenuchten.py” Python script from WOFOST8.1 was then used to derive the following soil water retention and hydraulic conductivity parameters:

- ❖ Soil water retention:
 - Soil moisture at wilting point (SMW) [cm^3/cm^3]
 - Soil moisture at field capacity (SMFCF) [cm^3/cm^3]
 - Soil moisture at saturation (SM0) [cm^3/cm^3]
- ❖ Hydraulic conductivity:
 - Hydraulic conductivity of saturated soil (K0) [cm/day]

Finally, these calculated parameters were compiled into a soil file for the use in WOFOST. The sowing date for each field was derived from the survey data. As the harvesting date was not included in the survey, it was set to the 30th of November. Lastly, WOFOST was run without any additional agricultural management practices (e.g., irrigation or fertiliser application).

2.3.3 Yield comparison

To compare the simulated output with the observations, the simulated fresh weight was calculated by dividing the simulated dry matter amount by 0.244 (also see Chapter 2.2.3). Subsequently, the simulated fresh weight was compared to the observations by calculating the mean absolute error (MAE) for every sugar beet field. Furthermore, the aim was to include the information regarding the BYV contamination: Since WOFOST simulates only the water-limited production, potential yield-limiting factors such as pests and diseases are not taken into account. Consequently, WOFOST is anticipated to overestimate the sugar beet yield for fields with significant BYV contamination. To quantify the fit between the simulated and the observed sugar beet yield, the Willmott's Index of Agreement (see Chapter 2.2.3) and the PBIAS (percent bias) were calculated. The PBIAS is a metric used to quantify the performance of a model: Negative values indicate overestimation, positive values indicate underestimation, and 0 indicates an optimal match between observed and simulated values (Gupta et al., 1999). PBIAS can be calculated with the following formula:

$$PBIAS = \frac{\sum_{t=1}^N (q_t^{obs} - q_t^{sim})}{\sum_{t=1}^N (q_t^{obs})} \times 100\%$$

Finally, the difference between the simulated and observed yields was calculated. Additionally, the results were grouped by the degree of virus contamination. Ultimately, four groups resulted, for which the differences between simulated and observed yield were analysed.

2.4 Model evaluation with reference data from Reckenholz

In addition to evaluating the sugar beet yield estimation of WOFOST, it is also possible to analyse various other simulated parameters to assess the model's performance. Here, the limiting factor is the availability of observational data. At the Agroscope site in Reckenholz, Zurich, Agroscope operates lysimeter systems that measure the evapotranspiration and soil moisture content of fields where various crops are grown. For the years 2011, 2014, 2017, and 2020, daily records of evapotranspiration and soil moisture content for four different soil depths (10 cm, 30 cm, 60 cm, and 90 cm) from an area where sugar beets were grown were available and used to evaluate the simulation accuracy of evapotranspiration and soil moisture content in WOFOST.

The soil in the lysimeter systems used for this analysis was from Grafenried. Table 4 summarises the properties of the Grafenried soil. As outlined in Chapter 2.3.2, soil hydraulic parameters can be calculated from soil texture and organic content using pedotransfer functions.

Two different pedotransfer functions, namely “ptf 01” and “ptf 02”, from the “eupft2” r-Package (Weber et al., 2020) were used to derive the Van Genuchten-Mualem parameters. Similarly to the process previously described in Chapter 2.3.2, the derived Van Genuchten-Mualem parameters were used to calculate soil water retention and hydraulic conductivity parameters, which can ultimately be included in the WOFOST simulations. In addition to soil property parameters, WOFOST also needs meteorological data to simulate the growth of a crop (see Chapter 2.1). In this study, daily measurements of minimum and maximum temperature, pressure, wind, precipitation, and radiation were obtained from the automatic weather station at Reckenholz operated by MeteoSwiss.

Table 4: Soil properties of the soil in the lysimeter systems

Depth (upper) [mm]	Depth (lower) [mm]	Clay content [%]	Silt content [%]	Sand content [%]	pH content	Organic carbon content [%]
0	25	16	32	51	6.9	1.0
25	65	20	26	53	6.6	0.2
65	110	18	24	58	6.7	0.1
110	135	16	27	57	6.8	0.0

While the WOFOST simulations described in the previous chapters aimed to compare the simulated yield to the actual harvested yield, WOFOST was used here to assess the model’s performance in simulating evapotranspiration and soil moisture. Here, the WOFOST8.1 model with a classical water balance was used. The Van Genuchten-Mualem parameters were calculated from soil property data (Table 4). Ultimately, specific soil water retention and hydraulic conductivity parameters were used (these were again calculated using the “vanguenuchten.py” Python script from WOFOST8.1). The estimated evapotranspiration and soil moisture simulated by WOFOST were then compared with observations from the lysimeter data. To evaluate the models’ accuracy, the coefficient of determination (R^2), the root mean square error (RMSE), and the normalised root mean square error (NRMSE) were calculated for both evapotranspiration and soil moisture content. Additionally, Willmott’s index of agreement (see Chapter 2.2.3) was also calculated.

$$R^2 = 1 - \frac{\sum_{i=1}^n (y_i - \tilde{y}_i)^2}{\sum_{i=1}^n (y_i - \bar{y})^2}$$

$$RMSE = \sqrt{\frac{\sum_{i=1}^n (y_i - \tilde{y}_i)^2}{n}}$$

$$NRMSE = \frac{\sqrt{\frac{\sum_{i=1}^n (y_i - \tilde{y}_i)^2}{n}}}{\bar{y}_i} \times 100$$

2.5 Remote sensing data

This thesis aims to identify the differences between healthy sugar beet fields and those contaminated with the BYV through remote sensing (as described in Chapter 1). The location and severity of BYV contamination assessed by farmers for each field in the 2020 survey dataset are available. Figure 5 shows the spatial distribution of the sugar beet fields from which data were collected in the 2020 survey, as well as their BYV contamination category (from 1 to 4). Generally, it is observed that most fields with moderate or high BYV contamination are located in the western part of Switzerland. In contrast, the sugar beet fields in the northeastern region predominantly show no or low contamination.

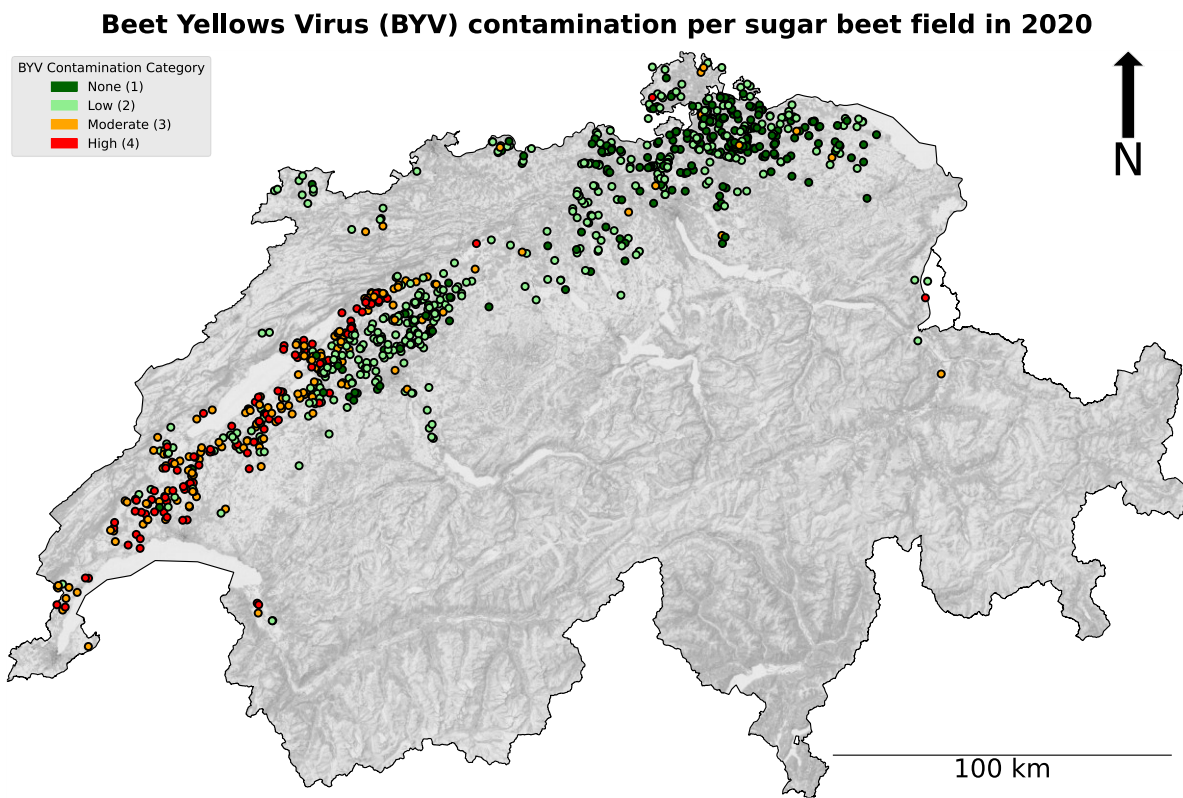


Figure 5: Map showing the location and the BYV contamination category for all sugar beet fields from the survey in 2020.

As outlined in Chapter 1, the reduced chlorophyll content of sugar beet leaves due to virus contamination could potentially be identified using vegetation indices. Many different vegetation indices exist, each possessing specific advantages or limitations in their application (Xue & Su, 2017). This analysis first examines which vegetation index is most suitable for identifying fields with higher virus contamination. Here, multispectral remote sensing data from

Sentinel-2 satellites (part of the Copernicus Programme from the European Space Agency) are ideally suited for vegetational and agricultural monitoring due to the presence of three red-edge bands essential for most vegetation indices (Phiri et al., 2020). Furthermore, the “rsi” R-package (Mahoney, 2025) facilitates the access, download, and processing of Sentinel-2 data in efficient manner, even for large calculations. It also includes the formulas for over 120 vegetation indices that can be computed from Sentinel-2 data. With the Copernicus Data Space Ecosystem Browser, it is possible to filter for dates with low cloud coverage. For the 2020 dataset, the Copernicus Data Space Ecosystem Browser was used to identify days with low cloud coverage to ensure clear remote sensing observations. Since the sugar beet plants were sown around the end of March and it takes time for the leaves to develop and be detectable through remote sensing, the earliest dates for the analysis were selected at the beginning of May. Available Sentinel-2 data, which covered nearly the entire area of Switzerland and exhibited minimal or no cloud coverage, were found for the following dates: 04.05.2020, 09.05.2020, 19.05.2020, 24.05.2020, 03.06.2020, 23.06.2020, 08.07.2020, 18.07.2020, and 07.08.2020. The available Sentinel-2 vegetation indices from the rsi-package were calculated for each date and sugar beet field. Ultimately, the calculated vegetation index values were compared to the farmers' assessments of BYV contamination to assess whether the vegetation index is suitable for detecting sugar beet fields infected with the BYV. Spearman's rank correlation coefficient was calculated for each vegetation index. Since the harvest yield amount was also collected in the survey, an additional regression analysis was carried out between the yield and each vegetation index. Here, Pearson's correlation coefficient was used to calculate the correlation between each vegetation index (independent variable) and the harvest sugar beet yield (dependent variable) as proposed by Bao et al. (2024).

Additionally, a random forest modelling approach was used to classify sugar beet fields as “healthy” (indicating no BYV contamination) or “ill” (BYV contaminated) based on vegetation index values derived from remote sensing. The workflow was modelled after Nguyen et al. (2021), where a machine learning pipeline was used to evaluate results from different vegetation indices calculated from hyperspectral images of healthy and virus-infected grapevine leaves. The random forest classification was performed with the Scikit-learn library in Python 3.10. The vegetation indices data from 08.07.2020 were used in this analysis since BYV contamination effects were expected to be highest in July. In the first step, a random forest model was set up for the calculated index values from all 101 examined vegetation indices to perform a 5-fold cross-validation. The vegetation indices were used as the predictor variables,

while the BYV contamination categories 1 and 2 were combined into a single class (coded as 0 representing “healthy” fields), and categories 3 and 4 were grouped into another class (coded as 1 indicating “ill” fields). The virus contamination category represents the target variable.

From the first model’s prediction, the most important predicting features were identified. In the second step, these ten most important predicting features were used to train a new random forest model. Lastly, a third random forest model was set up, using only the most predicting feature identified in the initial model. With the aim of improving the models' performance, the following hyperparameters were tuned using the `RandomizedSearchCV` class from the `sklearn` package: the number of trees (`n_estimators`), maximum depth (`max_depth`), minimum samples required to split an internal node (`min_samples_split`), minimum samples required at leaf node (`min_samples_leaf`), maximum number of features (`max_features`), bootstrap sampling (`bootstrap`) and class weights (`class_weight`). The performance of the models was evaluated based on the cross-validation accuracy and the classification reports.

3 Results

This chapter contains the obtained results. First, Chapter 3.1 presents the results from the WOFOST evaluation at Reckenholz regarding evapotranspiration and soil moisture. Afterwards, the results from the WOFOST simulations for the historical period 1990-2022 (Chapter 3.2) and the year 2020 (Chapter 3.3) are described. Lastly, Chapter 3.4 contains the results from the remote sensing analysis.

3.1 WOFOST evaluation at Reckenholz

This chapter presents the results from the WOFOST simulations at Reckenholz. As outlined in Chapter 2.4, WOFOST simulations were run for the years 2011, 2014, 2017, and 2020 using daily meteorological observations as well as specific soil parameters as inputs. The Van Genuchten-Mualem parameters (Table 5) were estimated from measured soil texture data using the “eupft2”-pedotransfer functions (Weber et al., 2020) to calculate soil water retention and hydraulic conductivity curves. Here, the resulting soil water retention and hydraulic conductivity curves for the two pedotransfer functions (PTF-01 and PTF-02) are presented. Additionally, the next two subchapters include the results of the comparison between the simulated and observed evapotranspiration and soil moisture content.

Table 5: Van Genuchten-Mualem parameters for the Grafenried soil at Reckenholz calculated with two pedotransfer functions

Pedo-transfer function	Soil layer [cm]	θ_r (Residual Water content) [cm ³ cm ⁻³]	θ_s (Saturated water content) [cm ³ cm ⁻³]	α (Inverse Air-Entry suction) [cm ⁻¹]	L (Mualem's pore-connectivity parameter)	n (pore-size distribution parameter)	K_s (Saturated hydraulic conductivity) [cmd ⁻¹]
PTF-01	0-25	0.005	0.460	0.061	-3.324	1.214	38.483
PTF-01	25-65	0.000	0.360	0.046	-1.638	1.142	40.114
PTF-01	65-110	0.000	0.347	0.057	-2.747	1.127	53.939
PTF-01	110-120	0.000	0.328	0.035	-3.196	1.129	19.073
PTF-02	0-25	0.005	0.426	0.080	-3.051	1.195	42.012
PTF-02	25-65	0.036	0.351	0.045	-2.564	1.180	18.173
PTF-02	65-110	0.055	0.348	0.065	-3.196	1.169	14.915
PTF-02	110-120	0.041	0.348	0.012	-1.240	1.190	7.472

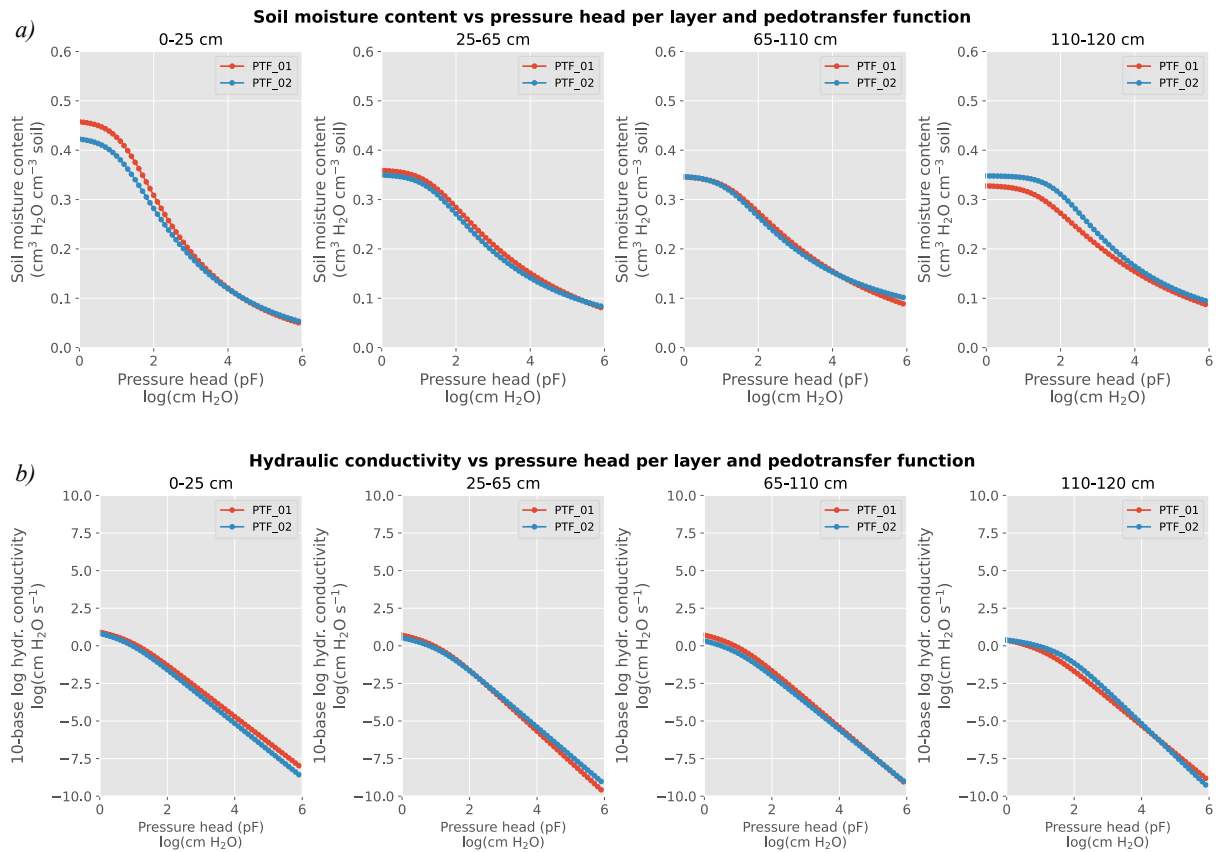


Figure 6: (a) Soil moisture content plotted against the pressure head for different soil depths (0-25 cm, 25-65 cm, 65-110 cm and 110-120 cm) and two pedotransfer functions (PTF 01 and PTF 02). (b) Hydraulic conductivity plotted against pressure the pressure head for different soil depths and two pedotransfer functions.

Figure 6a shows the water retention curves for the Grafenried soil at Reckenholz across four different soil depths (0-25 cm, 25-65 cm, 65-110 cm, and 110-120 cm). As previously described, two different pedotransfer functions were used: the results for PTF-01 are shown in red, while those for PTF-02 are shown in blue. Generally, the calculated soil-water retention curves follow a typical pattern for soils with varying pore sizes. Moreover, the results from the two different pedotransfer functions are similar, particularly for soil depths of 0-25 cm and 65-110 cm. Figure 6b indicates that hydraulic conductivity declines with an increasing pressure head across all soil depths. Here again, the findings from the two pedotransfer functions are similar, as both show a decrease in hydraulic conductivity with an increasing pressure head.

3.1.1 Evapotranspiration

The Van Genuchten-Mualem parameters calculated in the previous chapter were used to calculate soil property variables, which were ultimately used in the WOFOST simulation. As outlined in Chapter 2.4, the simulated evapotranspiration from WOFOST will be compared with the observations from the lysimeter systems at Reckenholz.

Figure 7 shows the daily observed and simulated amounts of evapotranspiration at Reckenholz for 2011, 2014, 2017, and 2020. Additionally, the selected statistical metrics used to quantify the relationship between the observed and simulated values are displayed in the upper left corner of each plot. In general, the simulated values follow the trend of the observed values, although the quantities are slightly lower. Consequently, the calculated PBIAS values are positive for all years, indicating that WOFOST underestimates the amount of evapotranspiration. While the coefficient of determination (R^2) ranges from 0.31 to 0.42 for 2011, 2014, and 2017, indicating weak model predictability, it reaches 0.69 for 2020, indicating improved model predictability. Similarly, Willmott's Index is highest for 2020, with lower values for the other years.

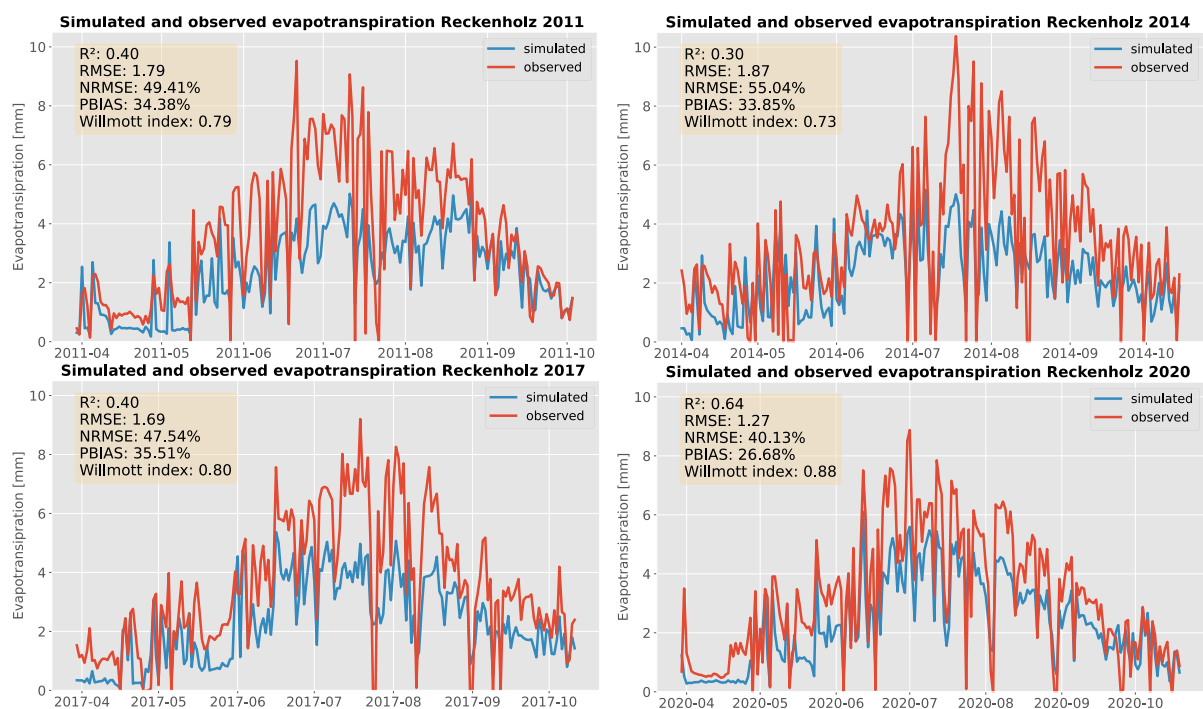


Figure 7: Simulated and observed evapotranspiration at Reckenholz in 2011 (upper left), 2014 (upper right), 2017 (lower left) and 2020 (lower right)

3.1.2 Soil moisture content

This chapter compares the observed soil moisture content from the lysimeter systems at Reckenholz with the simulated soil moisture content from WOFOST. Initially, WOFOST 8.1

was run using a classical water balance, using soil property variables derived from Van Genuchten-Mualem parameters calculated with pedotransfer functions PTF-01 and PTF-02. The daily soil moisture content simulated in WOFOST is shown in Figure 6 for PTF-01 (blue) and PTF-02 (violet), as well as the observed soil moisture values from the lysimeter systems at Reckenholz (red). Figure 8 includes the soil moisture values and the calculated statistical metrics for the relationship between the observed and simulated values for the years 2011 (upper left), 2014 (upper right), 2017 (lower left), and 2020 (lower right). Generally, the simulated soil moisture values are lower than the observed values, independent of the year and the used pedotransfer function. The positive PBIAS values indicate this as well. Regarding the simulated values, it can be observed that the simulated soil moisture values are lower with PTF-02 compared to PTF-01, consequently displaying higher PBIAS values, indicating greater underestimation. Similar to the comparison of evapotranspiration in the previous chapter, the fit between the observed and simulated values is best for 2020.

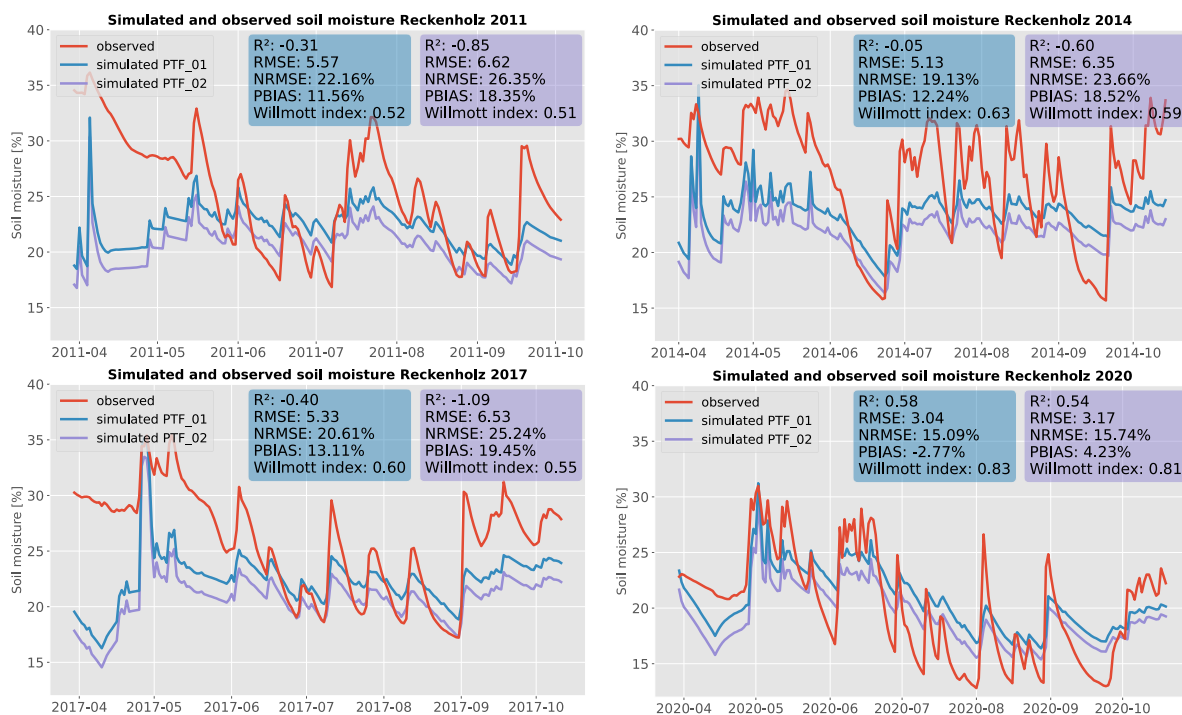


Figure 8: Simulated and observed (red) soil moisture contents at Reckenholz for PTF-01 (blue) and PTF-02 (violet) in 2011 (upper left), 2014 (upper right), 2017 (lower left) and 2020 (lower right)

3.2 WOFOST simulations 1990-2022

This chapter presents the results of the WOFOST simulations from 1990 to 2022 and compares them with observations. Chapter 2.2 provides detailed information about the data used and the WOFOST settings applied. The primary objective of this analysis is to identify which of the four available crop parameter sets is most suitable for estimating the harvested yield of sugar beet. To achieve this goal, Willmott’s Index of Agreement was calculated between the observed and simulated sugar beet yield for each location. For the simulated yield, four different crop parameter sets were used, leading to four different results, which are compared in this chapter.

Table 6 presents the calculated values of Willmott’s Index of Agreement for each location and crop parameter file. The highest value per location is highlighted in bold. For most locations, the Willmott’s Index of Agreement is highest for the crop parameter set “Sugar beet 601”, with declining d-values from crop parameter set “Sugar beet 601” to “Sugar beet 604”. The d-values show variability, with the lowest calculated d-value being 0.30 and the highest 0.83.

Table 6: Willmott’s Index of Agreement values (d) for all examined locations and the four crop parameter sets in WOFOST. Values in bold represent the highest value for the respective location.

Station	Sugar beet 601	Sugar beet 602	Sugar beet 603	Sugar beet 604
Aadorf / Tänikon	0.83	0.78	0.66	0.57
Bern / Zollikofen	0.67	0.67	0.64	0.59
Beznau	0.56	0.54	0.50	0.47
Buchs / Aarau	0.79	0.75	0.69	0.61
Fribourg / Grangeneuve	0.61	0.65	0.72	0.71
Gösgen	0.64	0.56	0.52	0.49
Güttingen	0.73	0.70	0.65	0.58
Koppigen	0.66	0.62	0.55	0.51
Leibstadt	0.62	0.56	0.51	0.45
Mühleberg	0.45	0.35	0.30	0.32
Neuchâtel	0.43	0.40	0.38	0.34
Payerne	0.47	0.46	0.42	0.38
Rünenberg	0.59	0.58	0.58	0.53
Salen-Reutenen	0.64	0.58	0.53	0.48
Schaffhausen	0.60	0.57	0.54	0.49
Vaduz	0.52	0.53	0.55	0.58
Wynau	0.64	0.64	0.61	0.56
Zürich / Affoltern	0.60	0.61	0.60	0.57
Zürich / Fluntern	0.72	0.72	0.71	0.64
Zürich / Kloten	0.65	0.64	0.62	0.55

Figure 9 shows the geographical distribution of the examined locations. The resulting d-values correspond to those displayed in Table 6, but only for the crop parameter set “Sugar beet 601”. The map shows that the three stations with the lowest d-values are situated in the western part of Switzerland, specifically in the Seeland region. Generally, the highest d-values are found in the northeastern part of Switzerland. The location "Aadorf/Tänikon," located in the Canton of Thurgau, reached the highest d-value with 0.83. The calculated d-values for the four locations between Bern and Olten all indicate very similar values, ranging from 0.64 to 0.67. Comparing the d-value for the location in Gösgen (0.64) with that of the location in Buchs/Aarau (0.79) reveals a difference of 0.15 despite the proximity of the locations to one another. Similar observations can be made for the three locations in Zurich, where the d-values range from 0.60 to 0.72.

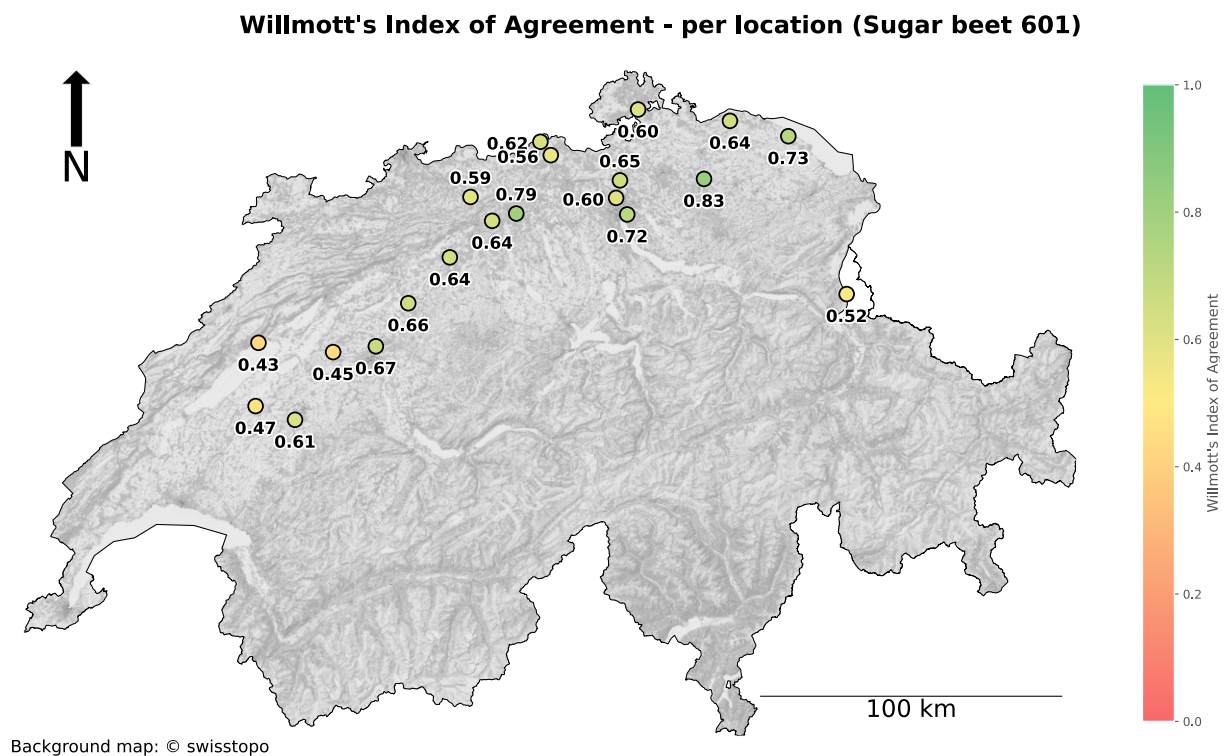


Figure 9: Map showing Willmott's Index of Agreement values (d) for all examined locations and the crop parameter set “Sugar beet 601”.

Lastly, Figure 10 shows the statistical distribution of the calculated d-values for each crop parameter set. The boxplot indicates that the median is highest for the crop parameter set “Sugarbeet 601.” Moving from “Sugarbeet 601” to “Sugarbeet 604,” the median decreases slightly from one crop parameter set to the next. While the first two crop parameter sets show higher values compared to the last two sets, their interquartile range (IQR) is greater, indicating larger variability.

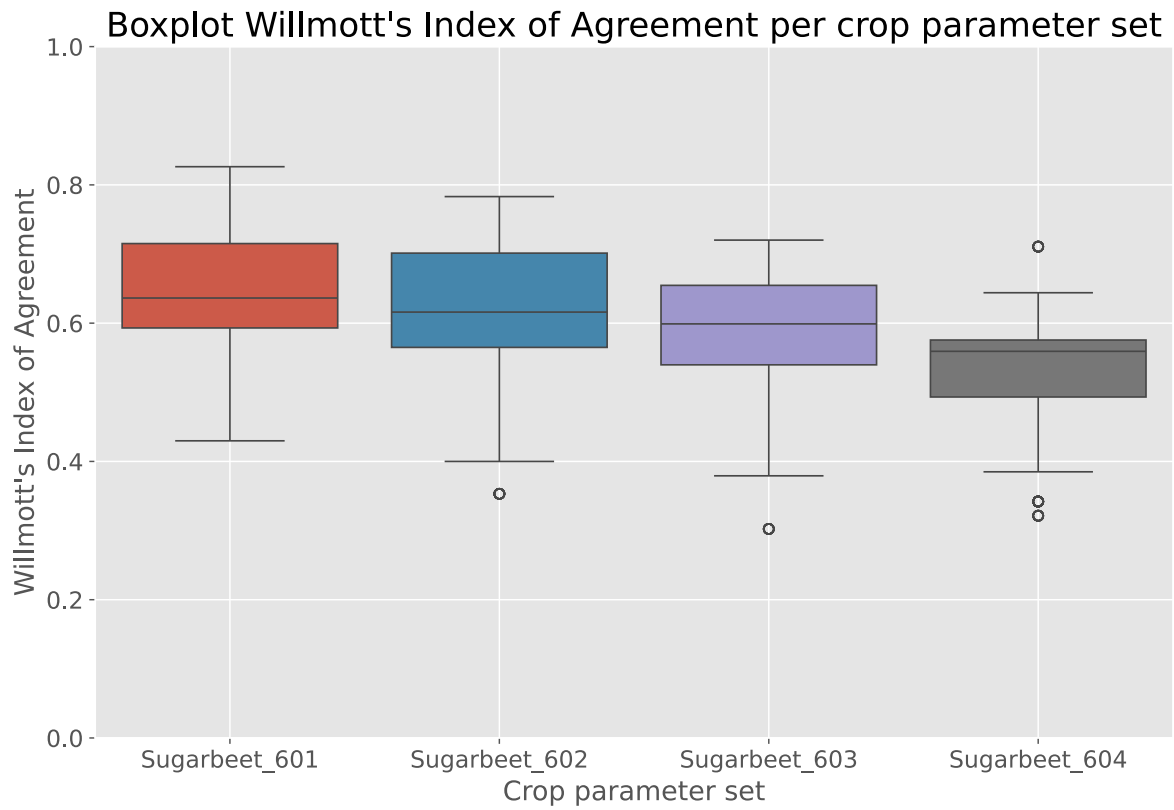


Figure 10: Boxplot showing the calculated values for Willmott's Index of Agreement per crop parameter set.

3.3 WOFOST simulations 2020

This chapter contains the WOFOST results generated based on the data collected in the survey about BYV contamination in 2020. Although preparing the meteorological data and calculating the soil parameters using pedotransfer functions for each of the 950 examined fields were complex and time-consuming, the results of these preparation steps are not included in this thesis due to the large volume of data. However, the detailed preparation steps are described in Chapters 2.3.1 and 2.3.2. In the first part of this chapter, the calculated Willmott's Index of Agreement values of the observed and simulated sugar beet yield will be presented, similar to the previous chapter. In the second part, the information about the BYV contamination will be included in the analysis of the results.

As described in Chapter 2.3, WOFOST was run for every sugar beet field using site-specific meteorological and soil property data. Additionally, similar to the data analysis in Chapter 3.2, the simulations were run using the four available crop parameter sets to ultimately identify the parameter set that yields the most accurate results. Figure 11 illustrates the statistical distribution of the difference between the observed and simulated yield across all examined fields, arranged by crop parameter set and applied pedotransfer function using a boxplot.

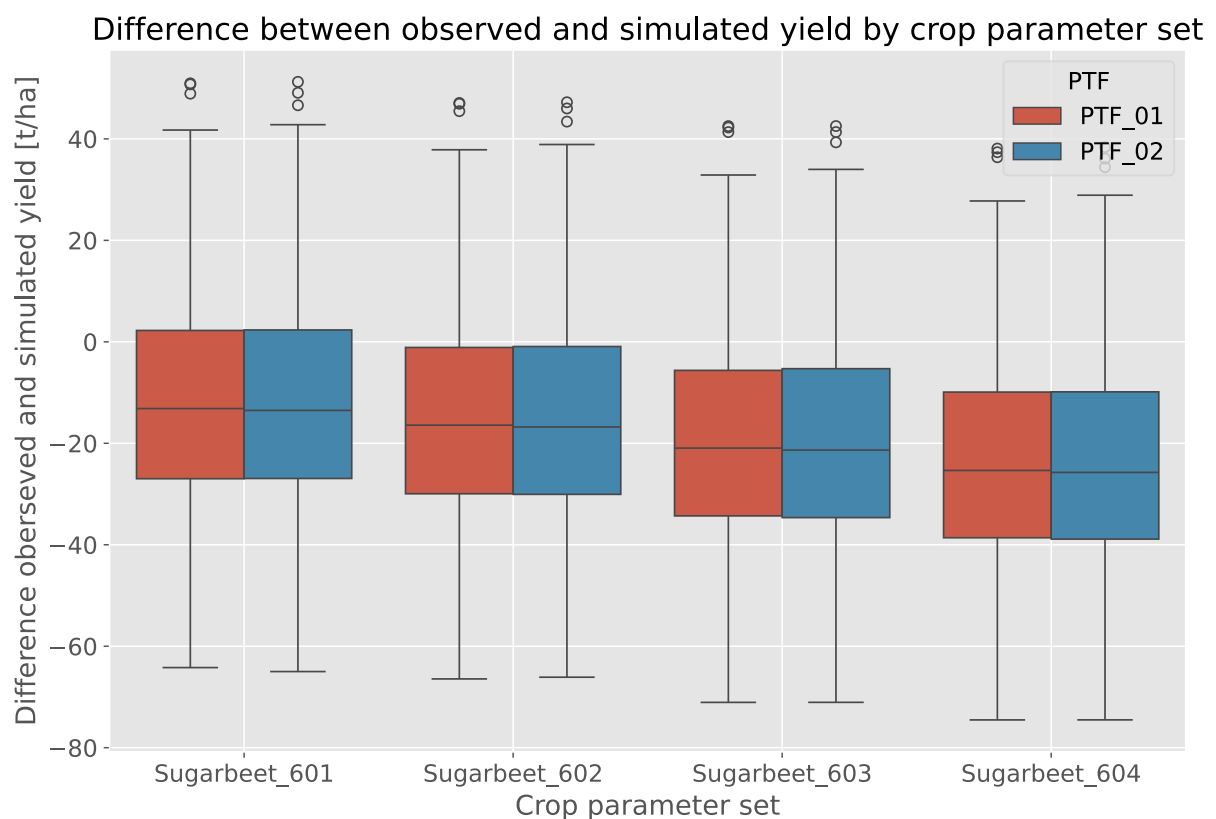


Figure 11: Boxplot showing the difference between observed and simulated amount of sugar beet yield per crop parameter set and pedotransfer function.

The results calculated for each crop parameter set derived from the two pedotransfer functions show almost no differences. In general, the median of every crop parameter set is negative, indicating that the model underestimates the actual yield. Additionally, the interquartile range and the extreme values show a large variability for all crop parameter sets. Again, the crop parameter set “Sugarbeet_601” shows the best results as its median is closest to 0. The underestimation increases from “Sugarbeet_601” to “Sugarbeet_604”.

As the crop parameter set “Sugarbeet_601” showed the most accurate results, Figure 12 presents a map displaying the mean absolute error between the observed yield and the yield simulated with the crop parameter set “Sugarbeet_601” for each examined sugar beet yield. While the results generally show high variability, a cluster with high mean absolute error values exists in the northeastern part of Switzerland. In the western part of Switzerland, lower mean absolute error values are observable.

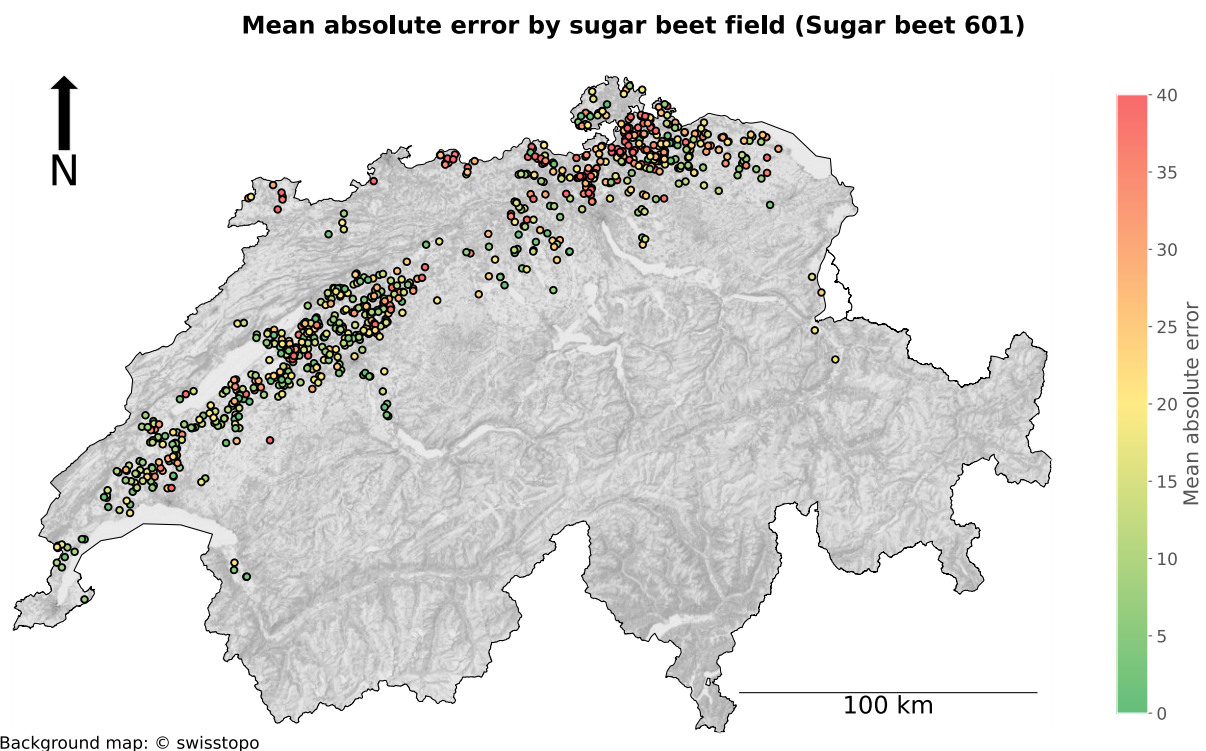


Figure 12: Map showing the mean absolute error (mae) for all examined fields and the crop parameter set “Sugar beet 601”. Numerous sugar beet fields were affected by BYV contamination in 2020. Data concerning the severity of BYV contamination (ranging from 1 “no contamination”, to 4 “more than 50% contaminated”) for each assessed field is available. In the initial step, the simulated sugar beet yields were classified according to their level of BYV contamination. Again, the difference between the observed and simulated output is of interest. Figure 13 shows the statistical distribution of the difference between the observed and simulated sugar beet yield per BYV

contamination category. Furthermore, the results for both pedotransfer functions are presented. Similar to the already discussed results presented in Figure 11, the results show a large variability and almost no differences between the two pedotransfer functions. However, clear differences can be observed in the results for BYV contamination categories 1 and 2 (none and low contamination) and 3 and 4 (medium to high contamination): While the median values for categories 1 and 2 lie at approximately -20 t/ha, indicating an underestimation of the model, it overestimates the yield for categories 3 and 4, with medians of approximately 1 and 10 respectively.

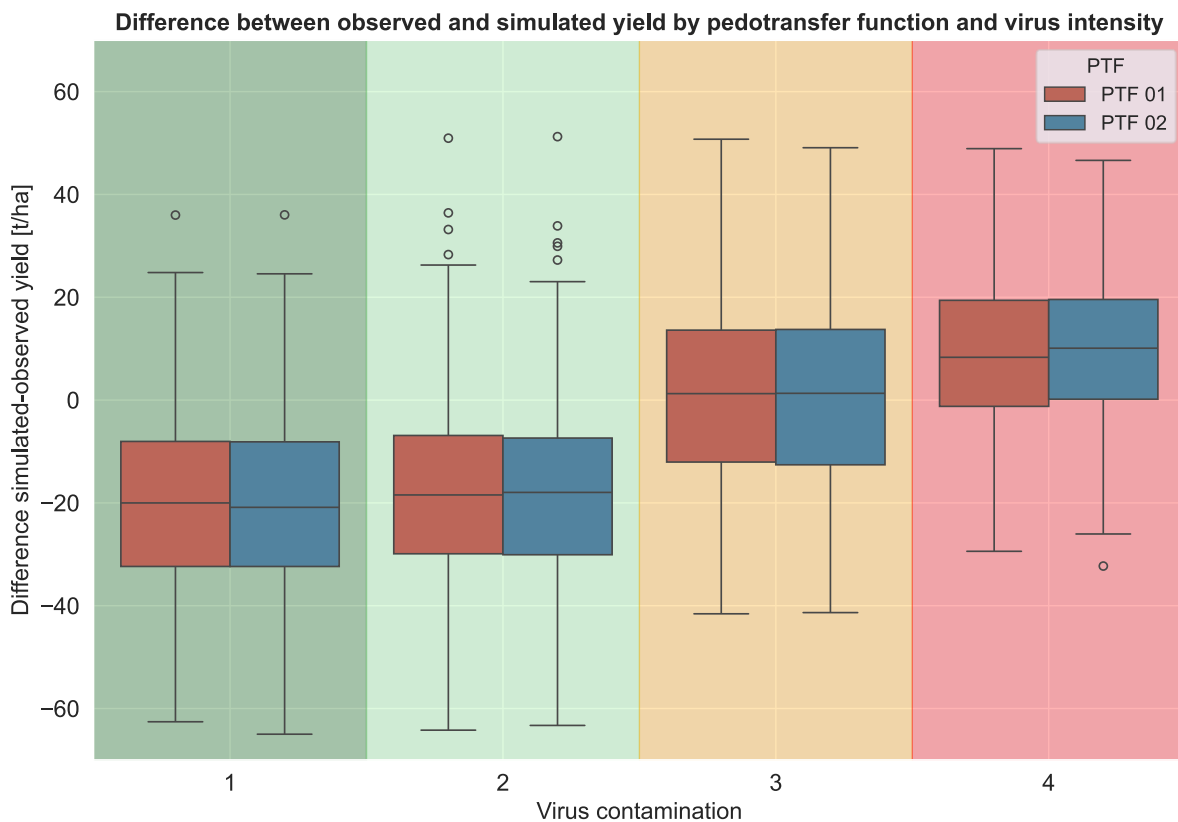


Figure 13: Boxplot showing the difference between observed and simulated amount of sugar beet yield per virus contamination category and used pedotransfer function for crop parameter set Sugarbeet_601.

In Chapter 2.5, it was shown that the four virus contamination categories are not evenly spatially distributed in Switzerland: Sugar beet fields with medium or high virus contamination were predominately located in the western part of Switzerland. In contrast, the majority of the sugar beet fields in the eastern part of Switzerland showed low or no virus contamination (Figure 5). Due to these regional differences, the calculated results were divided into a “west” and an “east” group. Again, the observed and the simulated amount of sugar beet yield were compared for each group. Figure 14 shows the relationship between the observed and simulated sugar beet yields for sugar beet fields in western (left) and northeastern Switzerland. As already

mentioned, the model generally underestimates the yield, which is also the case for both groups here, indicated by the positive PBIAS values. However, the underestimation is greater for the northeastern fields (23.41%) compared to the western fields (6.57%). Additionally, the Willmott's Index of Agreement for the northeastern fields is low (0.39), indicating weak model performance. In contrast, the Willmott's Index of Agreement for the western field is 0.68, indicating moderate to good model performance.

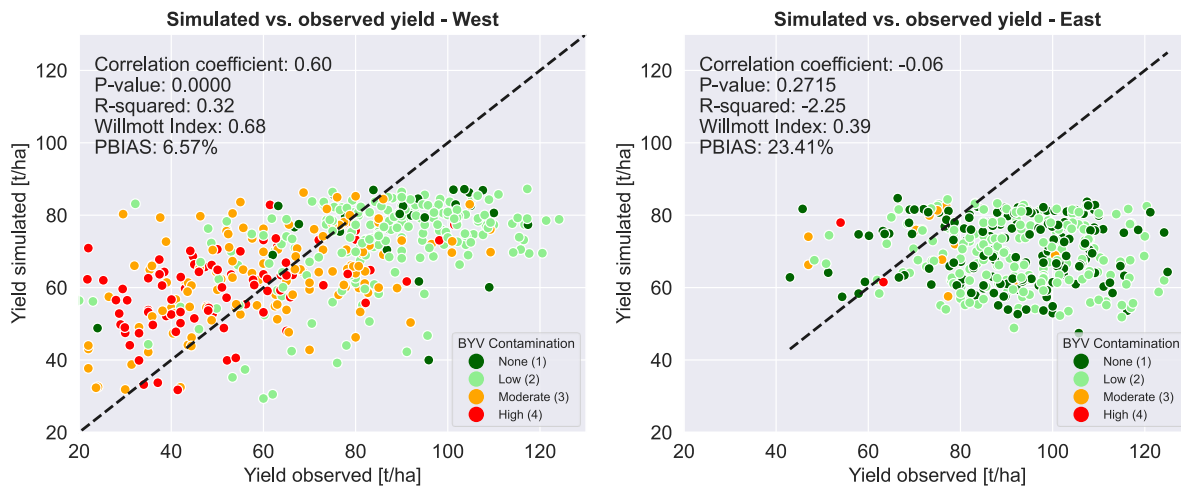


Figure 14: Scatterplot with the observed yield on the x-axis and the simulated yield on the y-axis for sugar beet field in western Switzerland (left) and northeastern Switzerland (right). The colour of each point indicates the level of BYV contamination.

Examining the distribution of BYV contamination in the western fields reveals that WOFOST projects fields with high BYV contamination (red points) to have slightly lower yields than other fields. Since WOFOST only simulates water-limited crop production and does not consider potential growth constraints due to pests, diseases, or viruses, lower simulated yields for fields with high virus contamination are surprising at first. However, these results indicate that specific meteorological and soil conditions (as these are the only inputs in WOFOST) are more likely to create an environment favouring BYV infections. Consequently, additional simulation results were analysed to identify stress factors in the growth process.

Four meteorological variables were exported from WOFOST, describing the meteorological conditions throughout the growing process of the sugar beet plants. The statistical distribution of these meteorological variables is shown in Figure 15 per virus contamination category. Figure 15a shows that the total amount of rainfall throughout the growing process is lowest in fields with no BYV contamination and highest in fields with high contamination. The same can be observed for the variable “number of days with water stress” (Figure 15b). However, the variability for fields with no BYV contamination is large, whereas fields with high BYV contamination show a smaller variability but higher overall values. Similarly, the variable

“Total evaporation from soil surface” (Figure 15c) shows the same trend, with increasing values from BYV contamination categories 1 to 4. In contrast, almost no differences between the BYV contamination categories are observable for the variable temperature sum (Figure 15d).

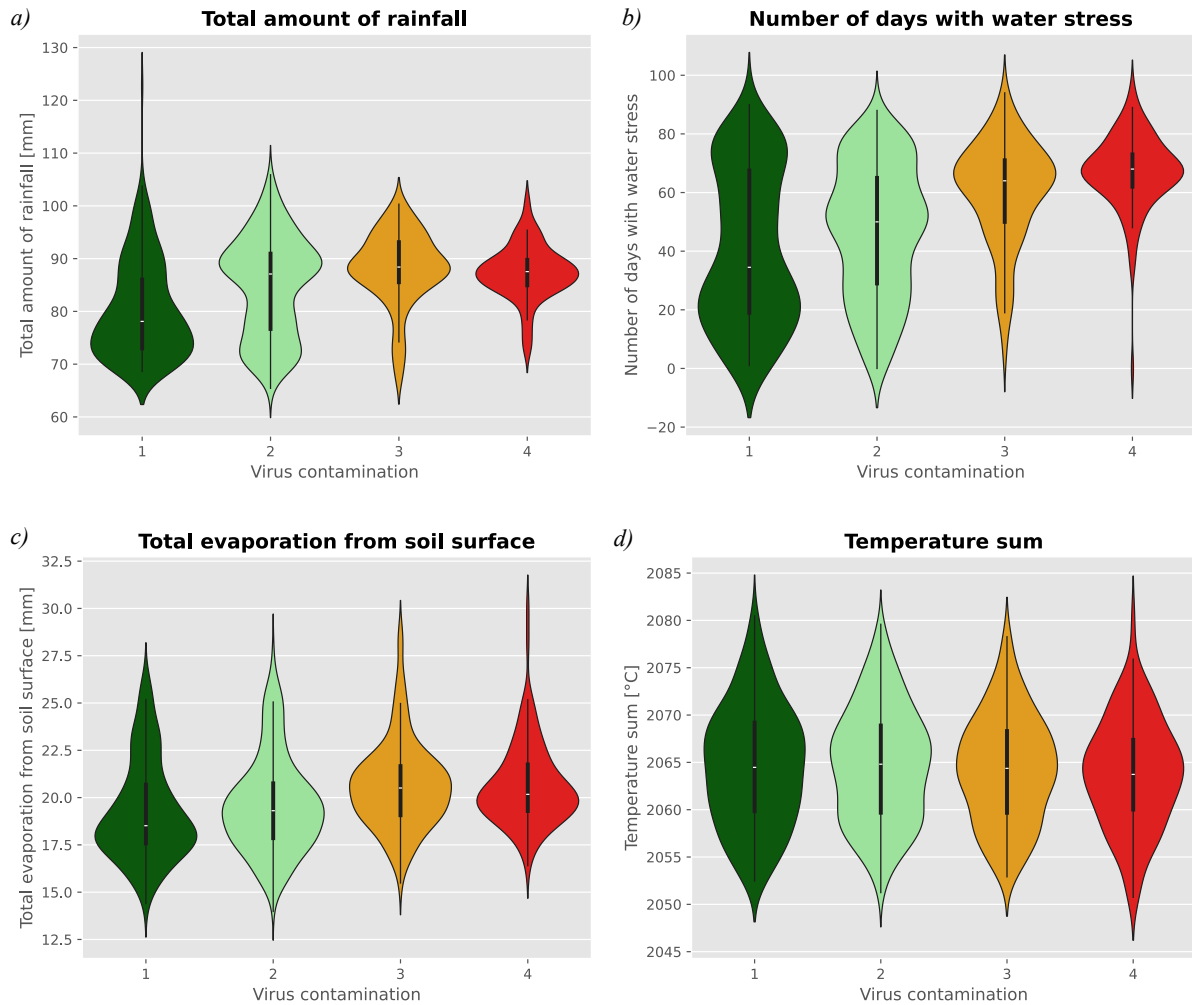


Figure 15: Violin plots showing the statistical distribution of selected meteorological variables per BYV contamination category for all examined western fields. Meteorological variables contains the total amount of rainfall (a), the number of days with water stress (b), the total amount of evaporation from soil surface (c) and the temperature sum (d).

3.4 Remote sensing results

To identify the vegetation index that correlates the strongest with the observed amount of harvest sugar beet yield, Pearson’s correlation coefficient was calculated. As outlined in Chapter 2.5, the vegetation indices were calculated for different days. For the correlation between the different vegetation indices and the harvested yield, it would be expected that the correlation would be the highest for vegetation indices calculated for days closest to the harvesting date. However, the highest correlation was between the vegetation indices and the harvested yield was calculated of the 8th of July. Therefore, this chapter presents the vegetation indices that were calculated for every examined sugar beet field on the 8th of July in 2020. Figure 16 contains the calculated Pearson’s correlation coefficients (R) with the amount of harvested sugar beet yield as the dependent variable and the values of each examined vegetation index as the independent variable. The highest calculated R-values resulted for the Chlorophyll Index Green (CIG), Simple Ration (SR2 800 and 550 nm) and the Green Ratio Vegetation Index (GRVI) with 0.71, indicating a moderate relationship. The Red-Edge Disease Stress Index (REDSI) showed the 26th best correlation coefficient. The results for all vegetation indices are listed in Annex B.

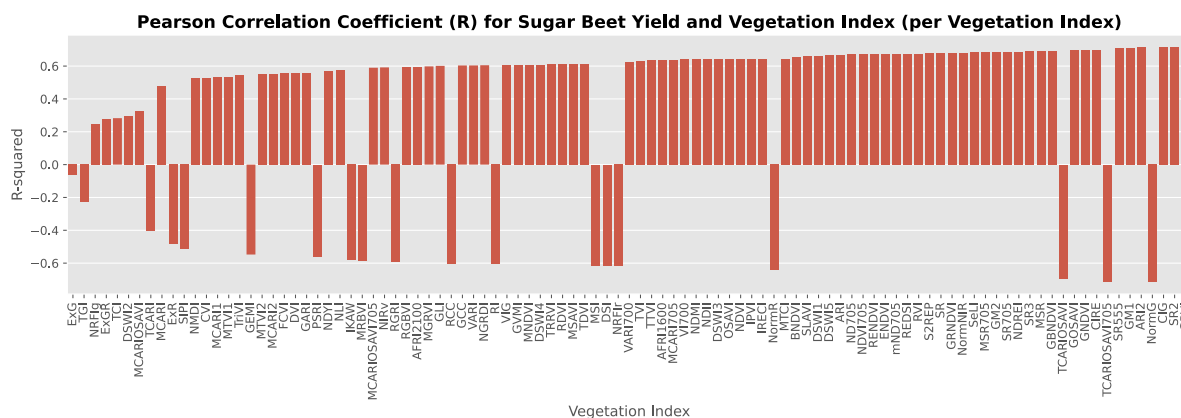


Figure 16: Pearson’s correlation coefficient (R) for observed sugar beet yield and various vegetation indices

To evaluate the relationship between each vegetation index and the BYV contamination severity estimated by the farmers that participated in the 2020 survey, Spearman’s rank correlation coefficient (ρ) was calculated. Here, again, the vegetation indices were calculated for the 8th of July in 2020. The complete table containing the results for all 101 examined vegetation indices can be found in Annex B. The Anthocyanin Reflectance Index (ARI) showed the highest correlation (-0.49), indicating a moderate relationship between the vegetation index and the BYV contamination categories. The differences between the calculated correlation coefficients are small. The REDSI showed a moderate Spearman’s correlation coefficient of 0.40.

As described in Chapter 2.5, the initial random forest model's most important features were identified and presented in Figure 17. Due to space constraints, this figure only displays the feature importance of the 20 most significant features. Eighty-one additional features were utilised in the first model but showed lesser feature importance. The second random forest model incorporated all predictive features above the red dashed line. The “Normalized Rapeseed Flowering Index Red” (NRFIr) was identified to be the most important feature in the initial model. Since the Anthocyanin Reflectance Index (ARI) was identified as the second most important feature, two additional random forest models were set up: One with the NRFIr as predictor and one with the ARI as predictor. Since the cross-validation accuracy, as well as the classification accuracy of the ARI model, was better, only this model was taken.

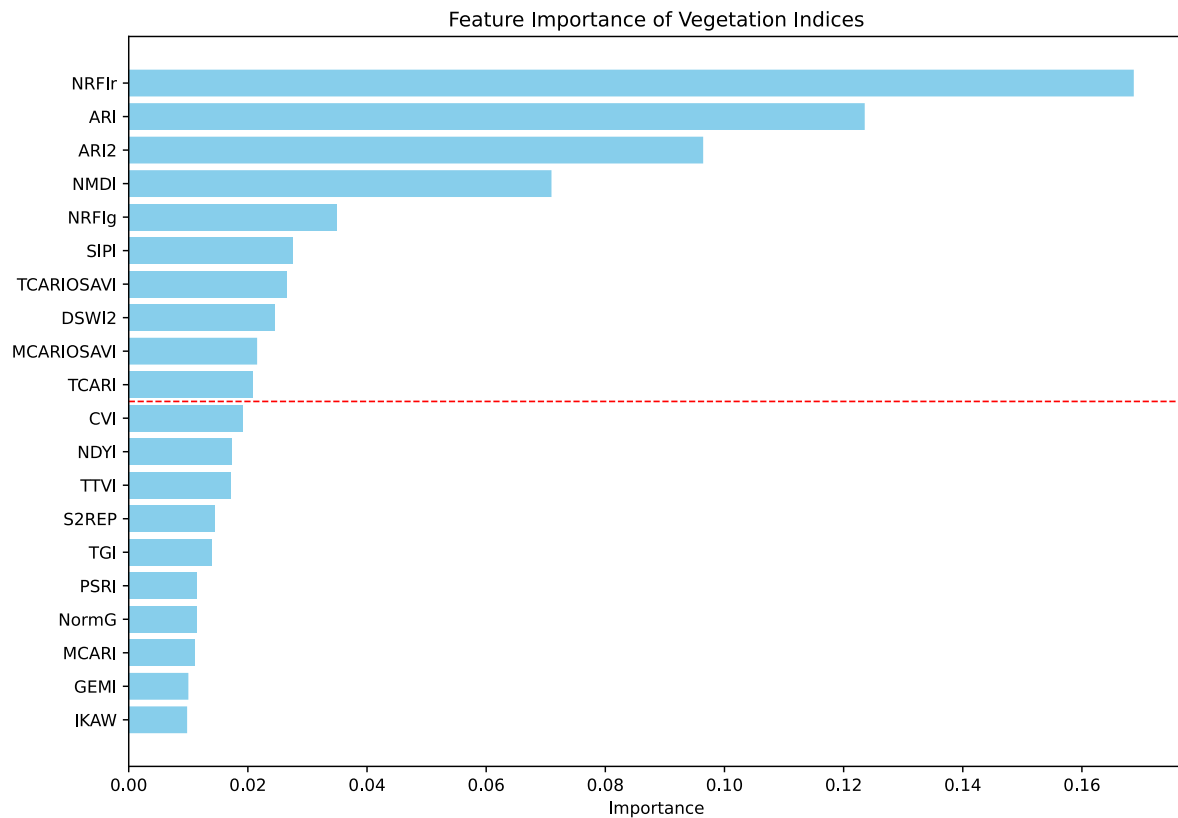


Figure 17: Feature importance derived from the initial random forest model.

The calculated cross-validation accuracy was 78% for the initial random forest model and 79% for the two model with 10 of the most important features as predictors. Finally, the model with only the vegetation index “ARI” as predictor showed a accuracy of 69% after cross-validation. Figure 18 shows the classification results of the three models in confusion matrices. The baseline model, with all vegetation indices, accurately identified 119 out of 135 as healthy, indicating that 88% of the healthy fields were correctly classified. However, only 24 out of a total of 47 ill fields were accurately classified (51%). The second model, which used the ten

most important vegetation indices, shows small improvement in the classification result for the ill fields (53% correctly classified) and slightly worse classification results for the healthy fields (85%). Lastly, the third model, based on the “ARI” vegetation index, classified only 77% of the healthy fields correctly but identified ill fields better (63%).

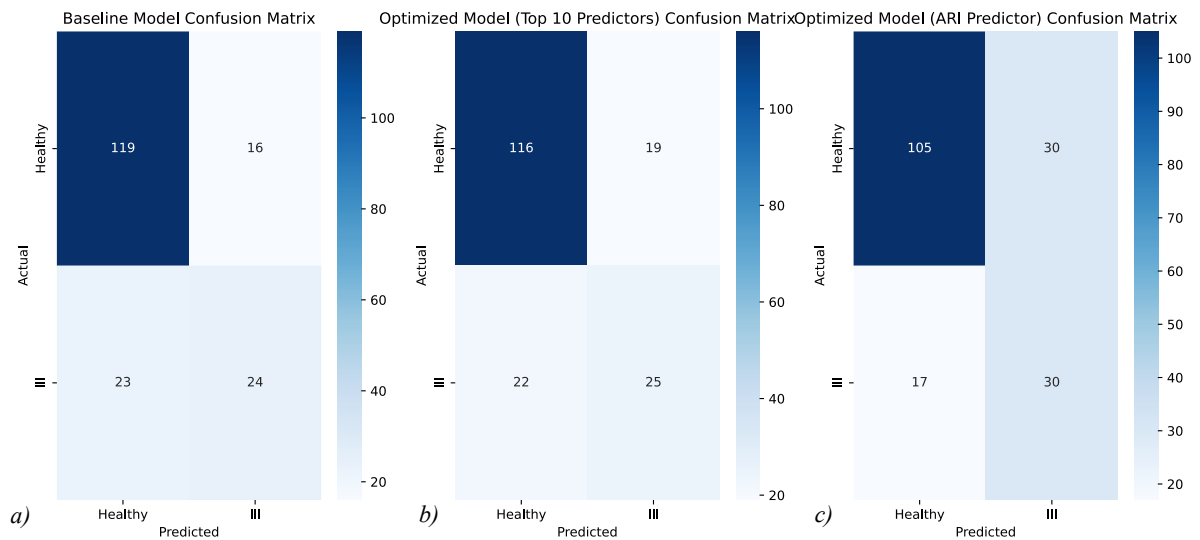


Figure 18: Confusion matrices for the three random forest models, utilising all vegetation indices (a), only the top ten vegetation indices (b), and the vegetation index “ARI” as a predictor feature.

4 Discussion

4.1 WOFOST simulations

The results of the WOFOST evaluation simulations at Reckenholz (see Chapter 3.1) showed that WOFOST underestimated the amount of evapotranspiration. The largest differences between the observations and the model's output occurred when the amount of observed evapotranspiration was high in summer. In 2020, the total observed evapotranspiration was lower than in the other years, resulting in less pronounced evapotranspiration amounts in summer. These findings suggest that WOFOST struggles to simulate high evapotranspiration amounts in summer when irradiance is high. Consequently, the statistical metrics (R^2 , RMSE, NRMSE) are worse for all years except 2020 compared to the findings of Dewenam et al. (2021). In their study, Dewenam et al. (2021) calibrated various crop parameters with data measured in the field, which could explain the better results. Contrarily, they found that WOFOST overestimated the amount of evapotranspiration. For soil moisture content, this study found that WOFOST underestimated the soil moisture content, which is in line with the findings of Dewenam et al. (2021). However, the statistical metrics are again worse than reported in Dewenam et al. (2021).

The results of the WOFOST simulations for the historical period 1990 to 2022 (Chapter 3.2) generally showed that the crop parameter set "SUG601" provided the best fit between the simulated and the observed amount of sugar beet yield. This finding is not surprising since this crop parameter set was calibrated for regions with similar climatic conditions as Switzerland. However, differences in the fit between the simulated and observed amount of sugar beet yield between the locations were identified. Three locations in western Switzerland (Neuchâtel, Payerne and Mühleberg) had notably low Willmott's Index of Agreement values, prompting further examination of why the fit for these locations was worse compared to the other stations. Therefore, the time series of simulated and observed sugar beet yield of these locations was studied (see Annex A). Comparing the results of the three locations showed that for the location "Mühleberg", only eleven years of observations were available (2010 to 2021). While the fit between the simulated and observed sugar beet yields is moderate for most years, WOFOST overestimates the sugar beet yield by approximately 20 t/ha (2016) and 30 t/ha (2021), which consequently leads to a comparably lower Willmott's Index of Agreement. Similarly, the results from the location "Payerne" also show that WOFOST overestimates the sugar beet yield in 2021 (by approx. 30 t/ha), 2016 (approx. 20 t/ha) and also for 2007 (approx. 30 t/ha). Since

WOFOST simulates water-limited production, factors such as diseases or pollutants could contribute to the lower observed sugar beet yields. In fact, it was stated in the “Agrarbericht 2021” that widespread leaf diseases in Western Switzerland reduced sugar beet production in 2021 (Bundesamt für Landwirtschaft, 2021). In contrast, in 2016, the “Agrarbericht 2016” reported that cold and wet conditions in spring, alongside hot and dry conditions in summer, led to decreased sugar beet production in that year (Bundesamt für Landwirtschaft, 2016). Here, it is surprising that WOFOST overestimates the sugar beet yield. Lastly, in 2007, WOFOST also overestimated the yield for the locations “Payerne” and “Neuchâtel”. Yield losses due to flooding in the area around Aarberg in Western Switzerland were reported in 2007 (Schweizerischer Verband der Zuckerrübenpflanzer, 2007). Since WOFOST does not take into account yield loss due to flooding, this may explain the overestimation.

WOFOST was also used to simulate the sugar beet yield for the year 2020. Here, site-specific meteorological and soil data were used for the simulation. Again, the crop parameter set “SUG601” showed the best simulation results. However, the results for all crop parameter sets showed that WOFOST underestimated the sugar beet yield. A potential reason for this underestimation could be inaccurate soil information which influence the water balance of the simulation. The simulation results per BYV contamination group showed, that WOFOST underestimated the yield for fields not or only slightly affected by the BYV (groups one and two). For fields stronger affected by the BYV (groups three and four) WOFOST slightly overestimated the yield. Here, this difference between groups one and two and groups three and four was expected: While the observed yield was reduced due to the BYV contamination for groups three and four, WOFOST did not account for this yield reducing factor which lead to an overestimation.

Evaluating the WOFOST simulation for 2020 spatially showed that the fit between observed and simulated sugar beet yield differs by region. While the Mean Absolute Error (MAE) for fields in the northeastern part of Switzerland was high indicating large differences between the observed and simulated yield, it was lower for fields in the western part of Switzerland. Dividing the results into a “west” and an “east” group provided various insights: First, WOFOST still underestimated the yield for both groups. However, the underestimation was not as pronounced for group “west” as for group “east”. Second, while no significant correlation between the observed and the simulated yield could be found for group “east”, the correlation was moderate for group “west” and statistically significant. Third, focusing on group “west” and dividing the results by BYV contamination category showed, that for fields heavily affected

by BYV (category 4), the simulated yield was lower compared to the other fields. From the last observation, the meteorological conditions for the fields of group “west” was carried out, since they were found to be related to the occurrence of the BYV. Here, it was shown, that for fields of BYV category 4 (heavily affected), the number of days with water stress from the WOFOST simulation was higher compared to the other categories. This finding indicates that fields where water stress occurred more frequently, were more vulnerable to BYV infections.

Overall, WOFOST showed good performance in simulating the temporal variability of the sugar beet yields (1990-2022). Simulation results can certainly be improved by calibrating for example the phenological development for specific locations or by including site-specific soil conditions. However, since the goal of the first analysis was to assess WOFOST’s performance under Swiss conditions and to identify the crop parameter set most suitable for Swiss conditions in general, further simulation improvements by including site-specific data were not considered. In contrast, the simulation results for 2020 showed generally larger differences between the observed and the simulated yields. Moreover, it was shown that the accuracy of the simulation results differed spatially. Even though site-specific meteorological and soil data were included in the simulation, the differences between the observed and simulated yield persisted. To summarise, WOFOST’s performance was more accurate regarding the temporal variability (1990-2022) than the spatial variability (2020).

4.2 Remote sensing

In this analysis, the Chlorophyll Index Green (CIG), the Simple Ration (SR) and the Green Ratio Vegetation Index (GRVI) were identified as the vegetation indices that correlated the best with the observed yield. Similarly, Peng & Gitelson (2011) also found that, among other vegetation indices, the Chlorophyll Index Green and the Simple Ration were useful for estimating the gross primary production of maize. The Red-Edge Disease Stress Index (REDSI) proposed by Zheng et al. (2018) showed the 26th best correlation coefficient. In general, it is important to note, that there are temporal differences regarding the used data. While the vegetation indices were calculated for the 8th of July, the sugar beets were harvested later in the year (approximately in November or December). This temporal shift in the data collection could induce uncertainties in the analysis. However, multiple dates were used to calculate the different vegetation indices and the highest correlation was found for the 8th of July. The findings suggest that for 2020, the time period around the 8th of July was a stage of the phenological development of the sugar beet plants that was very relevant for the yield formation.

The correlation analysis between the vegetation indices from the 8th of July and the BYV contamination categories revealed that the Anthocyanin Reflectance Index (ARI) showed the strongest correlation of all examined vegetation indices. Anthocyanins are red pigments in leaves that are related to the ability of plants to resist environmental stresses such as droughts or pathogens (Viña & Gitelson, 2011). Sugar beets are not anthocyanin-producing plants, instead they produce betalains (Karvansara & Razavi, 2019). Betalains are also associated with increasing a plant's resistance to environmental stresses: Karvansara & Razavi (2019) found increases in betalain production in sugar beets treated with ultraviolet radiation. Anthocyanins and betacyanins (betalains can be categorised in betacyanins and betaxanthins) are not only similar in their functions in plants, but they also both exhibit absorbance peaks at a wavelength of approximately 550 nm (Ceccanti et al., 2025). This is why the “Betacyanin Reflectance Index (BRI)” was proposed, which is calculated in exactly the same way as the ARI (Ceccanti et al., 2025). Considering that sugar beets do not produce anthocyanins and that betalains show a similar spectral reflectance pattern as anthocyanins, it can be assumed that the calculated ARI index values were, in fact, based on the betalain content of the examined sugar beet fields. The correlation analysis showed that ARI was highest for fields with no BYV contamination (category 1) and lowest for fields with high BYV contamination (category 4). These findings suggest that sugar beet plants with lower betalain contents were more often affected by BYV contamination.

Lastly, it was shown that the calculated vegetation indices were useful to identify healthy fields (BYV contamination categories 1 and 2) through a random forest model. However, the model with all vegetation indices as predictors only showed an accuracy of approximately 51% for identify infected (BYV contamination categories 3 and 4) fields. While the classification barley improved with only the ten most important predictors, the classification results changed with only the ARI values as predictors: While the accuracy for healthy fields decreased, it increased for ill fields. Since the correct identification of ill fields is more relevant in regards of potential BYV prevention measures, the model with only the ARI as a predictor is the most suitable. Additionally, the model is less resource consuming due to limited data requirements.

5 Conclusion

This thesis used the WOFOST cropping simulation model to identify the most suitable crop parameter set for simulating the growth of sugar beets under Swiss conditions. It was shown that the crop parameter set “SUG601” performed best compared to observations from 20 different locations across the Swiss Plateau. Regional differences in the model’s performance were identified: For three locations in western Switzerland, lower simulation accuracies were observed, while location in northeastern Switzerland showed the best results. One limitation of this analysis is that for some locations, sugar beet yield observations were only available for a shorter time period. Depending on the missing period, the fit between the observed and the simulated yield changes. Overall, WOFOST was able to replicate the variability of the sugar beet yields over time accurately, which is why it would be interesting to use climatic projections to assess the impact of climatic changes to the sugar beet production in Switzerland.

Additional WOFOST simulations were carried out for the year 2020 for 950 sugar beet fields, again to evaluate the model’s performance. Here, it was shown that for the year 2020, WOFOST underestimated the yield. Again, regional differences were identified: In contrast to the findings of the period 1990-2022, the model performed better for fields located in the western part of Switzerland compared to the northeastern part. Interestingly, combining the WOFOST results with the data the occurrence of BYV in 2020 showed, that WOFOST predicted lower yields for sugar beet fields that were heavily affected by the BYV. Analysing the meteorological conditions showed that water stress could have benefited BYV infections. Here, future research should focus on investigating how physical abiotic conditions are related to a plant’s vulnerability to pests and diseases. Furthermore, since water stress was shown to be related to the BYV contaminations in 2020, it would be interesting to examine if irrigation can lead to reductions in water stress and ultimately strengthen the resistance against diseases.

Lastly, remote sensing data was used in this thesis to calculate 101 different vegetation indices. The relationship between the obtained vegetation index values and the harvest sugar beet yield as well as the BYV contamination category was assessed to identify the vegetation index with the best correlation. Three different vegetation indices showed the best correlation with sugar beet yield: The Chlorophyll Index Green, the Simple Ratio and the Green Ratio Vegetation Index. Regarding the correlation between the vegetation indices and the four BYV contamination categories, the Anthocyanin Reflectance Index showed the best correlation. The calculated vegetation indices were ultimately used in a random forest classification. Here, the

ARI was the most useful predictor for classifying fields infected by BYV. All results were based on vegetation index values from the 8th of July in 2020, since this was identified as the day with the clear conditions and because symptoms of BYV infections would appear around this date. However, the farmer's assessment of BYV infection severity took place later in the year. Also, sugar beets are usually harvested in November and December. Therefore, this analysis compared data from different points in time, which induces uncertainties. Unfortunately, remote sensing data for dates in Autumn or Winter were not available. Additionally, uncertainties are added due to the fact that the BYV contamination severity was assessed by farmers that owned the belonging field. Here, it is possible that similar symptoms of other diseases or water stress were falsely classified as symptoms caused by the BYV. Additionally, it is very likely that some fields were classified in the wrong category, since the estimation of BYV contamination severity on a scale from 1 to 4 is subjective and thus varies from farmer to farmer. Nevertheless, this analysis still showed significant correlations between the calculated vegetation indices and the harvested yield as well as the BYV contamination estimates. Since remote sensing data are available and easily processible, future research should investigate how certain vegetation indices can be used to create an effective and precise vegetation monitoring with the goal to identify potential yield reducing factors such as pests and diseases.

6 References

- Bao, L., Li, X., Yu, J., Li, G., Chang, X., Yu, L., & Li, Y. (2024). Forecasting spring maize yield using vegetation indices and crop phenology metrics from UAV observations. *Food and Energy Security*, 13(1), e505. <https://doi.org/https://doi.org/10.1002/fes3.505>
- Bassu, S., Brisson, N., Durand, J. L., Boote, K., Lizaso, J., Jones, J. W., Rosenzweig, C., Ruane, A. C., Adam, M., Baron, C., Basso, B., Biernath, C., Boogaard, H., Conijn, S., Corbeels, M., Deryng, D., De Sanctis, G., Gayler, S., Grassini, P., ... Waha, K. (2014). How do various maize crop models vary in their responses to climate change factors? *Global Change Biology*, 20(7), 2301–2320. <https://doi.org/10.1111/gcb.12520>
- Bezner Kerr, R., Hasegawa, T., Lasco, R., Bhatt, I., Deryng, D., Farrell, A., Gurney-Smith, H., Ju, H., Lluch-Cota, S., Meza, F., Nelson, G., Neufeldt, H., & Thornton, P. (2022). *Food, fibre, and other ecosystem products*. In H.-O. Pörtner, D. C. Roberts, M. Tignor, E. S. Poloczanska, K. Mintenbeck, A. Alegría, M. Craig, S. Langsdorf, S. Löschke, V. Möller, A. Okem, & B. Rama (Eds.), *Climate change 2022: Impacts, adaptation and vulnerability. Contribution of Working Group II to the Sixth Assessment Report of the Intergovernmental Panel on Climate Change* (pp. 713–906). Cambridge University Press. <https://doi.org/10.1017/9781009325844.007>
- Boogaard, H., Wolf, J., Supit, I., Niemeyer, S., & van Ittersum, M. (2013). A regional implementation of WOFOST for calculating yield gaps of autumn-sown wheat across the European Union. *Field Crops Research*, 143, 130–142. <https://doi.org/10.1016/j.fcr.2012.11.005>
- Boons-Prins, E. R., De Koning, G. H. J., & Van Diepen, C. A. (1993). *Crop-specific simulation parameters for yield forecasting across the European Community*. CABO-DLO [etc.].
- Brönnimann, S., Appenzeller, C., Croci-Maspoli, M., Fuhrer, J., Grosjean, M., Hohmann, R., Ingold, K., Knutti, R., Liniger, M. A., Raible, C. C., Röthlisberger, R., Schär, C., Scherrer, S. C., Strassmann, K., & Thalmann, P. (2014). Climate change in Switzerland: A review of physical, institutional, and political aspects. In *Wiley Interdisciplinary Reviews: Climate Change* (Vol. 5, Issue 4, pp. 461–481). Wiley-Blackwell. <https://doi.org/10.1002/wcc.280>
- Bundesamt für Landwirtschaft. (2021). *Zucker*. In *Agrarbericht 2021*. Retrieved from <https://2021.agrarbericht.ch/de/markt/pflanzliche-produkte/zucker> (last visit: 17.03.2025)

- Bundesamt für Landwirtschaft. (2016). *Zucker*. In *Agrarbericht 2016*. Retrieved from <https://2016.agrarbericht.ch/de/markt/pflanzliche-produkte/zucker> (last visit: 17.03.2025)
- Bundesamt für Statistik. (2020). *Die Zuckerrübenproduktion in der Schweiz*. Retrieved from <https://www.swissstats.bfs.admin.ch/collection/ch.admin.bfs.swissstat.de.issue200711652000/article/issue200711652000-01> (last visit: 17.03.2025)
- Ceccanti, C., Landi, M. L., Landi, M., Lo Piccolo, E., Guidi, L., & Matteoli, S. (2025). Validation of betacyanin content in *Beta vulgaris* leaves by using non-destructive measurement with DualexTM leaf clip sensor or proximal sensing spectroscopy. *Computers and Electronics in Agriculture*, 230. <https://doi.org/10.1016/j.compag.2024.109872>
- CH2018 (2018). CH2018 – Climate Scenarios for Switzerland, Technical Report, National Centre for Climate Services, Zurich, 271 pp. ISBN: 978-3-9525031-4-0
- Challinor, A. J., Watson, J., Lobell, D. B., Howden, S. M., Smith, D. R., & Chhetri, N. (2014). A meta-analysis of crop yield under climate change and adaptation. *Nature Climate Change*, 4(4), 287–291. <https://doi.org/10.1038/nclimate2153>
- Conway, R., Holzkämper, P. D. D. A., & Hund, P. D. D. A. (2023). *Projecting Climate Change Impacts on Winter Wheat Growth in Switzerland*.
- Curnel, Y., de Wit, A. J. W., Duveiller, G., & Defourny, P. (2011). Potential performances of remotely sensed LAI assimilation in WOFOST model based on an OSS Experiment. *Agricultural and Forest Meteorology*, 151(12), 1843–1855. <https://doi.org/10.1016/j.agrformet.2011.08.002>
- de Wit, A. (2024a). *PCSE documentation*. Tech. Rep., 2019.[Online]. Available. <https://pcse.readthedocs.io/en/stable/> (last visit: 17.03.2025)
- de Wit, A. (2024b). *WOFOST_crop_parameters*. https://github.com/ajwdewit/WOFOST_crop_parameters
- de Wit, A., & Boogaard, H. (2024). *A gentle introduction to WOFOST*. Wageningen Environmental Research.
- de Wit, A., Baruth, B., Boogaard, H., Van Diepen, K., Van Kraalingen, D., Micale, F., Te Roller, J., Supit, I., & Van Den Wijngaart, R. (2010). Using ERA-INTERIM for regional crop yield forecasting in Europe. *Climate Research*, 44(1), 41–53. <https://doi.org/10.3354/cr00872>
-

- de Wit, A., Boogaard, H., Fumagalli, D., Janssen, S., Knapen, R., van Kraalingen, D., Supit, I., van der Wijngaart, R., & van Diepen, K. (2019). 25 years of the WOFOST cropping systems model. In *Agricultural Systems* (Vol. 168, pp. 154–167). Elsevier Ltd. <https://doi.org/10.1016/j.agry.2018.06.018>
- de Wit, A., Boogaard, H. L., Supit, I., & van den Berg, M. (2020). *System description of the WOFOST 7.2, cropping systems model*. Wageningen Environmental Research.
- Dewenam, L. E. F., Er-Raki, S., Ezzahar, J., & Chehbouni, A. (2021). Performance evaluation of the WOFOST model for estimating evapotranspiration, soil water content, grain yield and total above-ground biomass of winter wheat in tensift al haouz (Morocco): Application to yield gap estimation. *Agronomy*, *11*(12). <https://doi.org/10.3390/agronomy11122480>
- Fuhrer, J., Beniston, M., Fischlin, A., Frei, C., Goyette, S., Jasper, K., & Pfister, C. (2006). Climate risks and their impact on agriculture and forests in Switzerland. *Climatic Change*, *79*(1–2), 79–102. <https://doi.org/10.1007/s10584-006-9106-6>
- Gilardelli, C., Confalonieri, R., Cappelli, G. A., & Bellocchi, G. (2018). Sensitivity of WOFOST-based modelling solutions to crop parameters under climate change. *Ecological Modelling*, *368*, 1-14. <https://doi.org/10.1016/j.ecolmodel.2017.11.003>
- Groux, R., Mahillon, M., Bussereau, F., Brodard, J., Debonneville, C., Kellenberger, I., Steinger, T., & Schmupp, O. (2021). Distribution and intraspecific variation of Beet yellows virus (BYV) in Switzerland. *Rencontres Virologie Végétale*.
- Gupta, H. V., Sorooshian, S., & Yapo, P. O. (1999). Status of Automatic Calibration for Hydrologic Models: Comparison with Multilevel Expert Calibration. *Journal of Hydrologic Engineering*, *4*(2), 135–143. [https://doi.org/10.1061/\(asce\)1084-0699\(1999\)4:2\(135\)](https://doi.org/10.1061/(asce)1084-0699(1999)4:2(135))
- Henne, P. D., Bigalke, M., Büntgen, U., Colombaroli, D., Conedera, M., Feller, U., Frank, D., Fuhrer, J., Grosjean, M., Heiri, O., Luterbacher, J., Mestrot, A., Rigling, A., Rössler, O., Rohr, C., Rutishauser, T., Schwikowski, M., Stampfli, A., Szidat, S., ... Tinner, W. (2018). An empirical perspective for understanding climate change impacts in Switzerland. In *Regional Environmental Change* (Vol. 18, Issue 1, pp. 205–221). Springer Verlag. <https://doi.org/10.1007/s10113-017-1182-9>

- Holzkämper, A., Calanca, P., & Fuhrer, J. (2013). Identifying climatic limitations to grain maize yield potentials using a suitability evaluation approach. *Agricultural and Forest Meteorology*, 168, 149–159. <https://doi.org/10.1016/j.agrformet.2012.09.004>
- Holzworth, D. P., Snow, V., Janssen, S., Athanasiadis, I. N., Donatelli, M., Hoogenboom, G., White, J. W., & Thorburn, P. (2015). Agricultural production systems modelling and software: Current status and future prospects. *Environmental Modelling and Software*, 72, 276–286. <https://doi.org/10.1016/j.envsoft.2014.12.013>
- Hossain, R., Menzel, W., Lachmann, C., & Varrelmann, M. (2021). New insights into virus yellows distribution in Europe and effects of beet yellows virus, beet mild yellowing virus, and beet chlorosis virus on sugar beet yield following field inoculation. *Plant Pathology*, 70(3), 584–593. <https://doi.org/10.1111/ppa.13306>
- Huang, J., Ma, H., Sedano, F., Lewis, P., Liang, S., Wu, Q., Su, W., Zhang, X., & Zhu, D. (2019). Evaluation of regional estimates of winter wheat yield by assimilating three remotely sensed reflectance datasets into the coupled WOFOST–PROSAIL model. *European Journal of Agronomy*, 102, 1–13. <https://doi.org/10.1016/j.eja.2018.10.008>
- Imtiaz Safa and Shahid, S. and I. T. and I. M. and N. A. F. and S. J. and F. S. and A. M. (2024). Impact of Climate Change on Agriculture. In S. and N. T. and G. L. and A. M. and Z. R. Fahad Shah and Saud (Ed.), *Environment, Climate, Plant and Vegetation Growth* (pp. 285–305). Springer Nature Switzerland. https://doi.org/10.1007/978-3-031-69417-2_10
- Karvansara, P. R., & Razavi, S. M. (2019). Physiological and biochemical responses of sugar beet (*Beta vulgaris* L) to ultraviolet-B radiation. *PeerJ*, 7. <https://doi.org/10.7717/PEERJ.6790>
- Klein, T., Holzkämper, A., Calanca, P., & Fuhrer, J. (2014). Adaptation options under climate change for multifunctional agriculture: A simulation study for western Switzerland. *Regional Environmental Change*, 14(1), 167–184. <https://doi.org/10.1007/s10113-013-0470-2>
- Kremer, P. (2017). *Die Zuckerrübe im Klimawandel: Agrarökologische Auswirkungen in Rheinland-Pfalz und Hessen*. Springer Spektrum.

- Kulig, B., Skowera, B., Klimek-Kopyra, A., Kołodziej, S., & Grygierzec, W. (2020). The use of the WOFOST model to simulate water-limited yield of early potato cultivars. *Agronomy*, *10*(1), 81. <https://doi.org/10.3390/agronomy10010081>
- Lecerf, R., Ceglar, A., López-Lozano, R., Van Der Velde, M., & Baruth, B. (2019). Assessing the information in crop model and meteorological indicators to forecast crop yield over Europe. *Agricultural Systems*, *168*, 191–202. <https://doi.org/10.1016/j.agsy.2018.03.002>
- Mahoney, M. (2025). *rsi: Efficiently Retrieve and Process Satellite Imagery*. Zenodo. <https://doi.org/10.5281/zenodo.14722095>
- Martin, R. J. (1980). Yields and sugar contents of sugar beet and fodder beet cultivars. *Proceedings of the Agronomy Society of New Zealand*, *10*, 9–12.
- Mulla, S., Singh, S. K., Singh, K. K., & Praveen, B. (2020). Climate change and agriculture: a review of crop models. *Global Climate Change and Environmental Policy: Agriculture Perspectives*, 423–435.
- Nguyen, C., Sagan, V., Maimaitiyiming, M., Maimaitijiang, M., Bhadra, S., & Kwasniewski, M. T. (2021). Early detection of plant viral disease using hyperspectral imaging and deep learning. *Sensors (Switzerland)*, *21*(3), 1–23. <https://doi.org/10.3390/s21030742>
- Peng, Y., & Gitelson, A. A. (2011). Application of chlorophyll-related vegetation indices for remote estimation of maize productivity. *Agricultural and Forest Meteorology*, *151*(9), 1267–1276. <https://doi.org/10.1016/j.agrformet.2011.05.005>
- Phiri, D., Simwanda, M., Salekin, S., Nyirenda, V. R., Murayama, Y., & Ranagalage, M. (2020). Sentinel-2 data for land cover/use mapping: A review. *Remote sensing*, *12*(14), 2291. <https://doi.org/10.3390/rs12142291>
- Rammig, A., Jonas, T., Zimmermann, N. E., & Rixen, C. (2010). Changes in alpine plant growth under future climate conditions. *Biogeosciences*, *7*(6), 2013–2024. <https://doi.org/10.5194/bg-7-2013-2010>
- Schweizerischer Verband der Zuckerrübenpflanzer. (2007). *Jahresbericht 2007*. Retrieved from https://www.svz-fsb.ch/images/MedienNEUab052020/DE/5_Publikationen/2_Jahresbericht/Jahresbericht_2007.pdf (last visit: 17.03.02025)

- Service Center NABODAT. (2022). *Swiss Soil Dataset – Documentation Version 6* (April 2022).
- Swiss Competence Centre for Soil (KOBO). (2023). *Hinweiskarten für Bodeneigenschaften: Landesweit modellierte Karten für Bodeneigenschaften für drei Tiefenstufen* (Report). Swiss Competence Centre for Soil.
- Shindell, D., Faluvegi, G., Kasibhatla, P., & Van Dingenen, R. (2019). Spatial Patterns of Crop Yield Change by Emitted Pollutant. *Earth's Future*, 7(2), 101–112. <https://doi.org/10.1029/2018EF001030>
- Shindell, D. T. (2016). Crop yield changes induced by emissions of individual climate-altering pollutants. *Earth's Future*, 4(8), 373–380. <https://doi.org/10.1002/2016EF000377>
- Supit, I., van Diepen, C. A., De Wit, A. J. W., Wolf, J., Kabat, P., Baruth, B., & Ludwig, F. (2012). Assessing climate change effects on European crop yields using the Crop Growth Monitoring System and a weather generator. *Agricultural and Forest Meteorology*, 164, 96–111. <https://doi.org/10.1016/j.agrformet.2012.05.005>
- Timsina, J., Wolf, J., Guilpart, N., Van Bussel, L. G. J., Grassini, P., Van Wart, J., Hossain, A., Rashid, H., Islam, S., & Van Ittersum, M. K. (2018). Can Bangladesh produce enough cereals to meet future demand? *Agricultural Systems*, 163, 36–44. <https://doi.org/10.1016/j.agry.2016.11.003>
- Tschurr, F., Feigenwinter, I., Fischer, A. M., & Kotlarski, S. (2020). Climate scenarios and agricultural indices: A case study for Switzerland. *Atmosphere*, 11(5). <https://doi.org/10.3390/atmos11050535>
- Van Genuchten, M. T. (1980). A closed-form equation for predicting the hydraulic conductivity of unsaturated soils. *Soil science society of America journal*, 44(5), 892-898.
- van Ittersum, M. K., & Rabbinge, R. (1997). Concepts in production ecology for analysis and quantification of agricultural input-output combinations. *Field Crops Research*, 52(3), 197–208.
- Viña, A., & Gitelson, A. A. (2011). Sensitivity to foliar anthocyanin content of vegetation indices using green reflectance. *IEEE Geoscience and Remote Sensing Letters*, 8(3), 464–468. <https://doi.org/10.1109/LGRS.2010.2086430>

- Weber, T. K. D., Weynants, M., & Szabó, B. (2020). *tkdweber/euptf2: R package of updated European hydraulic pedotransfer functions (euptf2)*. Zenodo. <https://doi.org/10.5281/zenodo.4281046>
- Xue, J., & Su, B. (2017). Significant remote sensing vegetation indices: A review of developments and applications. *Journal of sensors*, 2017(1), 1353691. <https://doi.org/10.1155/2017/1353691>
- Zhang, J., Huang, Y., Pu, R., Gonzalez-Moreno, P., Yuan, L., Wu, K., & Huang, W. (2019). Monitoring plant diseases and pests through remote sensing technology: A review. *Computers and Electronics in Agriculture*, 165, 104943.
- Zheng, Q., Huang, W., Cui, X., Shi, Y., & Liu, L. (2018). New spectral index for detecting wheat yellow rust using Sentinel-2 multispectral imagery. *Sensors*, 18(3), 868.

Declaration of consent

on the basis of Article 30 of the RSL Phil.-nat. 18

Name/First Name:

Registration Number:

Study program:

Bachelor

Master

Dissertation

Title of the thesis:

Supervisor:

I declare herewith that this thesis is my own work and that I have not used any sources other than those stated. I have indicated the adoption of quotations as well as thoughts taken from other authors as such in the thesis. I am aware that the Senate pursuant to Article 36 paragraph 1 litera r of the University Act of 5 September, 1996 is authorized to revoke the title awarded on the basis of this thesis.

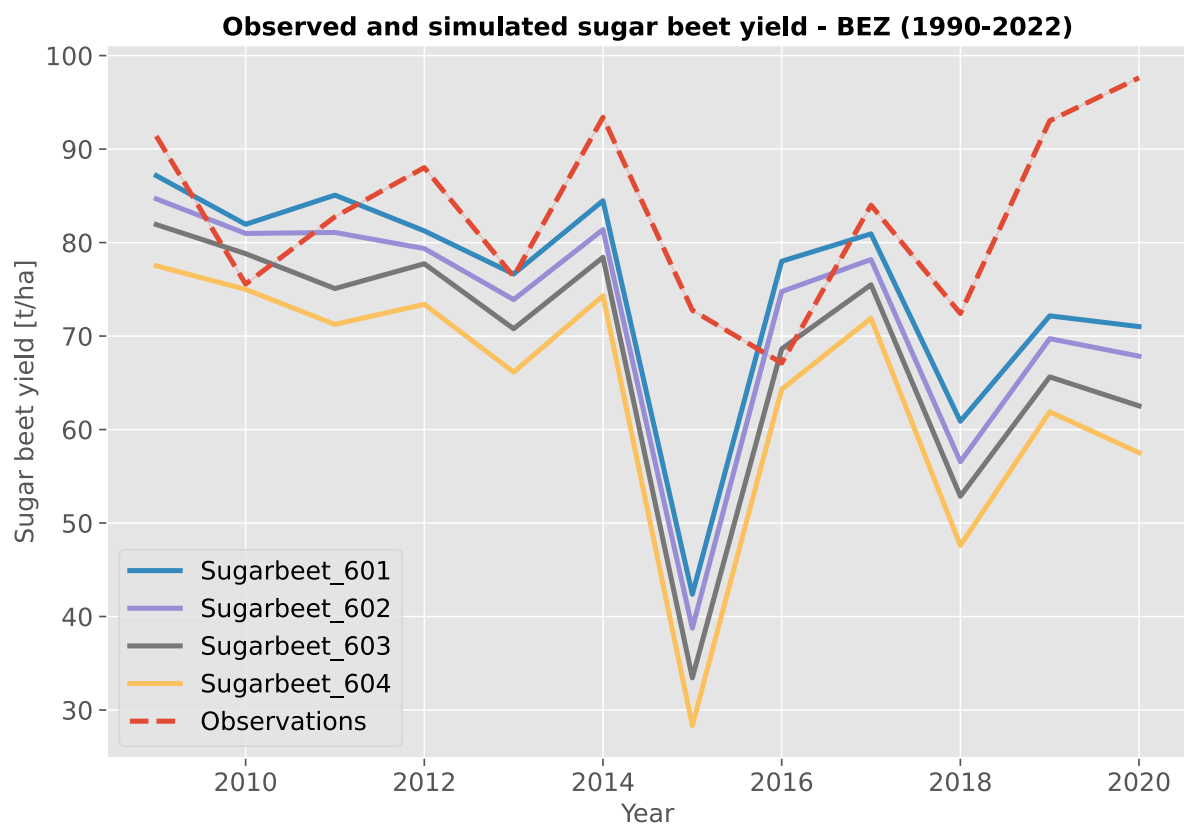
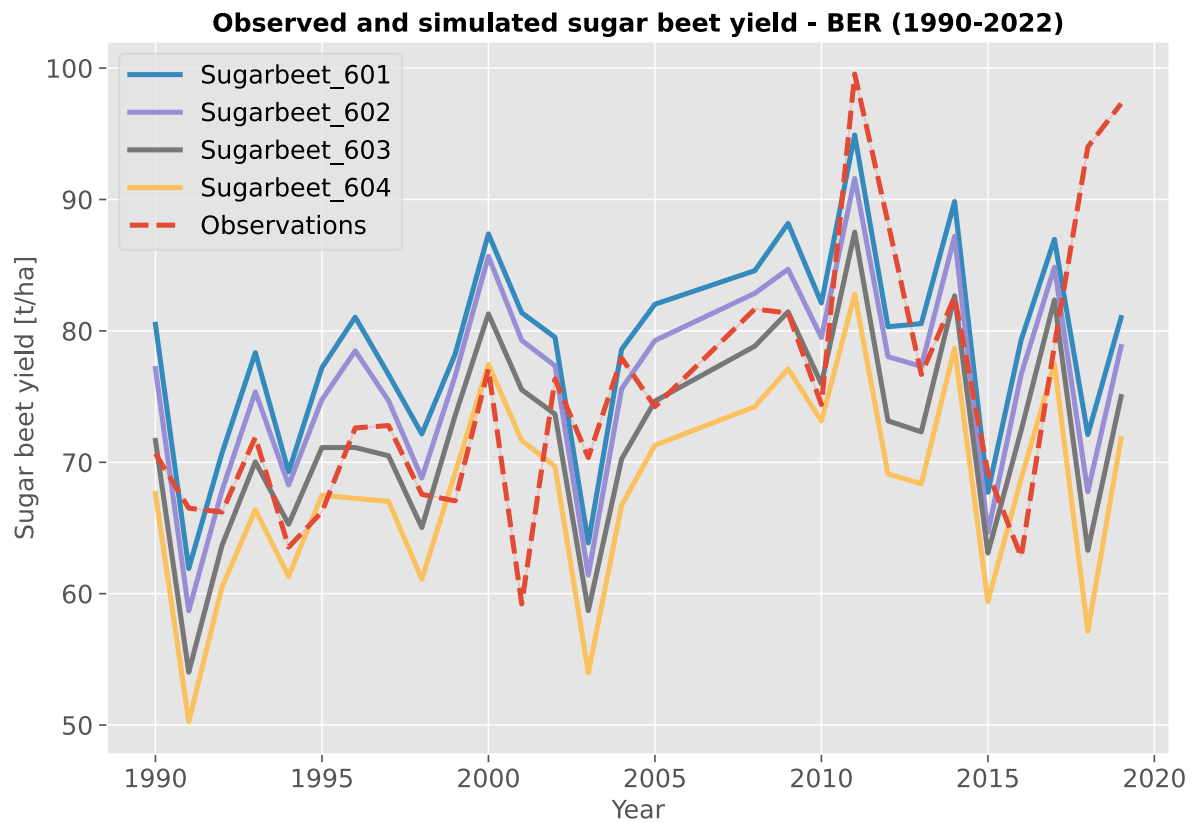
For the purposes of evaluation and verification of compliance with the declaration of originality and the regulations governing plagiarism, I hereby grant the University of Bern the right to process my personal data and to perform the acts of use this requires, in particular, to reproduce the written thesis and to store it permanently in a database, and to use said database, or to make said database available, to enable comparison with future theses submitted by others.

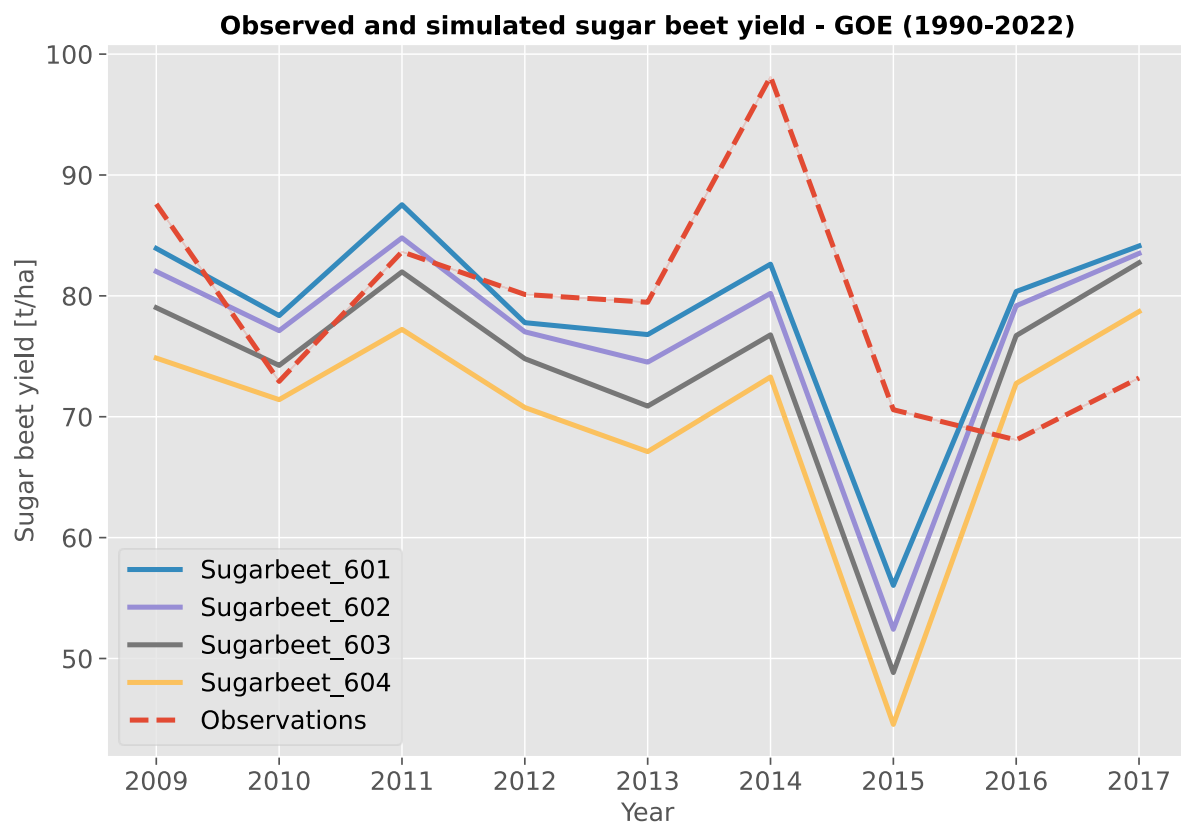
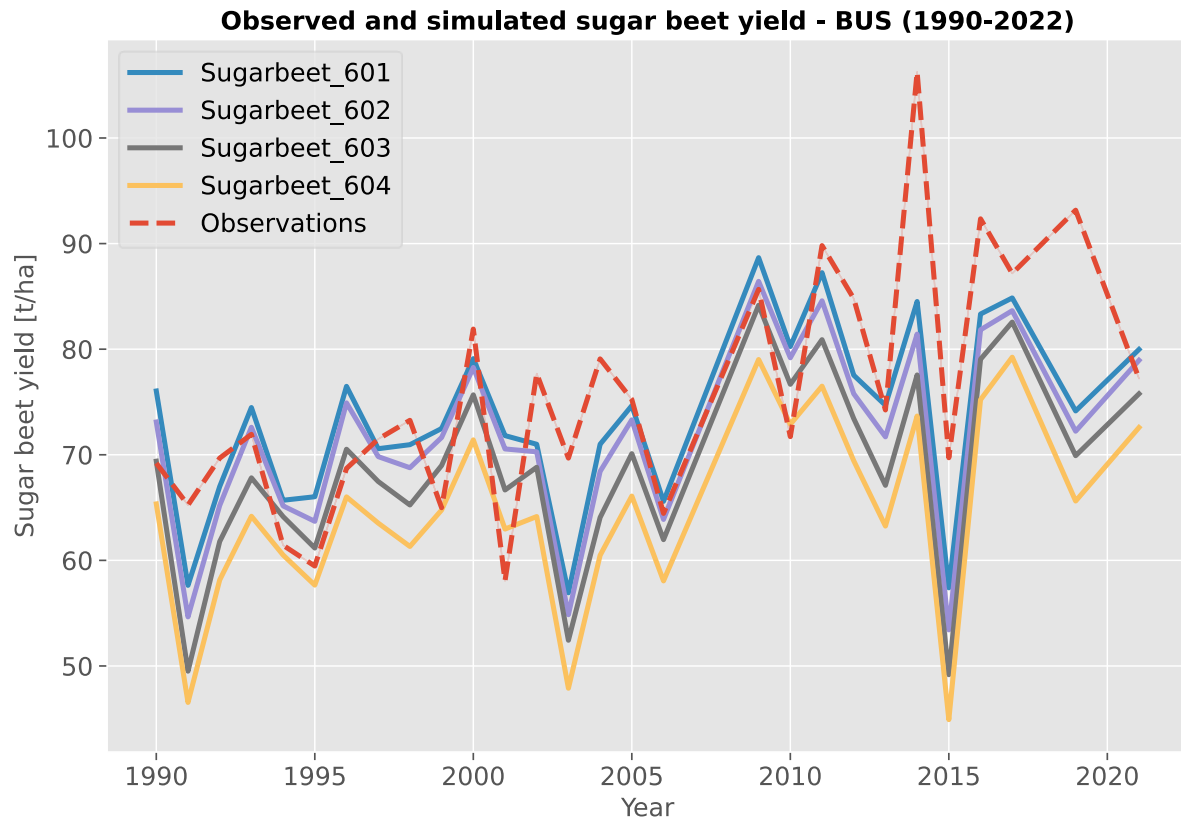
Place/Date

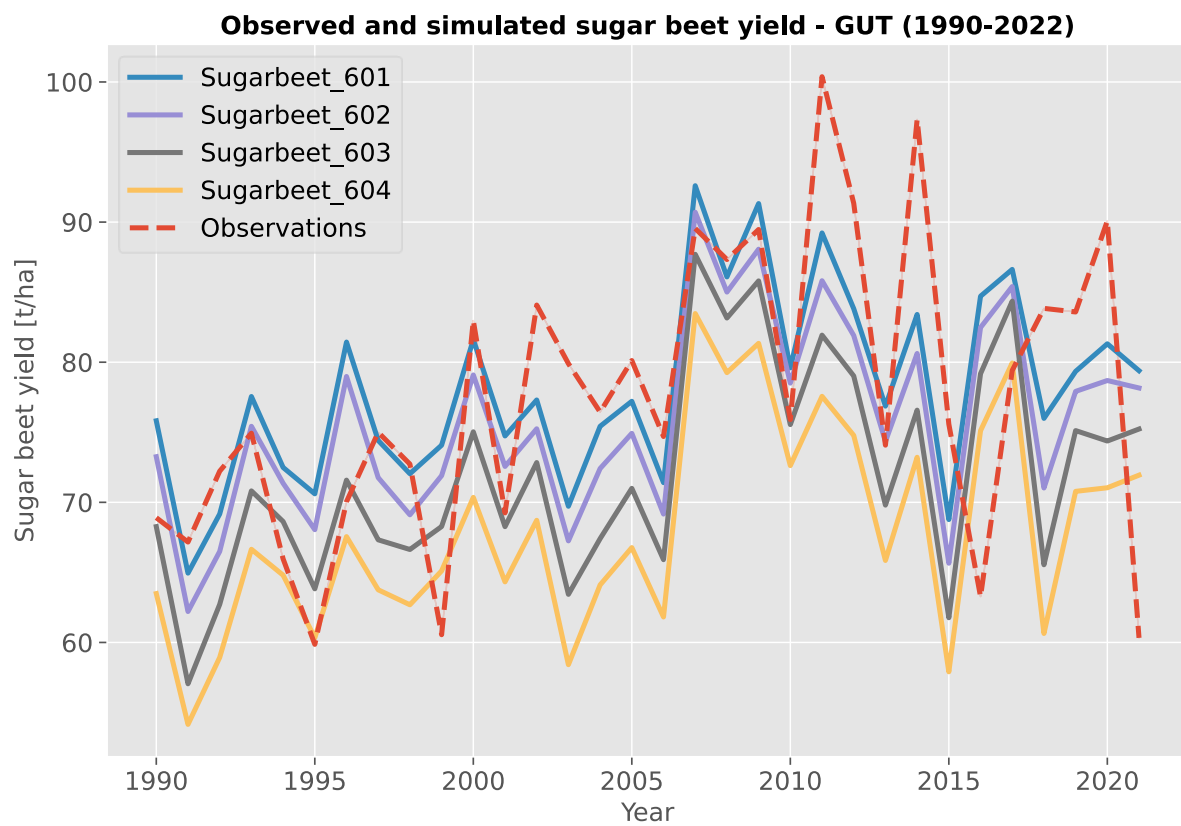
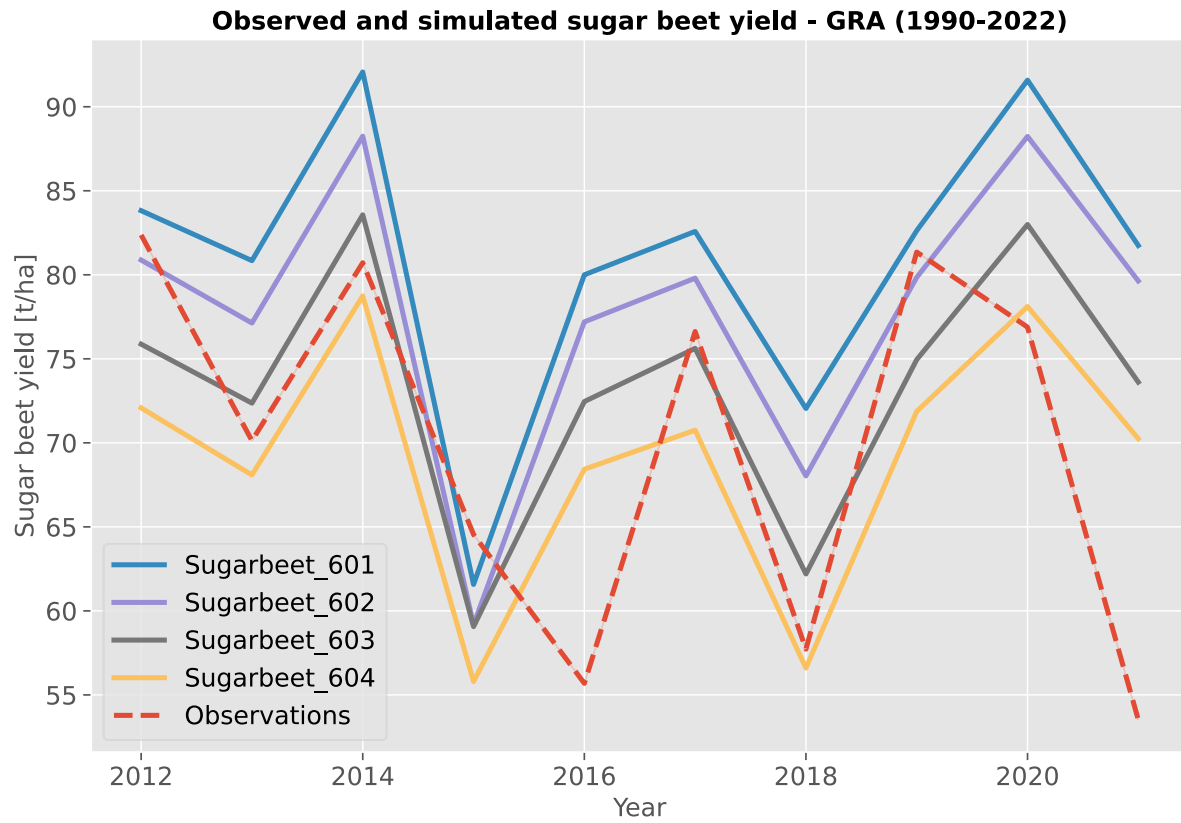

Signature

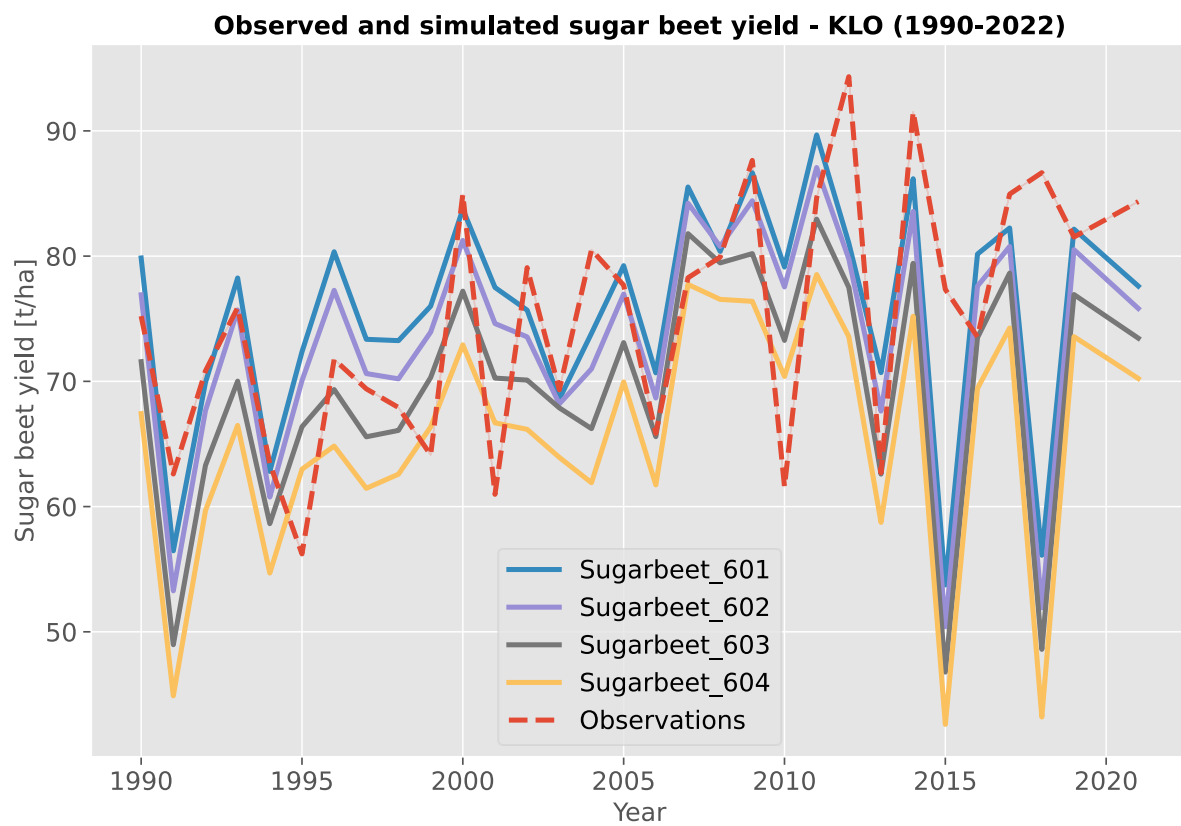
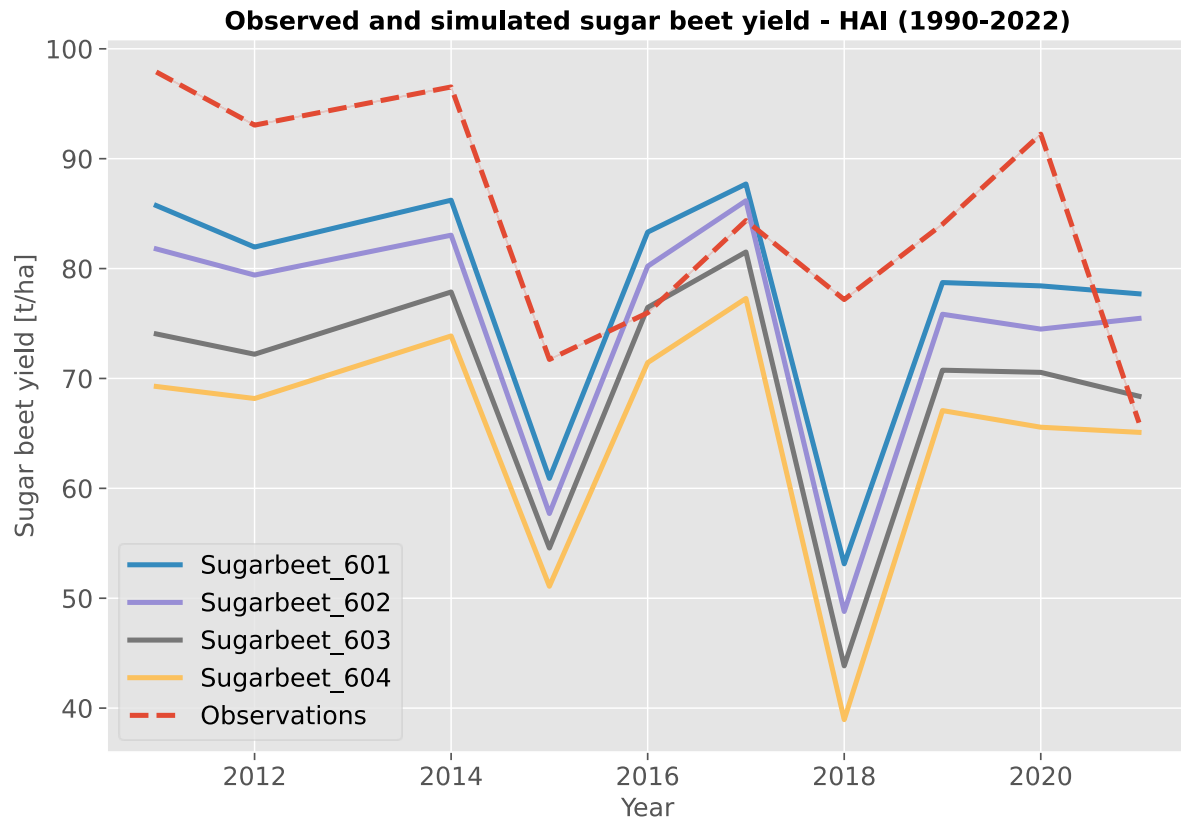
7 Annex

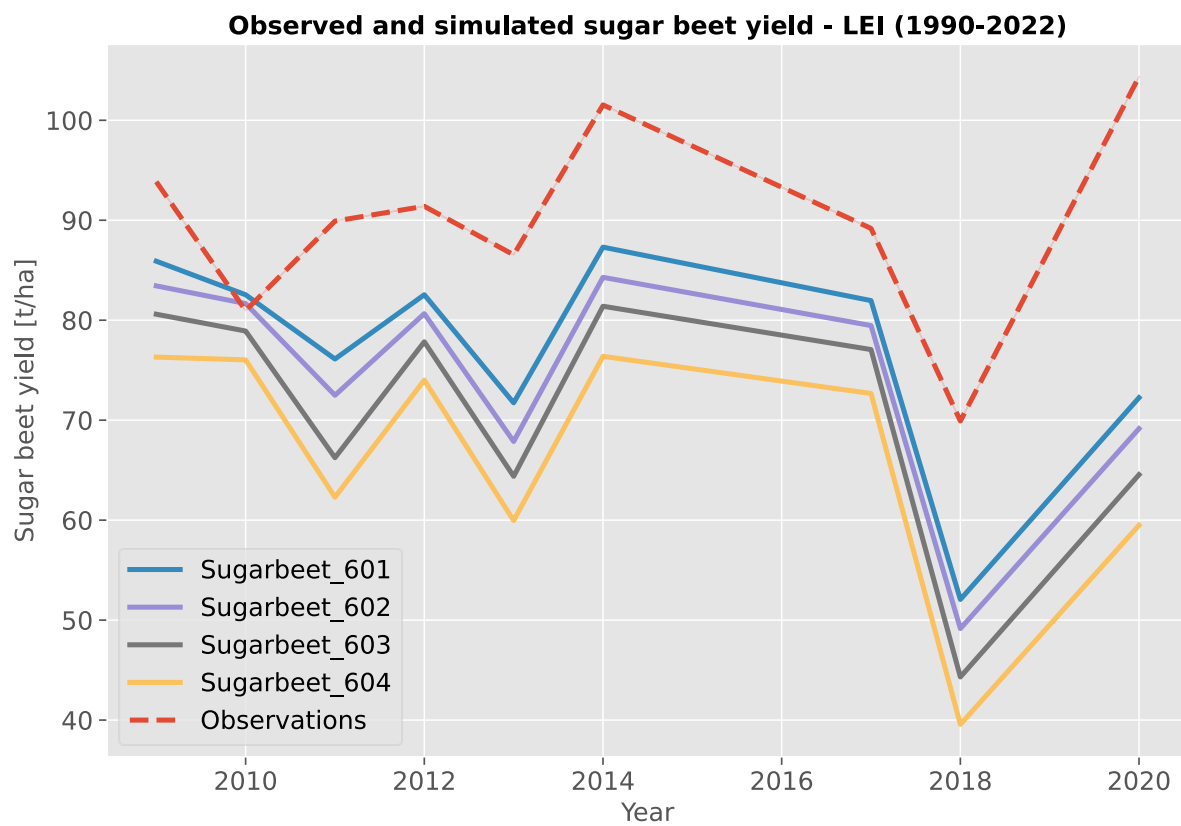
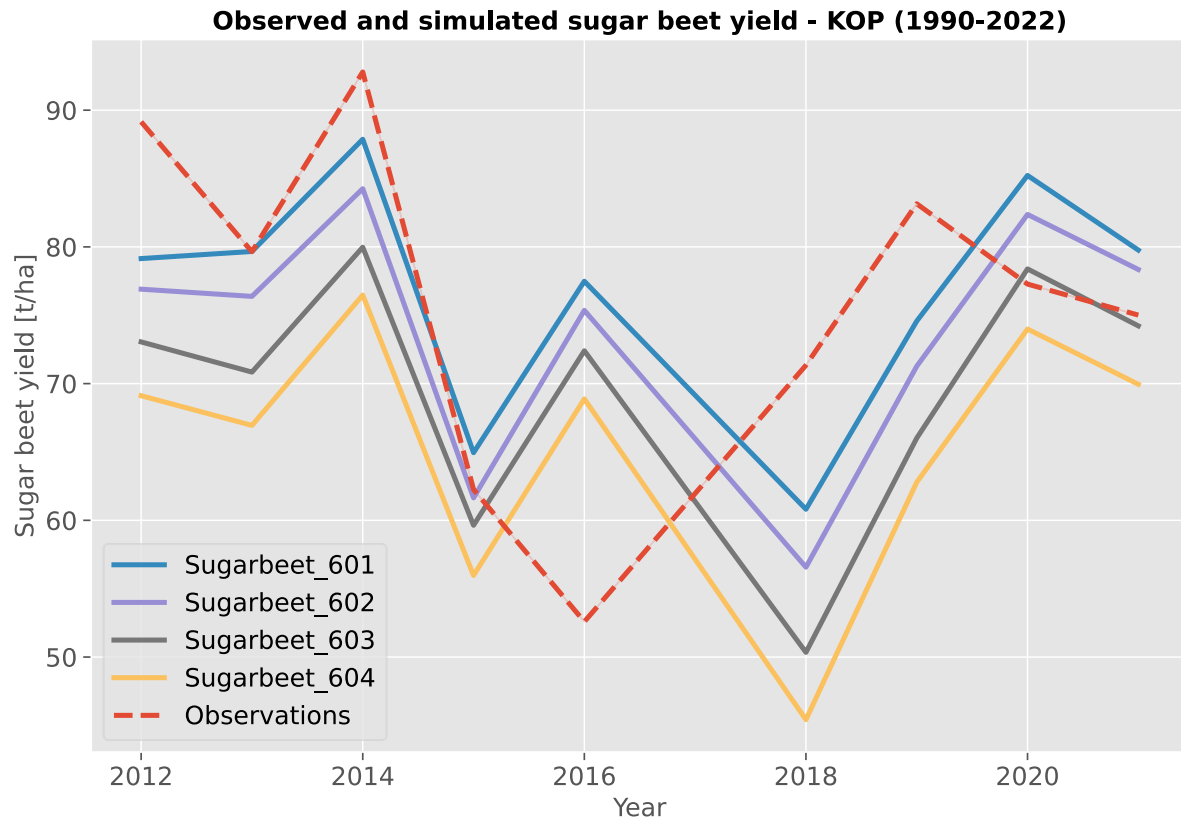
A) Simulated and observed yield historical period

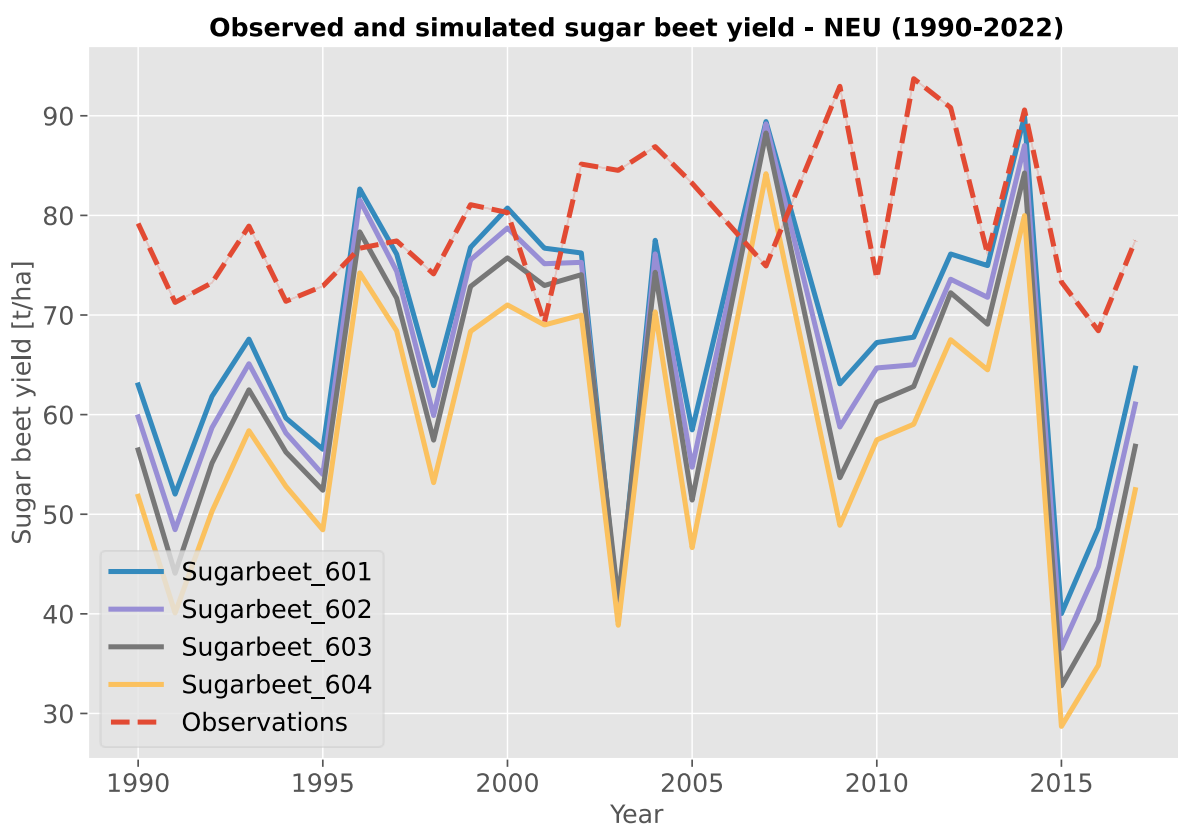
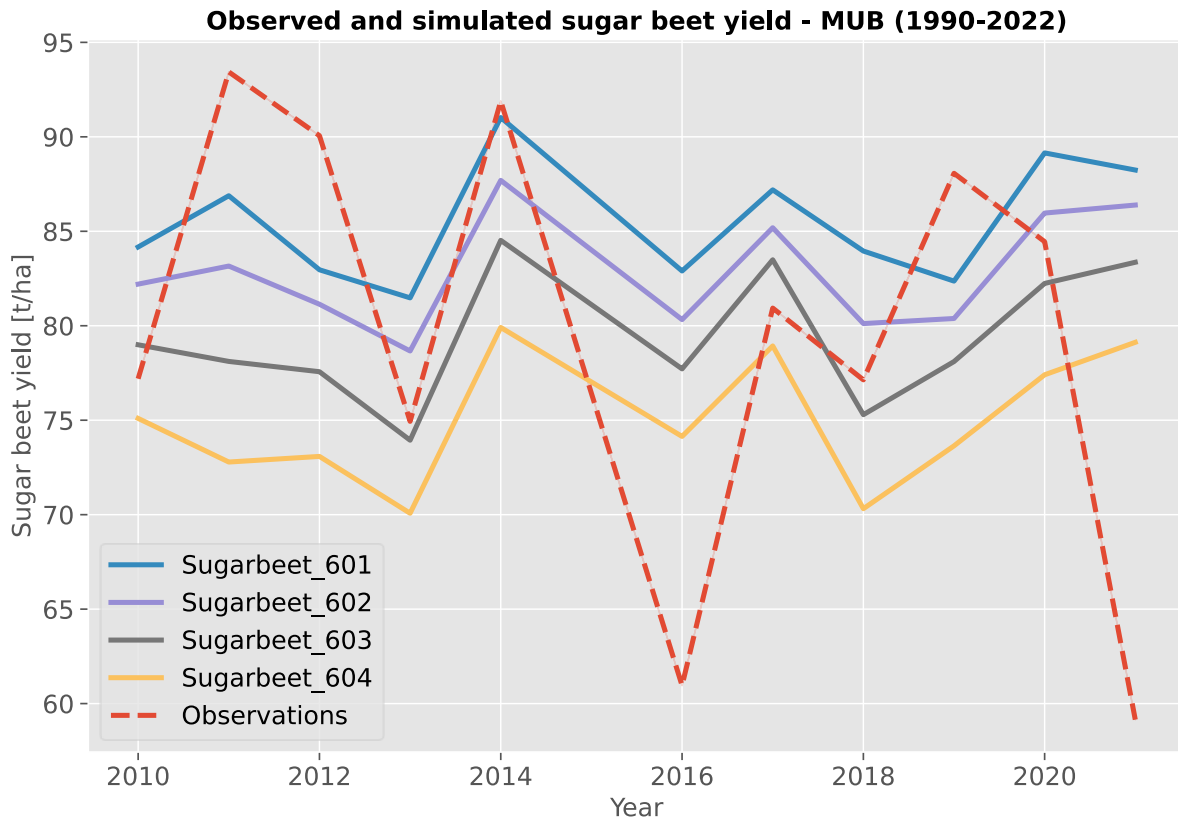


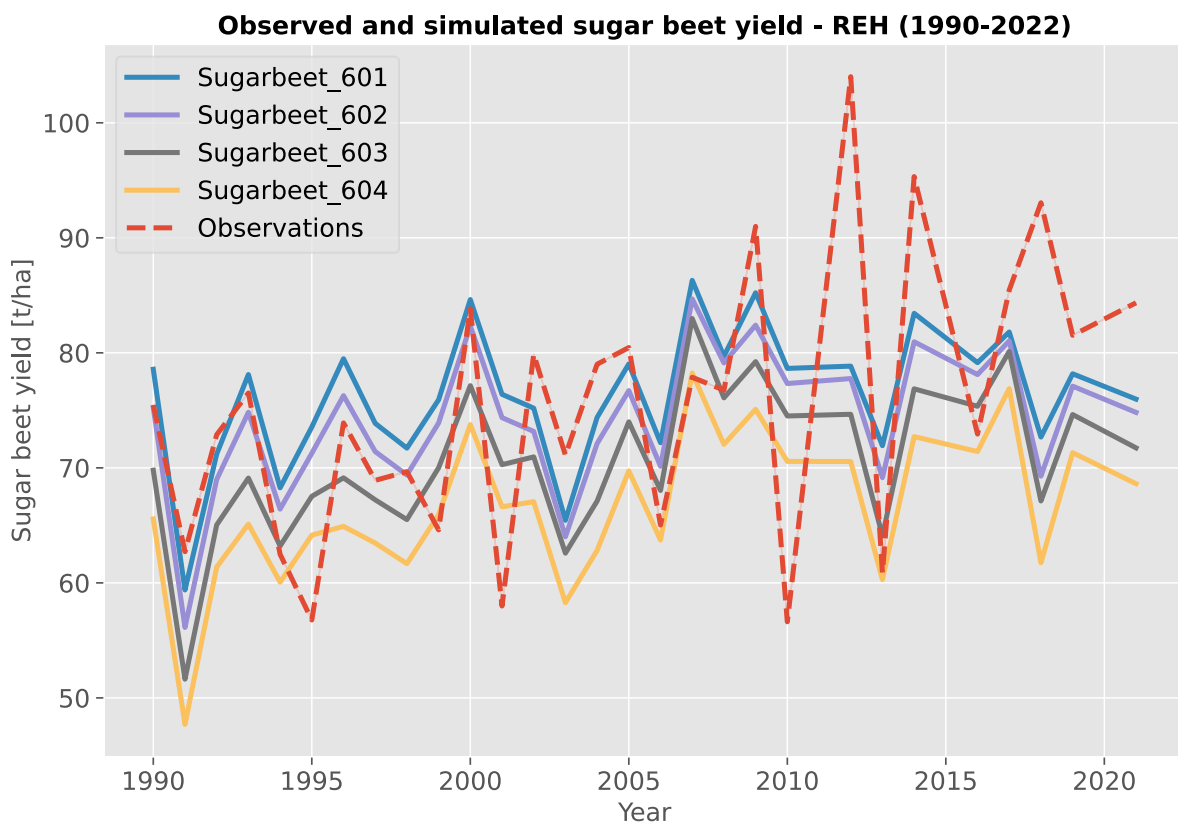
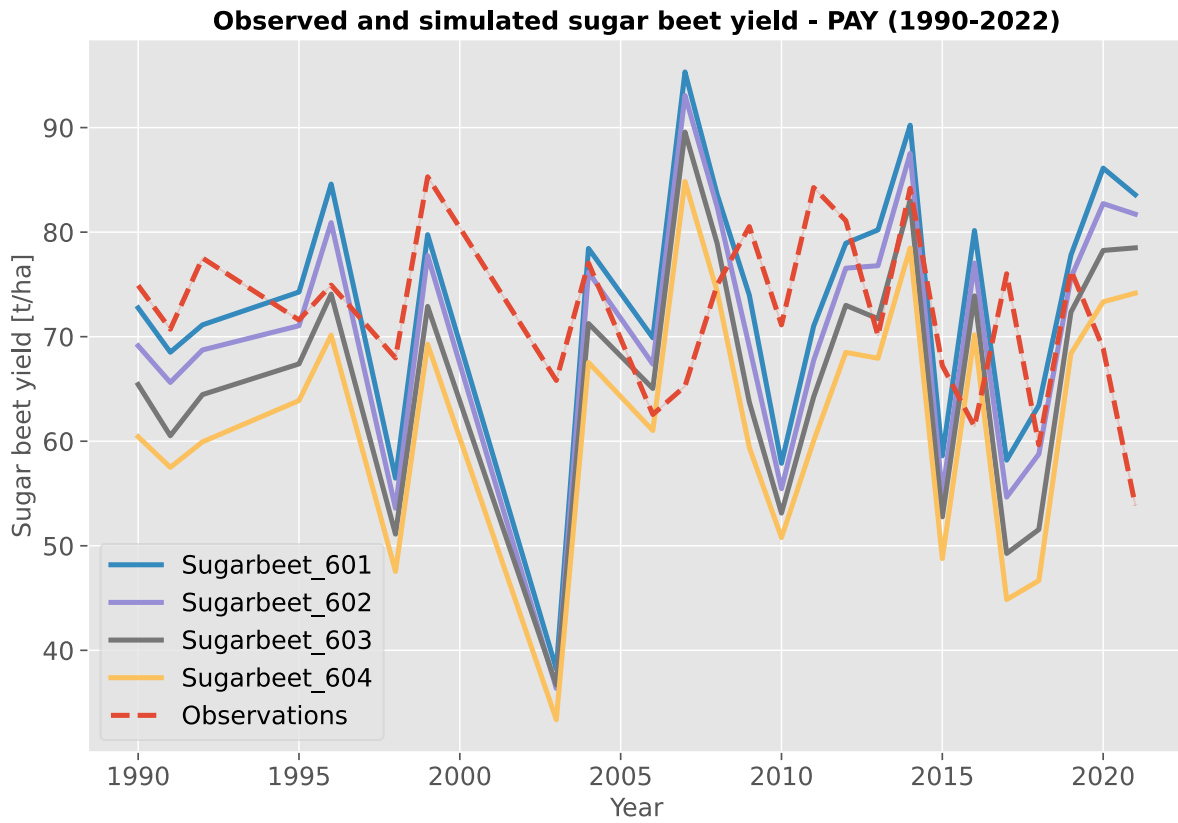


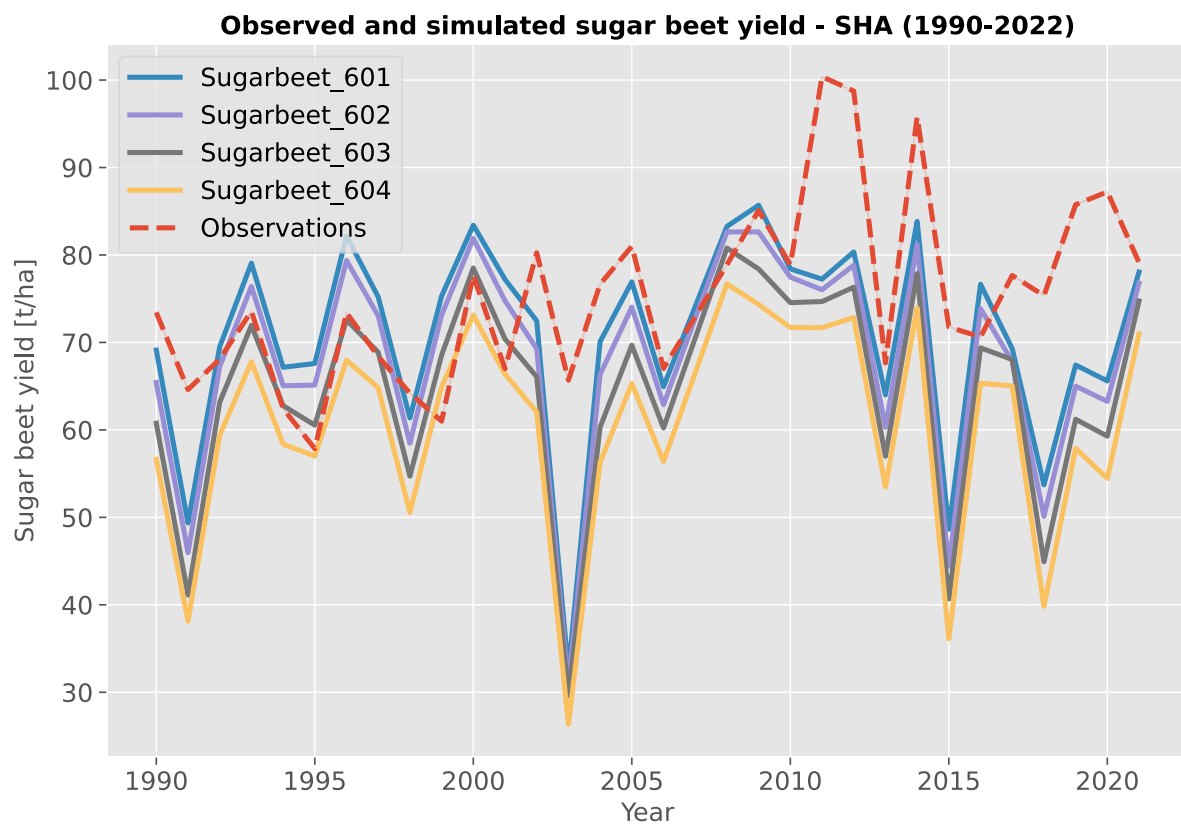
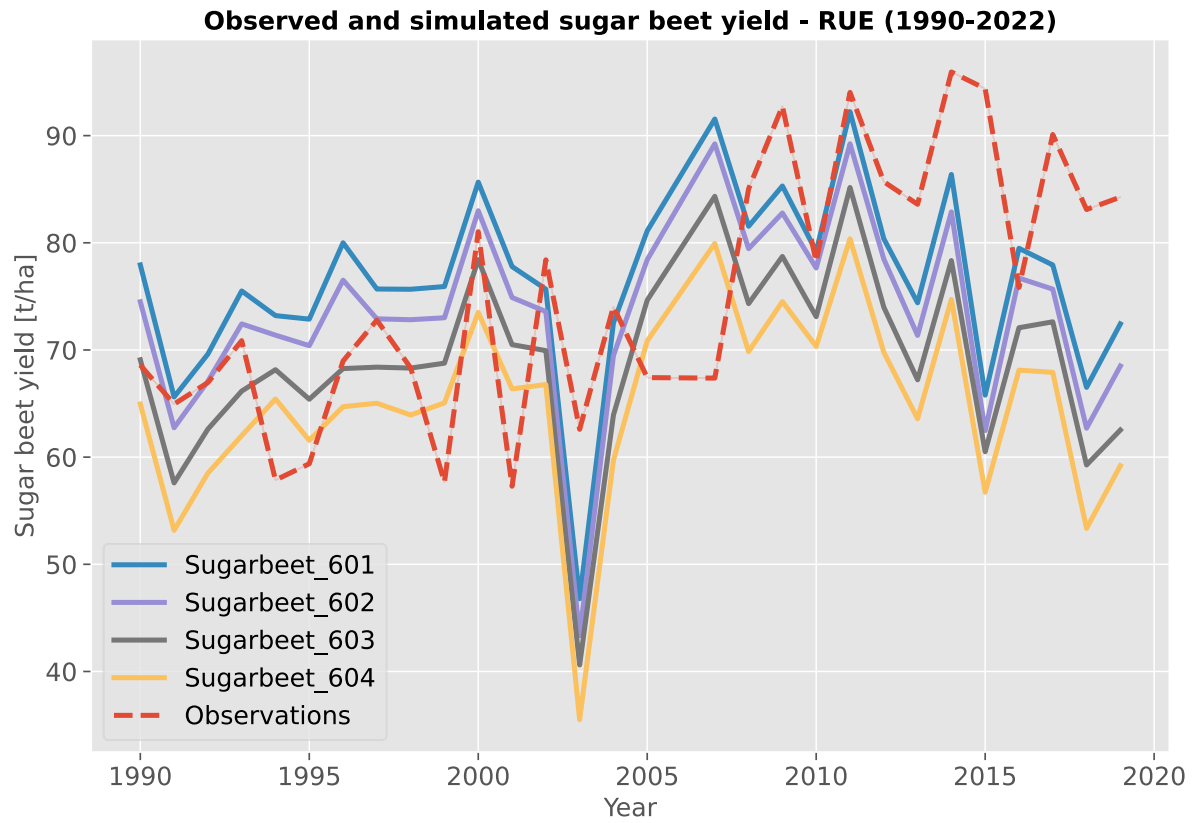


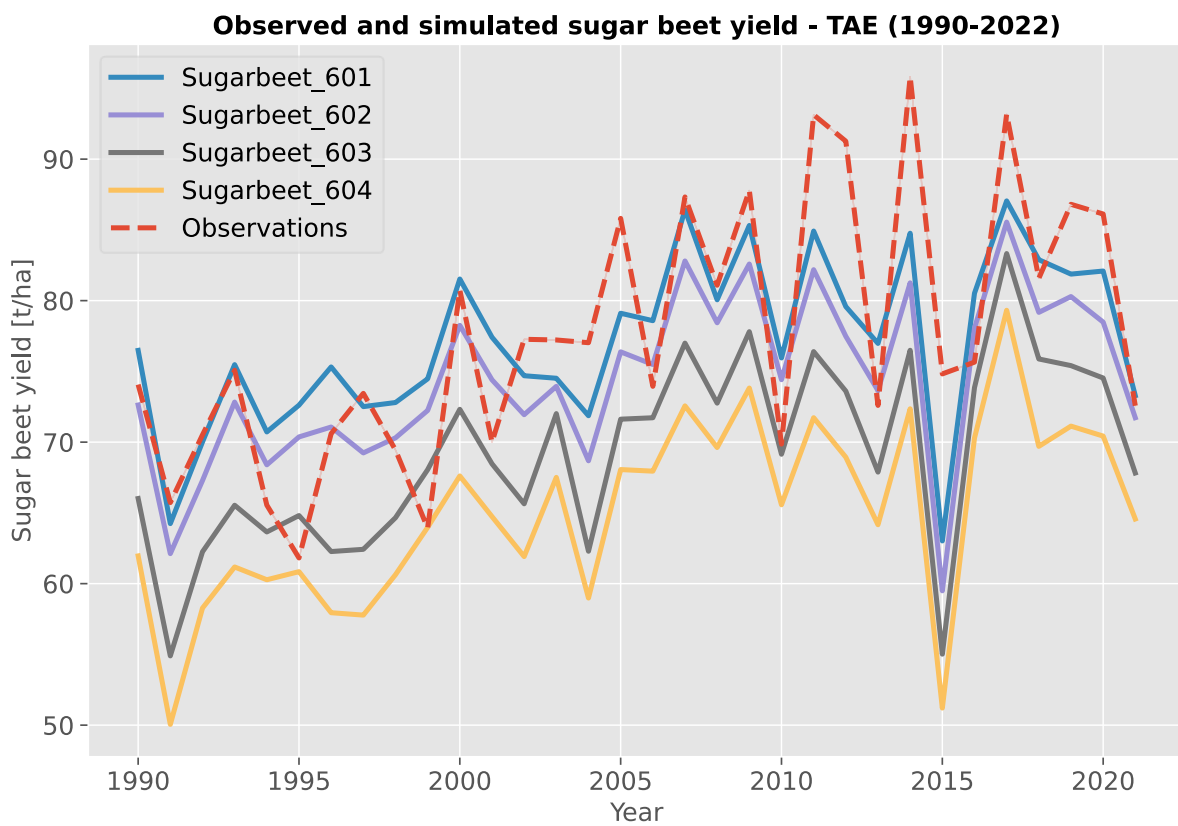
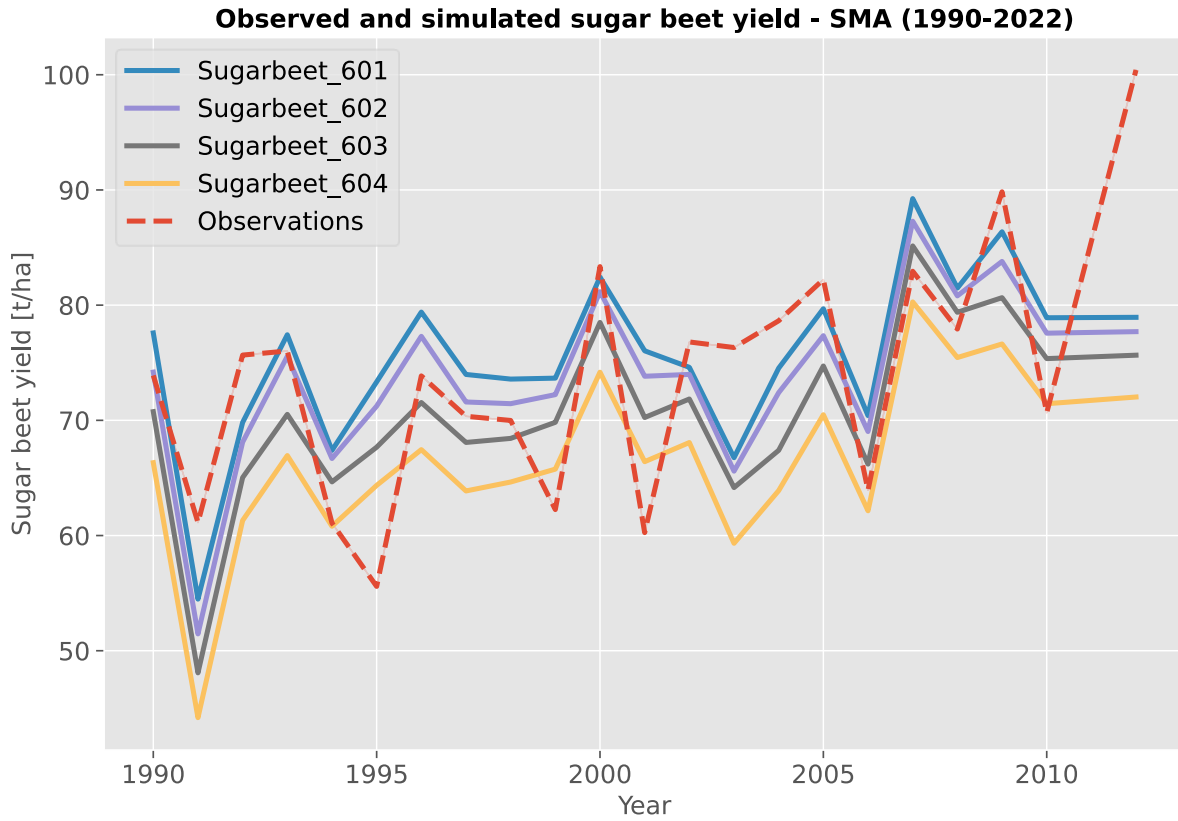


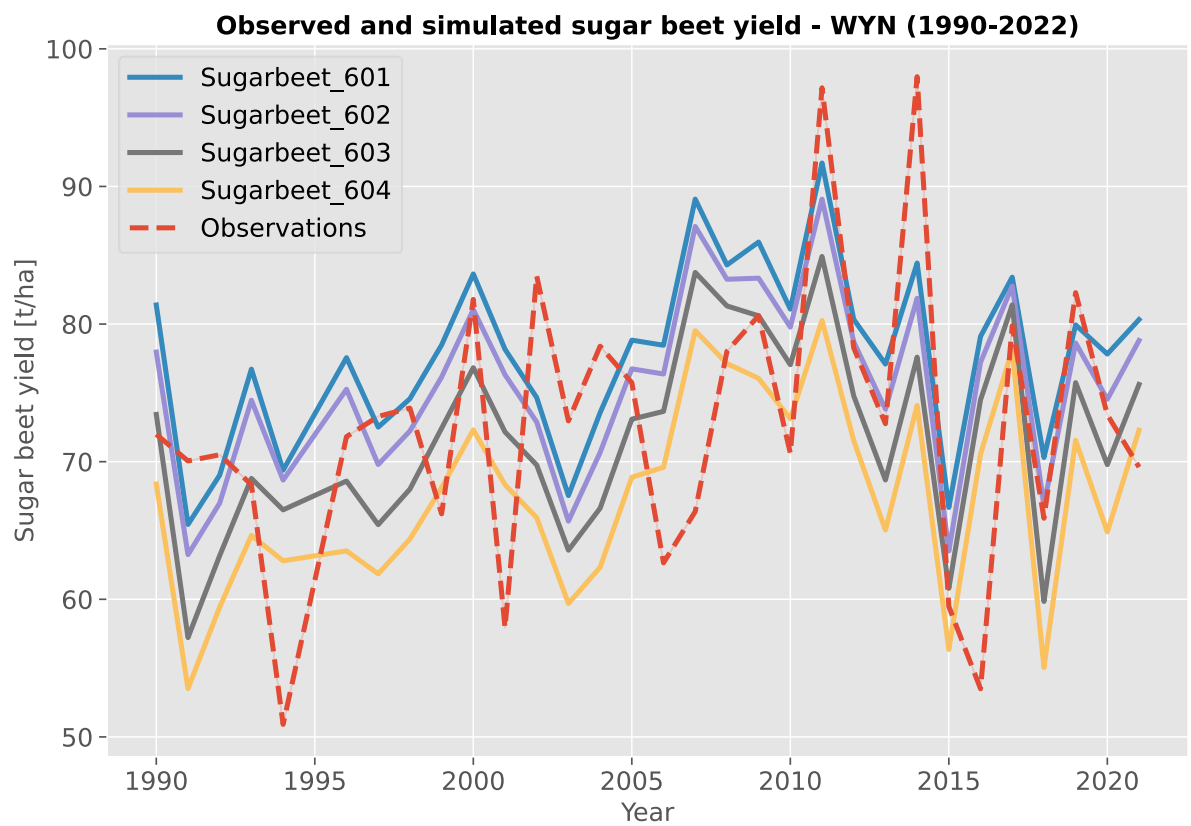
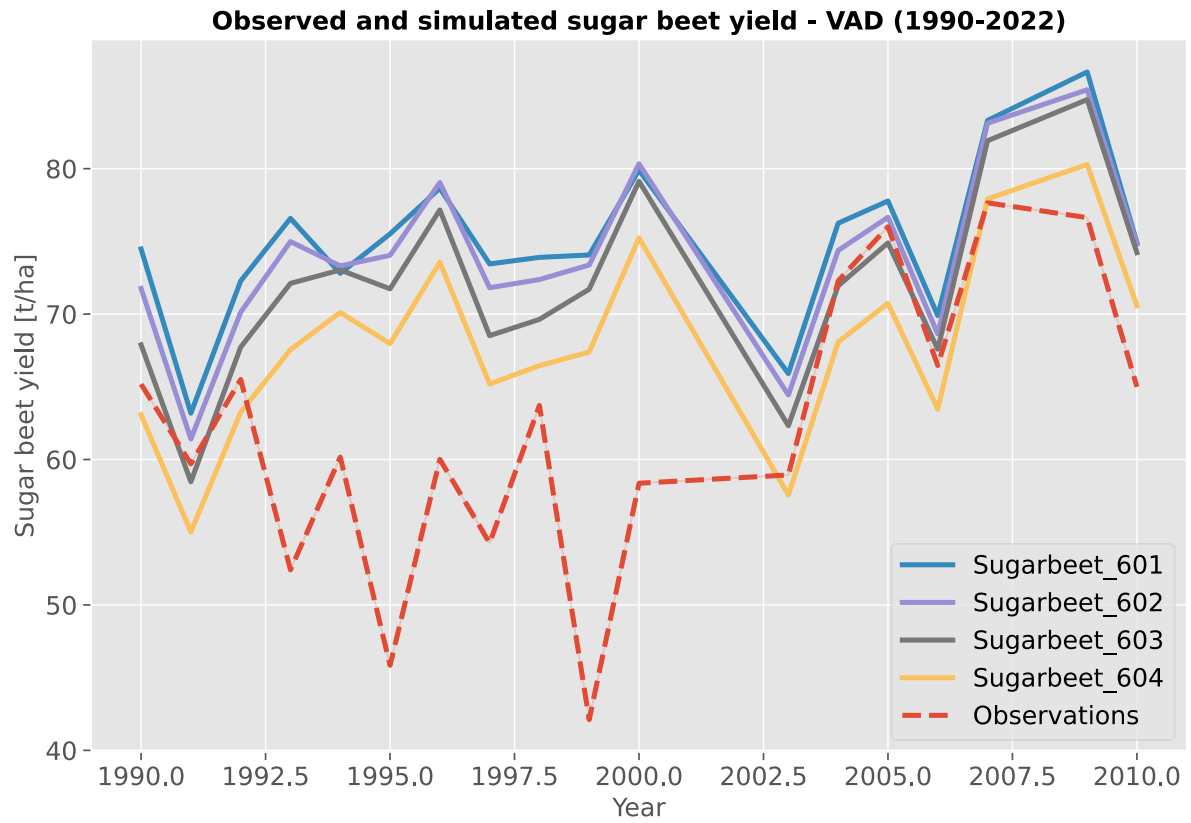












B) Used vegetation indices and Spearman's rank correlation coefficient

Vegetation index (abbreviation)*	Vegetaion index (full name)*	Pearson's coefficient	Spearman's coefficient	Formula*	Reference*
ARI	Anthocyanin Reflectance Index	0.67	-0.49	$(1 / G) - (1 / RE1)$	https://doi.org/10.1562/0031-8655(2001)074%3C0038:OPANEO%3E2.0.CO;2
TCARIOSAVI	TCARI/OSAVI Ratio	-0.69	0.47	$(3 * ((RE1 - R) - 0.2 * (RE1 - G) * (RE1 / R))) / (1.16 * (N - R) / (N + R + 0.16))$	https://doi.org/10.1016/S0034-4257(02)00018-4
ARI2	Anthocyanin Reflectance Index 2	0.72	-0.46	$N * ((1 / G) - (1 / RE1))$	https://doi.org/10.1562/0031-8655(2001)074%3C0038:OPANEO%3E2.0.CO;2
NRFIr	Normalized Rapeseed Flowering Index Red	-0.62	0.44	$(R - S2) / (R + S2)$	https://doi.org/10.3390/rs13010105
SR3	Simple Ratio (860, 550 and 708 nm)	0.69	-0.44	$N2 / (G * RE1)$	https://doi.org/10.1016/S0034-4257(98)00046-7
NormG	Normalized Green	-0.72	0.43	$G / (N + G + R)$	https://doi.org/10.2134/agronj2004.0314
GBNDVI	Green-Blue Normalized Difference Vegetation Index	0.69	-0.43	$(N - (G + B)) / (N + (G + B))$	https://doi.org/10.1016/S1672-6308(07)60027-4
GNDVI	Green Normalized Difference Vegetation Index	0.70	-0.43	$(N - G) / (N + G)$	https://doi.org/10.1016/S0034-4257(96)00072-7
GOSAVI	Green Optimized Soil Adjusted Vegetation Index	0.70	-0.43	$(N - G) / (N + G + 0.16)$	https://doi.org/10.2134/agronj2004.0314
CIG	Chlorophyll Index Green	0.72	-0.43	$(N / G) - 1.0$	https://doi.org/10.1078/0176-1617-00887
GRVI	Green Ratio Vegetation Index	0.72	-0.43	N / G	https://doi.org/10.2134/agronj2004.0314
SR2	Simple Ratio (800 and 550 nm)	0.72	-0.43	N / G	https://doi.org/10.1080/01431169308904370

Vegetation index (abbreviation)*	Vegetation index (full name)*	Pearson's coefficient	Spearman's coefficient	Formula*	Reference*
BNDVI	Blue Normalized Difference Vegetation Index	0.66	-0.43	$(N - B)/(N + B)$	https://doi.org/10.1016/S1672-6308(07)60027-4
ENDVI	Enhanced Normalized Difference Vegetation Index	0.67	-0.43	$((N + G) - (2 * B)) / ((N + G) + (2 * B))$	https://doi.org/10.1371/journal.pone.0186193
TCARIOSAVI705	TCARI/OSAVI Ratio (705 and 750 nm)	-0.71	0.43	$(3 * ((RE2 - RE1) - 0.2 * (RE2 - G)) * (RE2 / RE1)) / (1.16 * (RE2 - RE1) / (RE2 + RE1 + 0.16))$	https://doi.org/10.1016/j.agrformet.2008.03.005
GM1	Gitelson and Merzlyak Index 1	0.71	-0.43	$RE2/G$	https://doi.org/10.1016/S0176-1617(96)80284-7
SR555	Simple Ratio (555 and 750 nm)	0.71	-0.43	$RE2 / G$	https://doi.org/10.1016/S0176-1617(11)81633-0
NormNIR	Normalized NIR	0.68	-0.42	$N/(N + G + R)$	https://doi.org/10.2134/agronj2004.0314
GRNDVI	Green-Red Normalized Difference Vegetation Index	0.68	-0.42	$(N - (G + R))/(N + (G + R))$	https://doi.org/10.1016/S1672-6308(07)60027-4
SR	Simple Ratio	0.68	-0.41	N/R	https://doi.org/10.2307/1936256
MSR	Modified Simple Ratio	0.69	-0.41	$(N / R - 1) / ((N / R + 1)^{0.5})$	https://doi.org/10.1080/07038992.1996.10855178
DSWI3	Disease-Water Stress Index 3	0.64	-0.41	$S1/R$	https://doi.org/10.1080/01431160310001618031
RVI	Ratio Vegetation Index	0.67	-0.41	$RE2 / R$	https://doi.org/10.2134/agronj1968.00021962006000060016x
NDVI	Normalized Difference Vegetation Index	0.64	-0.41	$(N - R)/(N + R)$	https://ntrs.nasa.gov/citations/19740022614
IPVI	Infrared Percentage Vegetation Index	0.64	-0.41	$N/(N + R)$	https://doi.org/10.1016/0034-4257(90)90085-Z
OSAVI	Optimized Soil-Adjusted Vegetation Index	0.64	-0.41	$(N - R) / (N + R + 0.16)$	https://doi.org/10.1016/0034-4257(95)00186-7

Vegetation index (abbreviation)*	Vegetation index (full name)*	Pearson's coefficient	Spearman's coefficient	Formula*	Reference*
TVI	Transformed Vegetation Index	0.63	-0.40	$((N - R)/(N + R) + 0.5)^{0.5}$	https://ntrs.nasa.gov/citations/19740022614
TDVI	Transformed Difference Vegetation Index	0.61	-0.40	$1.5 * ((N - R)/((N^2.0 + R + 0.5)^{0.5}))$	https://doi.org/10.1109/IGARSS.2002.1026867
MSAVI	Modified Soil-Adjusted Vegetation Index	0.61	-0.40	$0.5 * (2.0 * N + 1 - (((2 * N + 1)^2) - 8 * (N - R))^{0.5})$	https://doi.org/10.1016/0034-4257(94)90134-1
NormR	Normalized Red	-0.64	0.40	$R/(N + G + R)$	https://doi.org/10.2134/agronj2004.0314
VI700	Vegetation Index (700 nm)	0.64	-0.40	$(RE1 - R) / (RE1 + R)$	https://doi.org/10.1016/S0034-4257(01)00289-9
NDREI	Normalized Difference Red Edge Index	0.68	-0.40	$(N - RE1) / (N + RE1)$	https://doi.org/10.1016/1011-1344(93)06963-4
CIRE	Chlorophyll Index Red Edge	0.70	-0.40	$(N / RE1) - 1$	https://doi.org/10.1078/0176-1617-00887
REDSI	Red-Edge Disease Stress Index	0.67	-0.40	$((705.0 - 665.0) * (RE3 - R) - (783.0 - 665.0) * (RE1 - R)) / (2.0 * R)$	https://doi.org/10.3390/s18030868
TRRVI	Transformed Red Range Vegetation Index	0.61	-0.39	$((RE2 - R) / (RE2 + R)) / (((N - R) / (N + R)) + 1.0)$	https://doi.org/10.3390/rs12152359
SeLI	Sentinel-2 LAI Green Index	0.68	-0.39	$(N2 - RE1) / (N2 + RE1)$	https://doi.org/10.3390/s19040904
MSR705	Modified Simple Ratio (705 and 750 nm)	0.68	-0.38	$(RE2 / RE1 - 1) / ((RE2 / RE1 + 1)^{0.5})$	https://doi.org/10.1016/j.agrformet.2008.03.005
SR705	Simple Ratio (705 and 750 nm)	0.68	-0.38	$RE2 / RE1$	https://doi.org/10.1016/S0176-1617(11)81633-0
GM2	Gitelson and Merzlyak Index 2	0.68	-0.38	$RE2/RE1$	https://doi.org/10.1016/S0176-1617(96)80284-7
ND705	Normalized Difference (705 and 750 nm)	0.67	-0.38	$(RE2 - RE1)/(RE2 + RE1)$	https://doi.org/10.1016/S0034-4257(02)00010-X

Vegetation index (abbreviation)*	Vegetation index (full name)*	Pearson's coefficient	Spearman's coefficient	Formula*	Reference*
RENDVI	Red Edge Normalized Difference Vegetation Index	0.67	-0.38	$(RE2 - RE1)/(RE2 + RE1)$	https://doi.org/10.1016/S0176-1617(11)81633-0
NDVI705	Normalized Difference Vegetation Index (705 and 750 nm)	0.67	-0.38	$(RE2 - RE1) / (RE2 + RE1)$	https://doi.org/10.1016/S0176-1617(11)81633-0
mND705	Modified Normalized Difference (705, 750 and 445 nm)	0.67	-0.38	$(RE2 - RE1)/(RE2 + RE1 - A)$	https://doi.org/10.1016/S0034-4257(02)00010-X
DSWI5	Disease-Water Stress Index 5	0.67	-0.37	$(N + G)/(S1 + R)$	https://doi.org/10.1080/01431160310001618031
NLI	Non-Linear Vegetation Index	0.58	-0.37	$((N^2) - R)/((N^2) + R)$	https://doi.org/10.1080/02757259409532252
VARI700	Visible Atmospherically Resistant Index (700 nm)	0.63	-0.37	$(RE1 - 1.7 * R + 0.7 * B) / (RE1 + 1.3 * R - 1.3 * B)$	https://doi.org/10.1016/S0034-4257(01)00289-9
NDYI	Normalized Difference Yellowness Index	0.57	-0.37	$(G - B) / (G + B)$	https://doi.org/10.1016/j.rse.2016.06.016
MSI	Moisture Stress Index	-0.61	0.37	$S1/N$	https://doi.org/10.1016/0034-4257(89)90046-1
DSI	Drought Stress Index	-0.61	0.37	$S1/N$	https://www.asprs.org/wp-content/uploads/pers/1999journal/apr/1999_apr_495-501.pdf
AFRI1600	Aerosol Free Vegetation Index (1600 nm)	0.63	-0.36	$(N - 0.66 * S1) / (N + 0.66 * S1)$	https://doi.org/10.1016/S0034-4257(01)00190-0
NDMI	Normalized Difference Moisture Index	0.64	-0.36	$(N - S1)/(N + S1)$	https://doi.org/10.1016/S0034-4257(01)00318-2
NDII	Normalized Difference Infrared Index	0.64	-0.36	$(N - S1)/(N + S1)$	https://www.asprs.org/wp-content/uploads/pers/1983journal/jan/1983_jan_77-83.pdf

Vegetation index (abbreviation)*	Vegetation index (full name)*	Pearson's coefficient	Spearman's coefficient	Formula*	Reference*
SLAVI	Specific Leaf Area Vegetation Index	0.66	-0.36	$N / (R + S2)$	https://www.asprs.org/wp-content/uploads/pers/2000journal/february/2000_feb_183-191.pdf
DSWI1	Disease-Water Stress Index 1	0.66	-0.36	$N/S1$	https://doi.org/10.1080/01431160310001618031
GCC	Green Chromatic Coordinate	0.60	-0.36	$G / (R + G + B)$	https://doi.org/10.1016/0034-4257(87)90088-5
GLI	Green Leaf Index	0.60	-0.36	$(2.0 * G - R - B) / (2.0 * G + R + B)$	http://dx.doi.org/10.1080/10106040108542184
RGBVI	Red Green Blue Vegetation Index	0.60	-0.36	$(G^2.0 - B * R) / (G^2.0 + B * R)$	https://doi.org/10.1016/j.jag.2015.02.012
DSWI4	Disease-Water Stress Index 4	0.61	-0.36	G/R	https://doi.org/10.1080/01431160310001618031
SIPI	Structure Insensitive Pigment Index	-0.51	0.36	$(N - A) / (N - R)$	https://eurekamag.com/research/009/395/009395053.php
TCARI	Transformed Chlorophyll Absorption in Reflectance Index	-0.40	0.35	$3 * ((RE1 - R) - 0.2 * (RE1 - G) * (RE1 / R))$	https://doi.org/10.1016/S0034-4257(02)00018-4
NGRDI	Normalized Green Red Difference Index	0.61	-0.35	$(G - R) / (G + R)$	https://doi.org/10.1016/0034-4257(79)90013-0
RI	Redness Index	-0.61	0.35	$(R - G) / (R + G)$	https://www.documentation.ird.fr/hor/fdi:34390
VIG	Vegetation Index Green	0.61	-0.35	$(G - R) / (G + R)$	https://doi.org/10.1016/S0034-4257(01)00289-9
MTVI2	Modified Triangular Vegetation Index 2	0.55	-0.35	$(1.5 * (1.2 * (N - G) - 2.5 * (R - G))) / (((2.0 * N + 1)^2) - (6.0 * N - 5 * (R^0.5)) - 0.5)^0.5)$	https://doi.org/10.1016/j.rse.2003.12.013
MCARI2	Modified Chlorophyll Absorption in Reflectance Index 2	0.55	-0.35	$(1.5 * (2.5 * (N - R) - 1.3 * (N - G))) / (((2.0 * N + 1)^2) - (6.0 * N - 5 * (R^0.5)) - 0.5)^0.5)$	https://doi.org/10.1016/j.rse.2003.12.013

Vegetation index (abbreviation)*	Vegetation index (full name)*	Pearson's coefficient	Spearman's coefficient	Formula*	Reference*
RGRI	Red-Green Ratio Index	-0.59	0.35	R/G	https://doi.org/10.1016/j.jag.2014.03.018
MGRVI	Modified Green Red Vegetation Index	0.60	-0.35	$(G^{2.0} - R^{2.0}) / (G^{2.0} + R^{2.0})$	https://doi.org/10.1016/j.jag.2015.02.012
VARI	Visible Atmospherically Resistant Index	0.60	-0.35	$(G - R) / (G + R - B)$	https://doi.org/10.1016/S0034-4257(01)00289-9
GARI	Green Atmospherically Resistant Vegetation Index	0.56	-0.35	$(N - (G - (B - R))) / (N - (G + (B - R)))$	https://doi.org/10.1016/S0034-4257(96)00072-7
S2REP	Sentinel-2 Red-Edge Position	0.68	-0.34	$705.0 + 35.0 * (((RE3 + R) / 2.0) - RE1) / (RE2 - RE1)$	https://doi.org/10.1016/j.isprsjprs.2013.04.007
RCC	Red Chromatic Coordinate	-0.60	0.34	$R / (R + G + B)$	https://doi.org/10.1016/0034-4257(87)90088-5
PSRI	Plant Senescing Reflectance Index	-0.56	0.33	$(R - B) / RE2$	https://doi.org/10.1034/j.1399-3054.1999.106119.x
AFRI2100	Aerosol Free Vegetation Index (2100 nm)	0.60	-0.33	$(N - 0.5 * S2) / (N + 0.5 * S2)$	https://doi.org/10.1016/S0034-4257(01)00190-0
GVMi	Global Vegetation Moisture Index	0.61	-0.33	$((N + 0.1) - (S2 + 0.02)) / ((N + 0.1) + (S2 + 0.02))$	https://doi.org/10.1016/S0034-4257(02)00037-8
MNDVI	Modified Normalized Difference Vegetation Index	0.61	-0.33	$(N - S2) / (N + S2)$	https://doi.org/10.1080/014311697216810
CVI	Chlorophyll Vegetation Index	0.53	-0.33	$(N * R) / (G^{2.0})$	https://doi.org/10.1007/s11119-010-9204-3
MTCI	MERIS Terrestrial Chlorophyll Index	0.65	-0.33	$(RE2 - RE1) / (RE1 - R)$	https://doi.org/10.1080/0143116042000274015
IRECI	Inverted Red-Edge Chlorophyll Index	0.64	-0.33	$(RE3 - R) / (RE1 / RE2)$	https://doi.org/10.1016/j.isprsjprs.2013.04.007

Vegetation index (abbreviation)*	Vegetation index (full name)*	Pearson's coefficient	Spearman's coefficient	Formula*	Reference*
MCARI705	Modified Chlorophyll Absorption in Reflectance Index (705 and 750 nm)	0.64	-0.33	$\frac{((RE2 - RE1) - 0.2 * (RE2 - G)) * (RE2 / RE1)}$	https://doi.org/10.1016/j.agrformet.2008.03.005
NMDI	Normalized Multi-band Drought Index	0.53	-0.32	$(N - (S1 - S2)) / (N + (S1 - S2))$	https://doi.org/10.1029/2007GL031021
MRBVI	Modified Red Blue Vegetation Index	-0.58	0.31	$(R^{2.0} - B^{2.0}) / (R^{2.0} + B^{2.0})$	https://doi.org/10.3390/s20185055
RDVI	Renormalized Difference Vegetation Index	0.61	-0.31	$(N - R) / ((N + R)^{0.5})$	https://doi.org/10.1016/0034-4257(94)00114-3
IKAW	Kawashima Index	-0.58	0.31	$(R - B) / (R + B)$	https://doi.org/10.1006/anbo.1997.0544
TTVI	Transformed Triangular Vegetation Index	0.63	-0.30	$0.5 * ((865.0 - 740.0) * (RE3 - RE2) - (N2 - RE2) * (783.0 - 740))$	https://doi.org/10.3390/rs12010016
NIRv	Near-Infrared Reflectance of Vegetation	0.59	-0.28	$((N - R) / (N + R)) * N$	https://doi.org/10.1126/sciadv.1602244
MCARIOSAVI705	MCARI/OSAVI Ratio (705 and 750 nm)	0.59	-0.28	$\frac{(((RE2 - RE1) - 0.2 * (RE2 - G)) * (RE2 / RE1))}{(1.16 * (RE2 - RE1) / (RE2 + RE1 + 0.16))}$	https://doi.org/10.1016/j.agrformet.2008.03.005
MCARI	Modified Chlorophyll Absorption in Reflectance Index	0.48	-0.27	$\frac{((RE1 - R) - 0.2 * (RE1 - G)) * (RE1 / R)}$	http://dx.doi.org/10.1016/S0034-4257(00)00113-9
DSWI2	Disease-Water Stress Index 2	0.29	-0.26	$S1/G$	https://doi.org/10.1080/01431160310001618031
DVI	Difference Vegetation Index	0.56	-0.25	$N - R$	https://doi.org/10.1016/0034-4257(94)00114-3
FCVI	Fluorescence Correction Vegetation Index	0.55	-0.25	$N - ((R + G + B) / 3.0)$	https://doi.org/10.1016/j.rse.2020.111676

Vegetation index (abbreviation)*	Vegetaion index (full name)*	Pearson's coefficient	Spearman's coefficient	Formula*	Reference*
GEMI	Global Environment Monitoring Index	-0.55	0.25	$\frac{((2.0 * ((N^2.0) - (R^2.0)) + 1.5 * N + 0.5 * R) / (N + R + 0.5)) * (1.0 - 0.25 * ((2.0 * ((N^2.0) - (R^2.0)) + 1.5 * N + 0.5 * R) / (N + R + 0.5))) - ((R - 0.125) / (1 - R))}{1}$	http://dx.doi.org/10.1007/bf00031911
TGI	Triangular Greenness Index	-0.23	0.24	$-0.5 * (190 * (R - G) - 120 * (R - B))$	http://dx.doi.org/10.1016/j.jag.2012.07.020
TriVI	Triangular Vegetation Index	0.54	-0.24	$0.5 * (120 * (N - G) - 200 * (R - G))$	http://dx.doi.org/10.1016/S0034-4257(00)00197-8
MCARI1	Modified Chlorophyll Absorption in Reflectance Index 1	0.54	-0.23	$1.2 * (2.5 * (N - R) - 1.3 * (N - G))$	https://doi.org/10.1016/j.rse.2003.12.013
MTVI1	Modified Triangular Vegetation Index 1	0.54	-0.23	$1.2 * (1.2 * (N - G) - 2.5 * (R - G))$	https://doi.org/10.1016/j.rse.2003.12.013
ExR	Excess Red Index	-0.48	0.22	$1.3 * R - G$	https://doi.org/10.1117/12.336896
MCARIOSAVI	MCARI/OSAVI Ratio	0.33	-0.18	$\frac{(((RE1 - R) - 0.2 * (RE1 - G)) * (RE1 / R)) / (1.16 * (N - R) / (N + R + 0.16))}{1}$	https://doi.org/10.1016/S0034-4257(00)00113-9
ExG	Excess Green Index	-0.06	0.16	$2 * G - R - B$	https://doi.org/10.13031/2013.27838
TCI	Triangular Chlorophyll Index	0.28	-0.09	$1.2 * (RE1 - G) - 1.5 * (R - G) * (RE1 / R)^{0.5}$	http://dx.doi.org/10.1109/TGRS.2007.904836
NRFIg	Normalized Rapeseed Flowering Index Green	0.25	-0.04	$(G - S2) / (G + S2)$	https://doi.org/10.3390/rs13010105
ExGR	ExG - ExR Vegetation Index	0.28	-0.04	$(2.0 * G - R - B) - (1.3 * R - G)$	https://doi.org/10.1016/j.compag.2008.03.009

* Information about each vegetation index (abbreviation and full name), the belonging formula and reference were all taken from the rsi-Package from Mahoney (2024)